THERMAL BREAKDOWN PROCESS IN POLYMERIC INSULATING MATERIALS

Masayuki HIKITA

報告番号 甲第1481号

THERMAL BREAKDOWN PROCESS IN POLYMERIC INSULATING MATERIALS

A Dissertation

for

the Degree of Doctor of Engineering

at

Faculty of Engineering

Nagoya University

by

Masayuki Hikita

1982

Acknowledgements

The author is deeply grateful to Professor Masayuki Ieda for his continuing guidance and encouragement throughout the course of this work.

The author also expresses his great appreciation to Professors Kenji Horii and Susumu Uchiyama for their helpful and instructive advices in completing this dissertation.

The author is greatly indebted to Professor Goro Sawa of Mie University and Dr. Masayuki Nagao of Toyohashi University of Technology for their frequent, stimulating and helpful duscussions in the course of this work.

The author wishes to thank deeply to Drs. Teruyoshi Mizutani, Akira Yoshida, Yoshiaki Takai and Yasuo Suzuoki for their helpful suggestions on experimental results.

The author is also grateful to his members of Professor Ieda's laboratory for their helps and encouragements, in paticular, to the author's coworkers, Mr. Teruaki Tsutsui, Mr. Akinori Matsuda and Mr. Masahiro Gotoh for their devoted helps and useful discussions.

The author also wishes to express his gratitude to the members of Mitsubishi Petrochemical Co. Ltd. and Kureha Chemical Industry Co. Ltd. for providing the specimens.

Lastly, but not least the author deeply acknowledges the help of Miss Rashmi in editing this thesis in English..

Contents

List of Principal Symbols

Symbol	Definition
A	Rate of energy gain from the applied field
B	Rate of energy transfer of conduciton electrons to the lattice
c	constant near 1
C_v	Specific heat per unit volume
d	Sample thickness
d_0	Original magnidude of thickness of the dielectric
D	Magnitude of infra-red absorption
D_α, D_β	Magnitude of infra-red absorption at the specific peak for α-phase at 530 cm^{-1} and for β-phase at 510 cm^{-1}, respectively.
e	Electronic charge
E	Electron energy
E_i	Ionization energy
F	Electric Field
F_B	Electric strength
F_{em}	Electric strength determined by the electromechanical breakdown theory
F_p	Prestress field
h	Planck's constant
hν	quantum of the phonon due to the lattice vibration
H	Constant field electric strength
i	Number of events of collision ionization
j	Current density
j_n	Current density due to electrons
j_p	Current density due to holes
j_0	Pre-exponential factor in ionic conduction current density
J_1	$j_0/2\lambda_i\alpha = 2\ q\ A_i\ N_i^{1/2}\ \nu_0/\alpha$
k	Boltzmann constant
l_0, l_f	Sample length before drawing and after drawing, respecrively.
m_0	Mass of free electron
m*	Effective mass of electron
n	Electron carrier density

Symbol	Definition
n_i	Density of ions
N, N_t	Total breakdown test number and the number of tests in which no breakdown takes place before the time t in a series of N tests under the same conditions, respectively
N_i	Density of supplying source of thermally dissociated ions
N_0	Effective density of states in the conduction band
p	Hole carrier density
q	Ionic charge
r_{max}	Length from a neutral state of ion to that at a maximum potential barrier
S	Cross-section of the film
t, t_f, t_s	Time, formative time lag, and statistical time lag
t_B	Voltage duration to breakdown
t_{BR}, t_{BS}	Time to breakdown obtained with a ramp voltage and a step voltage, respectively
t_{th}	Thermal time constant of the dielectric
T	Lattice temperature
T_c	Critical temperature required for thermal breakdown
T_{c1}, T_{c2}	Critical temperature at which temperature dependence of the electric strength changes
T_e	Electron temperature
T_m	Melting point
T_0	Ambient temperature or initial temperature
U	Potential barrier
v_e	Drift velocity of the electron
V	Voltage
V_{em}	Breakdown voltage determined by the electromechanical breakdown theory
V_t	Depth from the bottom of the conduction band to the Fermi level
W	Dissociation energy
W_m	Work function of the metal
x	Space
X	length along the direction towards the thickness
y	Load
Y	Young's modulus

Symbol	Definition
α	Field rising rate
α_e, α_n	Ionization coefficient per unit length and unit time
β_{PF}	$(q^3/\pi\varepsilon_0\varepsilon_r)^{1/2}$
ΔF^*	Free energy of the activation
ΔH^*	Activation enthalpy
ΔS^*	Activation entropy
ε_r	Relative Permittivity
ε_0	Permittivity (or dielectric constant) of vacuum
η	Recombination coefficient
κ	Thermal conductivity
λ	Heat transfer coefficient
λ_e	Mean free path of electron by collisions with phonons
$2\lambda_i$	Ionic jump distance
μ_n, μ_p	Mobilities of elelctrons and holes, respectively
ν_i	Vibration frequency of ions
ν	Frequency of lattice vibration
σ	Electrical conductivity
τ	Mean time between collisions
ϕ	Activation energy
Φ_D	Effective contact barrier height at the metal-insulator interface
χ	Electron affinity of the insulator

Chapter I Introduction

1-1 Introduction

The recent increasing demand for electric power has promoted the tendency to use ultra-high voltage (UHV) power transmission systems. This situation requires use of higher voltage and, at the same time, the miniaturization of the related electrical apparatuses along with an improvement of reliability and life. Also in the field of electronic engineering, the electric field intensity applied to the components such as MOS devices and thin film elements becomes extremely high as their miniaturization develops, though the voltage applied is relatively low. Therefore, both in electric power and in electronic engineerings, various problems have been introduced on electrical insulation at high fields. This means that the high electric field design becomes one of the most urgent problems to be solved nowadays in the field of electrical insulation.

With regard to insulating materials, a variety of organic polymers have been used because of their excellent mechanical and electrical properties. However, the rapid development of electrical and electronic devices in recent years has necessitated dielectric materials to operate under severe conditions of temperature, high energy radiation, and electric stress. This requires further elevation of electrical insulation properties, such as high resistivity, high dielectric strength, and low dielectric loss, as well as that of mechanical properties, such as high tensile strength.

The electrical insulation has been developed from two standpoints, i.e. materials and their manufacturing techniques. The actual procedures to realize this development so far have been much dependent on experiences based on trials. It is almost impossible, however, to fulfill the complex, high graded and severe demands only by such

empirical approaches. The material science has been trying to interpret the properties of materials based on the knoweldges of their constituent atoms and/or the molecules and of their atomic structure. In recent years, the progress of material science is so remarkable that it can greatly contribute to the molecular design of insulators and to the synthesis of new materials instead of old empirical approaches. At present, however, it is still difficult to understand perfectly the properties of various dielectrics such as polymers on the basis of the material science owing to their complex structure and/or to the difficulty in their purification. Therefore, practical situations, in many cases, still rely upon the empirical way. Thus, the material science approach should be taken positively for a more rapid advancement of the electrical insulation engineering.

In 1935 von Hippel[1] first interpreted the electrical breakdown in solid dielectrics on the basis of quantum mechanical solid state physics. He considered the situation in a pure crystalline material at low temperatures, and suggested that the electrons in the solids play an important role in the breakdown process. This promoted Fröhlich[2] and Seitz[3] to develop the breakdown theory for solids from the standpoint of solid state physics. These theories were successful in explaining the breakdown characteristics of ionic crystals qualitatively in the low temperature region. The order of magnitude of the electric strength could be calculated but many features of the breakdown process remain unexplained as discussed in Chapter II. Nevertheless, these theories should be evaluated in a sense that they give an indication to the increase in so-called intrinsic electric strength from the standpoint of solid state physics: The electric strength is expected to be raised with increasing the ionization energy of the material and with decreasing the drift mobility and mean free path of the electron.

In this thesis, fundamental electrical breakdown characteristics of several kinds of polymeric insulating materials are investigated, focussing attention to the high temperature region which is very important in practical application of insulators. In spite of many studies on the breakdown at high temperatures, any reasonable theories seem to have never been established so far owing to many complexies present in polymers. An approach is attempted throughout this thesis to consider the experimental results on dielectric breakdown from the thermal breakdown process.

This choice of consideration is mainly due to following two reasons: The first reason is that the electronic breakdown process in high temperature region presented by Fröhlich[4] has a problem in the development of the theory, which will be mentioned later in Chapter II. The second reason is that the breakdown in practical insulators is recognized as a structure destruction by temperature and conductivity increases, resulting in the evaporation or the melting of the material. Various problems are also left in a simple thermal breakdown theory, mainly concerning local heating in weak spots and space charge formation during voltage application. As a first approximation, however, an attempt is made, in the thesis, to interpret the obtained breakdown results in terms of the thermal breakdown theory as far as possible, assuming the sample is uniform. In other words, the large part of the thesis is devoted to make clear to what extent the obtained results are understood by the thermal breakdown theory.

1-2 Survey of the Thesis

The main aim of this thesis is to advance the understanding of the electrical breakdown process especially in a high temperature region for various polymers. The experimental results are attempted to be interpreted mainly in terms of the thermal breakdown process. From

the results, indications of designing a reasonable insulation for the electrical apparatuses and informations on synthesizing of new polymeric insulators are given. The outline of each chapter is as follows.

Chapter II summarizes the theories of electrical breakdown process, which are described to the extent to be required on discussion in each chapter.

Chapter III deals with the dielectric breakdown of polyimide in a high temperature region, which is the most representative high temperature polymer. Heat and hydrolytic treatment effects on dielectric breakdown strength are also discussed.

In Chapter IV, the dielectric breakdown of poly(vinylidene--fluoride) is studied. An attempt is made to apply the impulse thermal breakdown theory to the data obtained above 50°C. With the aid of computation, an estimation of the conduction parameters is made. Further, the influence of the crystalline phase of the polymer on the breakdown characteristics is discussed.

Chapter V deals with theoretical analysis of approximation required for numerical calculation of impulse thermal breakdown. The fundamental equation of thermal breakdown is solved numerically under the boundary conditions imposed by Newton's cooling law for various values of heat transfer coefficient λ from the dielectric surface to the surroundings. The influence of λ on breakdown characteristics is discussed.

Chapter VI deals with the dielectric breakdown of plasma polymerized styrene thin films (PPS) by taking advantage of self-healing. The breakdown mechanism of PPS is also discussed.

Chapter VII deals with a new simple thermal breakdown model, which discards the space charge and bulk processes, in order to explain the experimental results of PPS. Further, a steady state

avalanche is considered as a possible bulk conduction.

Chapter VIII deals with the dielectric breakdown of polyethylene. The discussion centers on the relation between morphology and the breakdown characteristics.

Chapter IX gives the conclusion drawn from the results presented in the thesis. The engineering significance of these results is also pointed out.

References

[1] A.von Hippel: Ergeb. Exak. Naturw. 14 79 (1935).

[2] H. Fröhlich: Proc. Roy. Soc. (London), A160 230 (1937).

[3] F. Seitz: Phys. Rev. 76 1376 (1949).

[4] H. Fröhlich: Proc. Roy. Soc. (London) A188 521 (1947).

Chapter II Electrical Breakdown in Solids

2-1 Introduction

As mentioned in the previous chapter, it is very significant in a practical use of insulators to understand the dielectric breakdown phenomena and to realize a molecular design of insulators. So far many studies on the breakdown phenomena of solid dielectrics have been done. Parallel to the experiments, many breakdown theories on solids have been proposed between 1930 and 1950, most of which were based on quantum mechanical solid state physics: It was von Hippel[1] who first interpreted the electric breakdown in alkali halide single crystal by electronic process, similar to the avalanche breakdown in gases. After his research, Fröhlich[2], and Fröhlich and Paranjape[3] modified the theory presented by von Hippel. Fröhlich presented the theories of breakdown of ionic crystal from the standpoint of solid state physics[2,4,5]. This was successful in explaining the experimental results for an alkali halide single crystal quantitatively[6]. These so-called intrinsic breakdown theories treat the energy balance of the conduction electrons differing from each other in the view of energy transfer process from the conduction electrons to the lattice, and assumption on the energy distribution of the conduction electrons. There are, however, many uncertainties in these theories, which will be described later. Moreover, in many materials except alkali halides, the quantitative agreement between the theory and experimental result has been scarcely obtained. Nevertheless, the distinguished idea of interpreting the breakdown phenomena from a viewpoint of the modern material science should be extremely admirable. This concept stimulated the development of new dielectric breakdown theories. A typical example is a single avalanche breakdown theory presented by Seitz[7]. He considered the situation in which a

single electron starting from the cathode causes an avalanche of electrons sufficient to destroy the solid dielectric.

On the other hand, at high temperatures, where electric strengths of most of the dielectrics fall with increasing temperature, various kinds of theoretical explanations have been given.

In 1922, Wagner[8] considered the heat balance between production of heat due to ionic conduction and heat dissipation due to heat conduction, deducing the thermal breakdown voltage from the condition in which the heat balance is broken. This concept has been supported by experiments after a little modification. However, the thermal breakdown theory is unable to explain experimental observations, for instance, time lag of breakdown and directional path of breakdown.

In 1947, Fröhlich[5] presented a new theory for breakdown at high temperatures on the basis of collective breakdown model. He recognized that, in crystals containing many impurities or in amorphous solids, the combined number of electrons in localized excited states and in conduction band will be relatively high, so that electron--electron scattering must predominate over electron-lattice interaction. This theory could give an qualitative interpretation to various experimental results at high temperatures. However, there still remain serious problems in Fröhlich's amorphous theory on the assumptions, such as a strong electron-electron interaction etc., as discussed in subsection 2-3-1-C. Later,Stark and Garton[9] proposed the electromechanical breakdown theory in which a mechanical deformation caused by Maxwell stress due to the applied field is considered. They recognized this behavior in polyethylene, but till now almost no experimental results have been reported except on polyethylene.

Another breakdown theory relevant to polymers is the free volume breakdown theory presented by Artbauer[10]. This was proposed to explain the breakdown phenomena of polymers around the glass transition

temperature region.

2-2 Classification of Electrical Breakdown

The term " electrical breakdown " is defined in two ways: One is associated with structure destruction by a large current increase, taking a form of evaporation or melting and consequently resulting in a short circuit of insulating part. For this case, the cirtical field strength refers to the field when the melting or evaporation occurs. The other case refers to an appearance of negative resistance region in current vs. voltage characteristics.

There are various ways to classify the electrical breakdown mechanisms. Among them, three major categories of classification are listed below:

1. the way to seperate them roughly into electronic and thermal breakdowns[11,12,13]. The former can be further divided into two, i.e. intrinsic breakdown and electron avalanche breakdown[14].
2. the way to classify the breakdown mechanisms as a combination of a current multiplication and a possitive feedback processes[15,16].
3. the way to classify them into two conditions for electrical breakdown. One is a condition in which a balance of physical parameters is broken and other is one in which a certain physical parameter reaches a critical value, which is summarized in Table 2.1[17].

In the next subsection, the principal features of the breakdown mechanisms, which will be used later for interpretation of experimental results, are discussed briefly, following the first of the classification. A summary of the breakdown mechanisms is given in Table 2.2[12].

Table 2.1. Condition for electrical breakdown

I. Losing of balance of physical quantities	
Pysical parameter	Type of breakdown
Electron energy	Intrinsic breakdown (Single electron approximation)
Electron temperature	Intrinsic breakdown (Collective breakdown theories)
Lattice temperature	Steady state thermal breakdown
Thickness	Electromechanical breakdown

II. Establishment of critical physical quantities	
Pysical parameter	Type of breakdown
Energy	Avalanche breakdown
Lattice temperature	Impulse thermal breakdown

2-3 Theories of Electrical Breakdown in Solid Dielectrics

2-3-1 Electronic Breakdown Process

[A] Intrinsic Breakdown Process

The intrinsic breakdown theory treats the energy balance of electrons. In an electric field F causing a current flow of density j, the rate of energy gain from the field is

$$A = j F. \tag{2.1}$$

Let the rate of energy transfer to the lattice by conduction electrons be denoted by B, then the condition for energy balance in the field is

$$A = B. \tag{2.2}$$

Table 2.2. Dielectric Breakdown theories of Solids[12]

I. Electronic breakdown process

- Intrinsic breakdown ($\partial F_B/\partial d = 0$), d: sample thickness
  - Theories based on the single electron approximation ($\partial F_B/\partial T_0 \geq 0$)
    - High energy criterion
    - Low energy criterion
  - Collective critical field theories
    - Single crystal ($\partial F_B/\partial T_0 > 0$)
    - Amorphous materials ($\partial F_B/\partial T_0 < 0$)
- Electron avalanche breakdown ($\partial F_B/\partial d < 0$) ($\partial F_B/\partial T_0 \geq 0$)
  - Single avalanche model
  - Collective avalanche model
- Field emission breakdown ($\partial F_B/\partial d = 0$) ($\partial F_B/\partial T_0 = 0$)
- Free volume breakdown ($\partial F_B/\partial T_0 < 0$)

II. Thermal breakdown process

- Steady state thermal breakdown ($\partial F_B/\partial T_0 < 0$)
- Impulse thermal breakdown

III. Mechanical breakdown process

- Electromechanical breakdown ($\partial F_B/\partial T_0 < 0$)

By considering different mechanisms of the energy transfer and different assumptions on energy distribution of the conduction electrons, intrinsic breakdown theories are classified further as shown in Table 2.2. It can be said that intrinsic critical field strength in each case corresponds to failure of some specific process to stabilize the conduction electron situation. Some criticisms were given about the electronic breakdown process by O'Dwyer[14] and Inuishi[16].

The intrinsic critical field strength in all cases refers to an infinite homogeneous medium and thus is not able to account for many features of the actual breakdown process. At first, electron emission from the cathode, which is either field induced or thermionic, is considered to take place. This will lead to the non-uniformity in electron density distribution due to trapping which introduces a disturbance of the uniform field distribution[14]. Secondly, it is also pointed out that another mechanism may take over the role of stabilizing the conduction electron system, even after the failure of some specified mechanism to stabilize it. For example, in a single electron approximation, only electron-lattice interaction is considered as energy loss mechanism. In this case, however, electron--electron collisions eventually prevent the consequences of failure of a steady state[14]. A more detailed discussion of intrinsic breakdown is given below.

The first theory of electronic breakdown presented by von Hippel [1] considered the situation in a pure, crystalline material at low temperatures. Under an applied electric field, the energy A transferred to one conduction electron per unit time, is written in the form

$$A = e\,F\,v_e = \mu_n\,e\,F^2 = e^2\,\tau(E)\,F^2/m^*, \qquad (2.3)$$

where v_e and μ_n are respectively the drift velocity and mobility of the electron, e the electronic charge, m^* the effective mass of electron and $\tau(E)$ the mean time between collisions. On the other hand, the energy B which the electron loses by collisions with lattice atoms per unit time is

$$B = h\nu/\tau(E), \qquad (2.4)$$

where $h\nu$ is the energy of optical phonon. Figure 2.1 illustrates a typical example of energy gain and loss of an electron as a function of the electron energy. von Hippel considered the critical field (F_{BH}) when the energy gain of every conduction electron exceeds the maxumum energy loss ($E = h\nu$), assuming that the electron interacts only with lattice vibrations. This corresponds to the condition in which the curves A and B in Fig.2.1. touch each other ($A \geq B$). The condition is also referred to as low energy criterion. This critical situation followed by accelerating the electron to ionization energy E_i leads to breakdown, unless recombination of all types could be balanced with ionization.

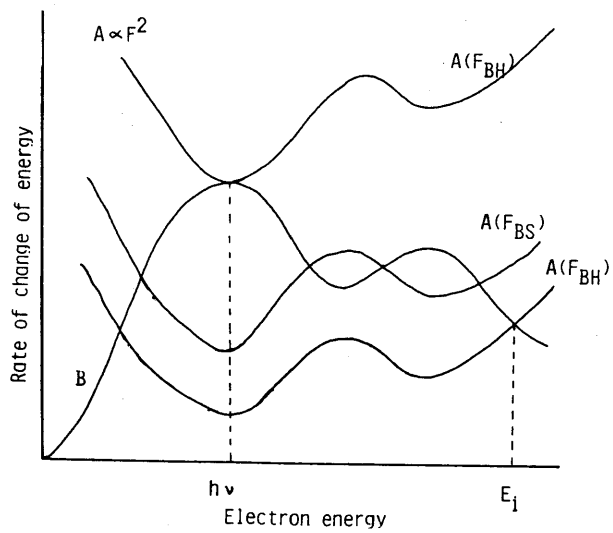

Fig.2.1. Graphical illustration of conditions for electronic breakdown.

O'Dwyer[14] claimed that there is a possibility of a state in which the number of conduction electrons is steady even though the energy loss through electron-lattice interaction can no longer cope with the energy gain of electrons from the power source. For example, collision ionization may increase the number of conduction electrons but it may be balanced by radiative recombination. Consequently, some of the energy gain from field is lost in light emission, keeping the number of conduction electrons steady[14]. In such s case, to calculate steady state electron distribution function, both ionization and recombination processes should be included, as well as the effects of the applied field and electron-lattice collision[18].

The critical field strength F_{BH} is given as [16]

$$F_{BH} = c\, h\nu/e\, \lambda_e, \tag{2.5}$$

where c and λ_e are a constant (≈1) and the mean free path of electron by collisions with phonons, respectively.

Fröhlich[2] insisted that condition for breakdown is to be $A \geq B$ for a small number of electrons with energy little below the ionization energy. The electric field F_{BF} shown in Fig.2.1 is the critical field strength, given by[16]

$$F_{BF} = F_{BH}(h\nu/E_i). \tag{2.6}$$

This is also referred to as Fröhlich high energy critical field. The critical situation is the failure of collision recombinations and collision ionizations to balance in such a way as to produce a steady state.

With respect to this theory, two types of criticism are presented[14]. The first criticism is whether these collision

processes could ever yield a steady state in the time available in an actual breakdown experiment for fields lower than the critical. The second is almost the same as the criticism levelled against the von Hippel low energy critical field, as mentioned earlier[14]. For example, the light emission was observed at the strong field well below breakdown. In this case, a steady state including radiative recombination as well as electron-lattice interaction must be considered.

If the rate of change of energy of an electron due to inter-electronic collisions exceeds that due to electron-phonon collisions, the energy distribution function in the steady state will be Maxwellian with an electron temperature T_e in excess of lattice temperature T. The electron temperature is determined by the energy balance. Fröhlich and Paranjape[3] considered that the critical condition occurs when the energy gain from the power source is greater than the energy loss for all electron temperature and the electron system is unstable.

The principal point of discussion for this theory exists in the possiblity of the existence of the high conduction electron densities in order that electron-electron collisions may be predominant. O'Dwyer[14] appoximately estimated the energy gain of the electrons below breakdown to be the order of a few hundred electron volts per ion volume per second by using a typical values for all the alkali halides. This energy must be transferred to the lattice and is sufficient to destroy it. Since this contradicts the assumption of a field below breakdown, the electron density assumed by the theory simply could not exist.

These three theories succeeded in explaining qualitatively and partly quantitatively the breakdown characteristics for alkali halides, and have the following common features:

i) An increase in temperature causes an increase in the scattering

of electron due to lattice vibrations, leading to a rise in electric strength.

ii) The electric strength is independent of sample thickness, electrode metal or form of applied voltage.

iii) An introduction of impurities or mechanical stress disturbs the periodicity of lattice, leading to an increase in electron scattering with a consequent increase in electric strength.

[B] Electron Avalanche Theory

Seitz[7] considered that some electrons can overcome energy loss B due to existence of fluctuation of electron distribution and can be accelerated to reach ionization energy (see Fig.2.1). The ionization coefficient α_e was calculated[7] as

$$\alpha_e = \frac{1}{\lambda_e} \exp (-h\nu/e\lambda_e F). \qquad (2.7)$$

An initial electron which starts from the cathode grows to an avalanche containing $\exp(\alpha_e d)$ electrons before it reaches the anode apart from the cathode with a distance d. The avalanche also diffuses to the transverse direction and thus determines its volume. The breakdown occurs when the total energy of the avalanche exceeds the energy requried for the destruction of the lattice in this small volume. From this consideration the following equation was obtained:

$$\alpha_e d = 40. \qquad (2.8)$$

This is also referred to as forty generation theory. The critical field is calculated as[14,16,18]

$$F_{BS} \simeq H/ \ln(d/ F_{BS} \mu(E_{av}) \tau(E_{av}) i), \qquad (2.9)$$

where i is the number of events of collision ionization and

$$H = (m^*/2)^{1/2} \frac{1}{e} \int_{E_{av}}^{E_i} \frac{dE}{E^{1/2}\,\tau(E)} . \qquad (2.10)$$

However, questions concerning the above discussion have been pointed out[14,16,19]. Inuishi[16] pointed out that a free electron may disappear by the process of capture recombination within short time (10^{-9} to 10^{-6} sec) in solids or loquids. Consequently, in these dielectrics, $\alpha_{eff} = \alpha_e - \eta$ in place of α_e should be used, where η is the recombination coefficient.

O'Dwyer discussed the problem occuring in deducing eq.(2.9) as follows: If conduction electron density becomes sufficiently high, electron-electron collisions will prevent electrons from attaining ionization energy, and avalanche multiplication will not continue. This situation may take place especially for long breakdown path lengths. A more sophisticated treatment of the Fröhlich-Paranjape collective theory is required.

Forlani and Minnaja[19] questioned the assumptions made in the Seitz's model. One question is whether avalanche starts when an electron energy is equal to the ionization energy. Another one is on dealing with τ as independent of the electron energy.

[C] Fröhlich's Amorphous Theory

Fröhlich[5] presented the electronic thermal breakdown theory to explain the negative temperature dependence of electric strength at high temperatures. His calculations were based on the hypothesis of the energy level scheme illustrated in Fig.2.2, where conduction electrons are derived from impurity levels lying deep in the forbidden zone. There is also a set of shallow traps spread below the conduction band edge ($V_t >> \Delta V_t >> kT$). The outline of the theory

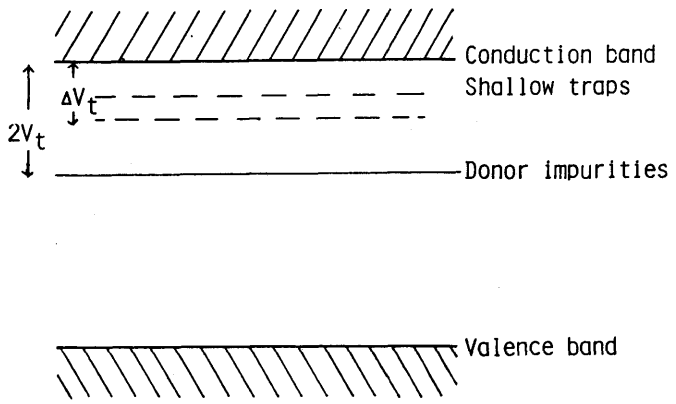

Fig.2.2. Model energy-level scheme for an amorphous solid.

is as follows:

i) It is assumed that the interaction between the conduction electrons and electrons in localized exited states is so strong that their electron temperature is equal each other. It means electron-electron scattering predominates over electron-lattice scattering, as in the case of the collective breakdown theory.

ii) When an electric field is applied, the energy supplied from the power source is transferred through the conduction electron with a large mobility to the electron system at a rate A

$$A = N_0 \exp (-V_t/kT_e) e \mu_e F^2, \qquad (2.11)$$

where N_0, V_t, and k are the effective density of states in the conduction band, the depth from the bottom of the conduction band to the Fermi level, and the Boltzmann constant, respectively. This energy is directly transferred to the electrons in localized states, raising them to the exited localized states.

iii) The principal mode of energy transfer to the lattice is the emission of phonons by the exited electrons. According to Fröhlich, the rate of energy transfer, B to the lattice is

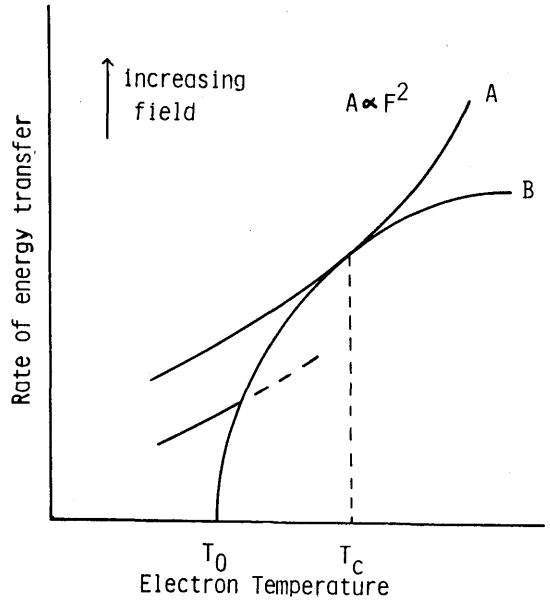

Fig.2.3. Energy transfer curves for increasing applied fields.

$$B = N\ (h\nu/\tau)\ [\exp(h/kT_e) - 1]^{-1}\ [\exp\ (h\nu/k)(1/T - 1/T_e) - 1], \tag{2.12}$$

where τ is the mean time between collisions of localized electrons with phonons and $h\nu$ is the quantum of the phonon due to the lattice vibration.

iv) When the inequality $A \geq B$ holds, the critical situation occurs in which a stable electron temperature is impossible. The critical field strength F_c is determined as a field at which the curves A and B touch each other as shown in Fig.2.3. Consequently, F_c is written in the form

$$F_c = C \exp (\Delta V_t/2kT), \tag{2.13}$$

where C is nearly constant with a weak dependence of temperature.

The main feature expected for this type of breakdown is that time lag is very short, of the order of 10^{-8} to 10^{-9} sec, because of the

small electron heat capacity. Simpson[20] calculated the time lag to be of the order of 10^{-10} to 10^{-12} sec, which is considered as the time required for electron in impurity level to go up to the conduction band from the deep trap under the influence of high electric field.

Inuishi[16] insisted that there is a problem in this theory on neglecting the interaction between the conduction electron and the lattice, and the energy transfer from the applied field to the hopping electron. Inuishi also presented a modified theory[21] which considers the balance between the rate of the energy transferred to the hopping electron from the applied field and that to the lattice vibrations from the hopping electron.

This Fröhlich's theory has been criticized by O'Dwyer on two points. One is the possiblility of strong field emission from the shallow traps. The other is excessive idealization of the electronic structure, which may be hard to maintain to represent the electronic structure of dielectric polymers.

[D] Field Emission Type of Breakdown

The electric strength determined by the electron avalanche theory mentioned in subsection 2-3-1-C is inversely proportional to the mean free path of the electron and increases with decreasing sample thickness. Thus, in such a material with a small mean free path as in amorphous solid or liquid, or in a thin sample such as semiconductor p-n junction, a large number of electrons are emitted from the electrode metal or the valence band to the conduction band by tunnelling effect under the influence of the high field. The former and the latter processes are called as field emission[22] and Zener effect[23], respectively. When the lattice temperature is raised up to a critical temperature by the input energy due to the tunnelling electrons, the dielectric is melt or evaporated, leading to a breakdown. In

this type of breakdown, the electric strength is scarcely influenced by temperature or sample thickness.

2-3-2 Thermal Breakdown Process

In many solid dielectrics there is a region in which the electric strength falls with increasing temperature. In this region, Wagner[8] introduced the idea that the breakdown can be treated as a problem of a balance between heat generation due to ionic conduction and heat conduction. This was the first approach to the thermal breakdown theory. In general, thermal breakdown is classified into the following two types; temperature increase in the lattice temperature due to an ionic conduction or due to electron conduction, and increase in electron temperature due to localized electrons in an amorphous solid (Fröhlich's electronic thermal breakdown)[16]. Through the thesis, only the first term of thermal breakdown process will be referred. An outline of thermal breakdown process is given below[14].

In the thermal breakdown, as in the case of the electronic breakdown process, the rate of energy transfer to the lattice due to an applied field can be written

$$A = \sigma F^2, \tag{2.14}$$

where σ is the electrical conductivity. This is always true for ionic conductivity since the charge carriers are material particles. For electronic conductivity, however, there must always be a quasi--steady state, namely the variation of the applied field with time must be sufficiently slow so that the electron distribution is, at all times, a function only of the field strength and not of its time derivatives. In this case, the energy transfer to the lattice is also

accord with eq.(2.14). The lattice temperature then increases to an extent depending on energy loss processes. If heat conduction is considered as the only significant loss process, the lattice energy balance equation, also called as the heat balance equation, is expressed by the following:

$$C_v \left(dT/dt \right) - \text{div} \left(\kappa \, \text{grad} \, T \right) = \sigma F^2, \qquad (2.15)$$

where C_v is the specific heat per unit volume, κ is the thermal conductivity, dT/dt is the time derivative, and grad T is the space gradient of the temperature.

Thermal breakdown occurs in two forms; one is destructive breakdown obtained by raising the temperature to a critical value and the other is thermal instability at which the heat input cannot be balanced by heat loss from the sample, depending on the time of application of the field. The former criterion for breakdown is adopted in impulse thermal breakdown, which is one of paticular case of eq.(2.15), when the heat conduction term is ignored. Thus, the heat balance equation becomes

$$C_v \left(dT/dt \right) = \sigma F^2. \qquad (2.16)$$

The other case is used when the electric field is increased slowly so that the temperature rise of the lattice remains steady state. The time dependent term of eq.(2.15) becomes

$$- \text{div} \left(\kappa \, \text{grad} \, T \right) = \sigma F^2. \qquad (2.17)$$

This limiting case is called the steady state thermal breakdown, and gives the minimum thermal critical field appropriate to the case in which the field is applied for a very long time.

The main features of thermal breakdown are as follows:

i) Thermal breakdown is observed for pulse durations from 10^{-6} sec into dc range.

ii) Electric strength decreases with increasing sample thickness (for steady state thermal breakdown), pulse duration, temperature and dielectric losses.

iii) Electric strength increases with increasing the resistivity and thermal conductance of the sample.

2-3-3 Electromechanical Breakdown Process

The attraction of the charges on opposite electrodes causes mechanical stress by mutual Coulombic force as the voltage V is imposed. This stress can cause a considerable decrease in thickness of the dielectric from an original magnitude d_0 in the vicinity of breakdown fields. At equilibrium, the electrical attractive force causing compression is balanced by the elastic restoring force, as expressed by the equation

$$\frac{1}{2} \varepsilon_0 \varepsilon_r (V/d)^2 = Y \ln (d_0/d), \qquad (2.18)$$

where ε_0 and ε_r are the permittivity of empty space and the relative dielectric constant, respectively, and Y is Young's modulus. The quantity $d^2 \ln (d_0/d)$ has a maximum for $d/d_0 = \exp(-1/2) \simeq 0.6$. No actual value of V can produce a stable situation for values of d/d_0 less than 0.6. When the electronic or thermal breakdown voltage is larger than this maximum voltage V_{em}, the dielectric collapses. Thus, the critical electric strength F_{em} is

$$F_{em} = V_{em}/d_0 = (Y/e \varepsilon_0 \varepsilon_r)^{1/2}, \qquad (2.19)$$

where e is the base of the natural logarithm. This process is

denoted as electromechanical breakdown. Electric strength determined by the electromechanical breakdown theory decreases with increasing temperature since Y decreases with increasing temperature.

2-3-4 Other Electrical Breakdown Mechanisms by Multi-step Processes

In the previous subsections, the main breakdown mechanisms were summarized. However, it is usually difficult to interpret the breakdown phenomena in solid dielectrics, especially polymers, by a single breakdown mechanism. The multi-step processes of breakdown have therefore been presented in which injection process from the electrode, bulk conduction and various secondary effects are taken into consideration. For convenience, these theories are roughly classified into three categories; electronic impact ionization model, ion--induced model and electro-chemical breakdown model. These models are described briefly below.

[A] Electronic Impact Ionization Model

The general concept of electronic impact ionization model is as follows[24]. It is assumed that the ionizing carriers are electrons only. At first, electrons are injected from the cathode by tunnelling emission or Schottky emission and traverse the insulator rapidly. They can produce electron-hole pairs by impact ionization. Holes produced may be deeply trapped to form the positive space charge because of the relatively small mobility of holes. These trapped holes enhance the field near the cathode, and hence the current injection and impact ionization. This whole sequence of events acts as positive feedback situation with a consequent current runaway above a certain critical field F_r. Two types of opposing effects against the regenerative processes are considered. One is hole removal by drift and the other is hole-electron recombination.

O'Dwyer[25,26], and Kashat and Klein[27] considered the case in which impact ionization is opposed by drift. The theory of the case in which the effect of impact ionization is opposed by recombination was treated by DiStefano and Shatzkes[28,29,30] and by Klein and Solomon[31].

Here the model proposed by O'Dwyer will be mentioned more explicitly since it is used for the discussion of breakdown phenomena of plasma polymerized styrene thin films in Chapter VII. He presented calculations for the high-field conduction characteristics with plane electrode geometry. The following assumptions are made:

i) Continuum electromagnetic theory can be applied. This means the electron and hole densities can be considered as continuous functions of position.

ii) The cathode emits electrons following a Fowler-Nordheim law, and the anode blocks the emission of holes.

iii) The electrons have a much larger mobility than the holes, and are capable of causing collision ionization.

iv) The steady state conduction characteristics are treated.

v) The current density and electric field are functions only of position within the dielectric.

vi) Recombination, displacement current and diffusion of both types of carriers are neglected.

The basic equations in one-dimensional form are given as follows:

The total current density j is

$$j = j_n + j_p \tag{2.20}$$

$$= ne\mu_n F + pe\mu_p F. \tag{2.21}$$

Poisson's equation is

$$\partial E/\partial x = e\,(p-n)/\varepsilon_0\varepsilon_r. \tag{2.22}$$

Taking into accuont the empirical result of collision ionization, the continuity equations are

$$\partial n/\partial t = n\,\alpha_n \exp(-H/F) + \frac{\partial}{\partial x}(n\,\mu_n F), \tag{2.23}$$

$$\partial p/\partial t = n\,\alpha_n \exp(-H/F) + \frac{\partial}{\partial x}(p\,\mu_p F). \tag{2.24}$$

Here n and p are the electron and hole densities, and μ_n and μ_p the respective mobilities, and t is the time. α_n and H are a constant ionization coefficient and a constant field strength, respectively, being characteristic of the dielectric material. The dielectric between infinite plane parallel electrodes with the anode at x=0 and the cathode at x=L is assumed. Elimination of the electron and hole densities n and p leads to the following pair of differential equations for j_n and F.

$$dj_n/dx = -(\alpha_n/\mu_n)\, j_n \exp(-H/F)/F, \tag{2.25}$$

$$dF/dx = [\, j - j_n\,(1-\mu_p/\mu_n)\,]/(\varepsilon_0\varepsilon_r\mu_p F),$$

$$\simeq (j - j_n)/(\varepsilon_0\varepsilon_r\mu_p F). \tag{2.26}$$

Equations (2.25) and (2.26) correspond to eqs.(7.8) and (7.9) given in Chapter VII, respectively. These equations can be numerically solved with the following boundary conditions.

$$\text{at } x=o, \qquad j_n = j, \tag{2.27}$$

$$\text{at } x=L, \qquad j_n = A_{FN}F^2 \exp(-B_{FN}/F), \tag{2.28}$$

which is the Fowler-Nordheim tunnelling emission current density. Further, taking the interelectrode potential to be

$$V = \int_0^L F \, dx, \tag{2.29}$$

the current density for a given voltage can be determined.

Klein presented succession of avalanche model[32] by taking into account the effect of fluctuations. In this model, most of the avalanches produced by electrons injected into the insulator are not effective in causing breakdown. Breakdown can arise only in the stochastic event when a sufficiently rapid succession of avalanches occurs at one place in the insulator.

Forlani and Minnaja[33] assumed avalanche of electrons as the cause of breakdown, but considered also the electrons to initiate the process. They considered the tunnelling injection of electrons from the cathode and the electron-accoustic phonon scattering process in the bulk. The breakdown field could be determined by calculating Joule's heat which causes irreversible changes in the dielectric. They derived the theoretical thickness dependence of electric strength F_B; $F_B \propto d^{-1/2}$ for thick sample, and $F_B \propto d^{-1/4}$ for thin sample.

[B] Ion-induced Breakdown Process

Redley[34] presented the model of breakdown mechanism for SiO_2 films. Electrons injected from a cathodic protuberance 10 to 100 Å in diameter by Fowler-Nordheim tunnelling emission cause filamentary Joule's heating path due to current densities of the order of 10^5 to 10^8 A/cm^2. It follows that the temperature is raised locally by hundreds of degrees Celsius. The positive ions produced move towards the protrusion and enhance the field and the current injection; this positive feedback effect causes current runaway above a critical field. Although no explicit relations were derived for the critical

field, it seems that in this model electric strength decreases with increasing ambient temperature and depends strongly on the electrode metal.

Another purely ion-induced mechanism was proposed by Gundlach and Schnupp[35] to explain the breakdown in aluminum oxide films less than 100 Å thick. In this model, ionic transport of the anode metal to the cathode and formation of metallic protrusions at the cathode are postulated. The increasing field enhancement at a protrusion accelerates its growth by cations, and positive feedback effect leads to runaway in the growth and to local breakdown.

[C] Electro-Chemical Breakdown Process

Budenstein[36] claimed that the dielectric breakdown in solids can not be explained by avalanche theories when the experimental results on light emission, damage morphology[37] and chemical effects, which were observed in a practical breakdown test, were taken into account. He presented a new breakdown model assuming that a complete breakdown occurs only when a gaseous channel extends through the dielectric from one electrode to the other. The whole breakdown sequences consist of the following five stages.

(1) Breakdown starts when critical charge density is reached. This is a basic assumption in this model. The source of the excess charge may be field emission, collision ionization, injection electrons from an external accelerator or electrons by ionization process by laser light.

(2) Bond disruption takes place, and the products include exited atoms and ions of several eV, and free electrons.

(3) The next step is chain reaction. Free electrons produced break other bonds, and release atoms, ions and additional electrons. A gaseous plasma is formed, and electrons striking the wall cause

further dissociation, and produce an additional electron.

(4) Establishment of a gaseous channel is the forth step. A gaseous cavity is formed after the chain reaction. High pressure inside gas cavity leads to cracks formation.

(5) The final stage of the model is completion of the channel. Gaseous channels produced in the previous steps bridge the electrodes, and then breakdown channel is produced. Joule's heat generated enlarges the conducting channel, resulting in a completion of breakdown.

The main results expected from this model are as follows:

i) Lower limit for the time to breakdown is 10^{-11} sec from Uncertainty Principle. Upper limit is of the order of 10^{-9}sec, taking into accout heat conduction at the walls of the cavity.

ii) Electric strength in a brittle medium is lower because of easier crack propagation.

iii) The material with a high dielectric permittivity has a lower electric strength because of larger local charge densities.

References

[1] A.von Hippel: Ergb. Exak. Naturw. 14 79 (1935).

[2] H. Fröhlich: Proc. Roy. Soc. (London) A160 230 (1937).

[3] H. Fröhlich and B.V.Paranjape: Proc. Phys. Soc. (London) B69 866 (1956).

[4] H.Fröhlich: Proc. Roy. Soc. (London) A172 94 (1939).

[5] H.Fröhlich: Proc. Roy. Soc. (London) A188 532 (1947).

[6] Buhel and A.von Hippel: Phys. Rev. 56 941 (1939).

[7] F.Seitz: Phys. Rev. 76 1376 (1949).

[8] K.W.Wagner: Trans. AIEE 41 288 (1922).

[9] K.H.Stark and C.G.Garton: Nature 176 1225 (1955).

[10] J.Artbauer: Kolloid Z. und Z. Polymere 202 15 (1965).

[11] N.Klein: Adv. in Electronics & Electron Physics, 26 309 (1969).

[12] M.Ieda: IEEE Trans. on Elect. Insulation EI-15 206 (1980).

[13] M.Ieda and G.Sawa: OYOBUTSURI 48 1177 (1979) in Japanese.

[14] J.J.O'Dwyer:"The Theory of Dielectric Breakdown of Solids" Oxford Clarenden Press (1964).

[15] Y.Inuishi: Ph.D thesis, Osaka University (195) in Japanese.

[16] Y.Inuishi: J.I.E.E. Japan 95 357 (1975) in Japanese.

[17] G.Sawa: Proceeding on Young's Seminar on Electrical Insulating Materials pp:1-10 (1980). in Japanese.

[18] Stratton:"Progress in Dielectrics"

[19] F.Forlani and N.Minnaja: J. Vac. Sci. Technol. 6 518 (1969).

[20] J.H.Simpson: E.R.A. Report L/T 178 (1947).

[21] Y.Inuishi: J.I.E.E.Japan 94 779 (1974). in Japanese.

[22] W.Franz: Z. Phys. 113 607 (1939).

[23] C.Zener: Proc. Roy. Soc. A145 523 (1934)

[24] N.Klein: Thin Solid Films 50 223 (1978).

[25] J.J.O'Dwyer: J. Appl. Phys. 40 3887 (1969).

[26] J.J.O'Dwyer : IEEE Trans. on Elect. Insulation EI-15 264 (1980).

[27] I.Kashat and N.Klein: J. Appl. Phys. 48 5217 (1978).

[28] T.M.DiStefano and M.Shatzkes: Appl. Phys. Lett. 25 685 (1974).

[29] T.M.DiStefano: J. Vac. Sci. Technol. 12 37 (1975).

[30] T.M.DiStefano: J. Vac. Sci. Technol. 13 50 (1976).

[31] N.Klein and P.Solomon: J. Appl. Phys. 47 4364 (1976).

[32] N.Klein: Adv. Phys. 21 605 (1972).

[33] F.Forlani and N.Minnaja: Phys. Status Solidi 4 311 (1964).

[34] B.K.Ridley: J. Appl. Phys. 46 998 (1975).

[35] K.H.Gundlach and P.Schunupp: Z. Ang. Phys. 21 468 (1966).

[36] P.P.Budenstein and J.M.Lloyd: CEIDP 303 (1975).

[37] R.Cooper and C.T.Elliott: J.Phys. D 1 121 (1968).

Chapter III Electrical Breakdown of Polyimide

3-1 Introduction

In general, high temperature polymers possess not only excellent electrical properties —— high resistivity, high dielectric strength and low loss, but also outstanding mechanical properties —— high tensile strength and an ease of manufacturing. Among them, polyimide has been accepted as superior electrical insulating materials to be applied at very high temperatures because of its excellent thermal properties[1,2]. The mechanical and chemical properties of polyimide (PI) have been investigated by many authors[3-7]. Electrical insulating materials are used generally in two ways: as insulation and capacitor dielectric. The dielectric properties, important in the latter category, i.e. the dielectric constant and the dissipation factor, have been extensively studied by many authors[8,9]. On the other hand, many parts about the electrical insulaing properties remain unknown, which are important in the former category[8,10,11,12]. Especially, there are a few reports concerning the dielectric breakdown of PI[10,11,12].

Nagao[12] reported that the electric strength of PI above room temperature decreased with rising temperature, and that the dielectric breakdown mechanism of PI in high temperature region was considered to be thermal breakdown due to ionic conduction. This result implies that if ionic conductivity is decreased, the breakdown characteristics at high temperatures are possibly improved.

It was suggested that during the course of manufacturing of PI film, imidization does not proceed to completion, and polyamic acid is left as a result[13,14]. It was also suggested that there is a possibility of further imidization with heating[14]. Sacher[15] suggested that the charge carrier is protonic and supplied from residual

non-reacted polamic acid. These results indicate that the electric strength of PI at high temperatures is improved by heat treatment.

On the basis of the results on the breakdown mechanism and of the above suggestions, Nagao[12] investigated heat treatment effect on the electric strength, and concluded that the heat treatment of PI results in a decrease in electrical conductivity and an increase in electric strength at high temperatures.

In this chapter, the dielectric breakdown of PI and the effect of heating on the electric strength of PI is summarized firstly. In order to elucidate further the relation between polyamic acid in PI and the dielectric breakdown, the effects of hydrolysis, which increases the concentration of polyamic acid with a process opposite to the imidization, and water absorption on the breakdown characteristics are studied.

3-2 Polyimide Polymer

Polyimide film (KAPTON-H Du pont) resulting from the condensation reaction between pyromellitic dianhydride and an aromatic diamine has the most excellent thermal endurance among existing commercial polymers[16,17,18]. The condensation reaction of PI is shown in Fig.3.1 [3]. It has outstanding mechanical properties and excellent electrical properties over the temperatue range from liquid helium temperature to 500°C, usable in class H (180°C) conditions. It does not undergo glass transition up to 500°C and does not char up to 800°C. This polymer has no known solvent and is also infusible. It has also a high degree of radiation resistance (no changes after 10^9 r. dosage of gamma rays[8]). The unique stability of this organic polymer is attributed to its cyclic structure, possessing both aromatic and heterocyclic rings[2].

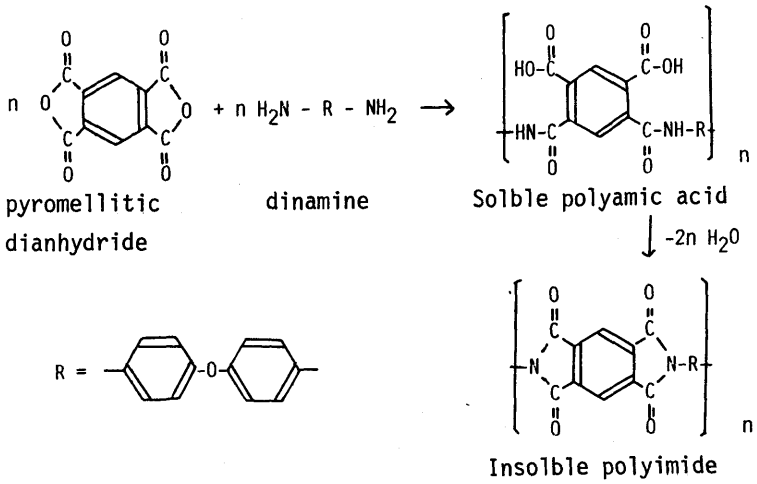

Fig.3.1. Condensation reaction of pyromellitic dianhydride and an aromatic diamine.

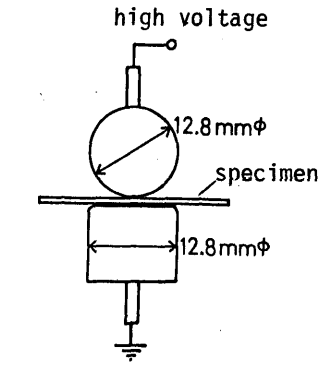

Fig.3.2. Electrode system.

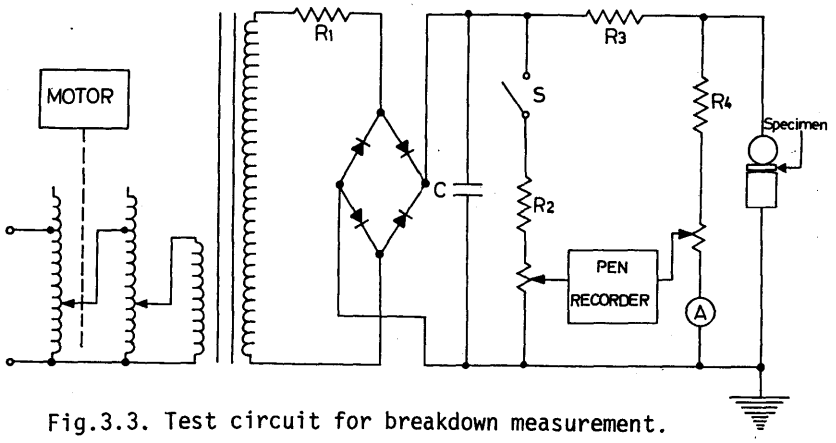

Fig.3.3. Test circuit for breakdown measurement.

3-3 Experimental Procedure

Measurements were made on polyimide films of thickness about 26 μm. Sample were sandwiched with the sphere-plane electrodes, as shown in Fig.3.2., and immersed in silicone oil (KF-965, 100cs, Shin-etsu Chemical Industry Co. Ltd.) which was kept at a given temperature or in liq.N_2. The test circuit for the breakdown measurement is illustrated in Fig.3.3. After the sample was immersed for about 5 min., a linearly rising voltage was applied to the sample until a breakdown occurred.

3-4 Summary of Breakdown Characteristics of as-received Polyimide Film[12]

The temperature dependence of electric strength F_B of as-received 26μm-thick PI film at a rising rate of electric field of about 0.2 MV/cm·sec was measured. In low temperature region from -196°C to room temperature (Region I), F_B scarcely varied with temperature. On the contrary, F_B decreased with temperature from room temperature to 200°C (Region II), more sharply especially above about 200°C (Region III). The breakdown characteristics obtained are given again in Table 3.1. After discussing the breakdown mechanism on the basis of the results, it was concluded as follows[12]: In Region I, the electronic breakdown process is dominant because of the small variation of F_B with temperature; and in the Regions II and III, the thermal breakdown process is considered as a possible mechanism. Especially it was shown that the impulse thermal breakdown is dominant in Region III.

3-5 Summary of Effect of Heat Treatment on Breakdown Characteristics

The effects of heat treatment on variation of F_B with temperature, field rising rate and thickness were examined. Below 200°C, the

Table 3.1. Feature of breakdown characteristics of as-received polyimide.

Room Temp.		200°C
$\partial F_B/\partial T_0 \simeq 0$	$\partial F_B/\partial T_0 < 0$	$\partial F_B/\partial T_0 < 0$
	$\partial F_B/\partial d < 0$	$\partial F_B/\partial d \simeq 0$
$\partial F_B/\partial \alpha \simeq 0$	$\partial F_B/\partial \alpha > 0$	$\partial F_B/\partial \alpha > 0$

F_B: electric strength, T_0: temperature,
α : field rising rate, and d : thickness.

breakdown strength of PI scarcely varied with the heat treatment, while above 200°C it was raised with the heat treatment. The temperature range above room temperature corresponds to Regions II and III in which the thermal breakdown is dominant. The increase of F_B above 200°C, therefore, could be consistent with an expected lowering of electrical conductivity due to the heat treatment.

The variation of F_B with time of the heat treatment at 300°C was measured. At the measuring temperature of 150°C, F_B was almost independent of the time of heat treatment. At 200 and 300°C, F_B increased with increasing time of the heat treatment. Especially at 300°C, F_B increased sharply with time of heat treatment up to one day.

The electrical conductivity σ of PI as a function of time obtained by applying a step voltage of 1200V to a 26 μm thick sample was also observed. The electrical conductivity σ at measuring temperature of 150°C changed only slightly with the heat treatment in air at 300°C for 7 days, but was appreciably reduced at measuring temperature of 200°C with the heat treatment. From these results, Nagao concluded that the elevation of F_B with the heat treatment can be qualitatively understood by the lowering of σ , being consistent with the thermal breakdown.

3-6 Effect of Hydrolytic Treatment on Breakdown Characteristics

The electrical conduction of PI at high temperatures is considered to be ionic[19,20,21]. It is also suggested that mobile ions are likely supplied from residual polyamic acid[19]. Further, it is indicated that the residual polyamic acid can be reduced with heating through imidization process[14]. With respect to this suggestion, infra-red spectrum of PI film was measured in order to elucidate conversion of polyamic acid with the heat treatment. No direct evidence for further imidization, however, could be obtained with infra-red

spectroscopy, as the concentration of polyamic acid might be very small. Therefore, the effect of hydrolysis, which increases the concentration of polyamic acid through a reverse process against imidization, was studied.

Hydrolytic reaction of PI is shown in Fig.3.4[22]. The hydrolytic treatment was done at room temperature by the following process: as-received PI film was immersed in about 2N KOH solution for 12 or 18 hr., resulting in ring-opening of imide bond with consequent generation of potassium salt of polyamic acid. After drying in vacuum for a given period, the sample was immersed in about 1N HCl solution for 6 hr., which resulted in replacement of K by H, and washed by water to remove the adhering HCl, and followed by drying in vacuum for 2 weeks.

Breakdown measurements on hydrolyzed samples were made. The variation of F_B of 18 hr. hydrolyzed PI followed by drying in vacuum for about 2 weeks with time of the heat treatment in silicone oil kept at 200°C is shown in Fig.3.5. It can be seen that F_B decreases with hydrolytic treatment, leading to a lower value than that of an as--received sample. However, it increases with increasing immersion time in silicone oil, which corresponds to heat treatment time at 200 °C, and approaches gradually the value for as-received one.

Figure 3.6 shows infra-red spectrum of as-received (a), 18 hr. hydrolyzed sample followed by heat treatment in silicone oil at 200°C for 5 min. (c) and 30 min. (d), respectively. Base line of each infra-red spectrum is shifted for convenience of comparison. Here, an attention is focussed on imide bands at 1780, 1360, and 720 cm^{-1}, especially the one at 720 cm^{-1} which is not disturbed by other absorption bands and is the clearest. It can be considered that imide bonds in polyimide undergo hydrolytic scission, resulting in production of polyamic acid. Then, it turns to the original polyimide through

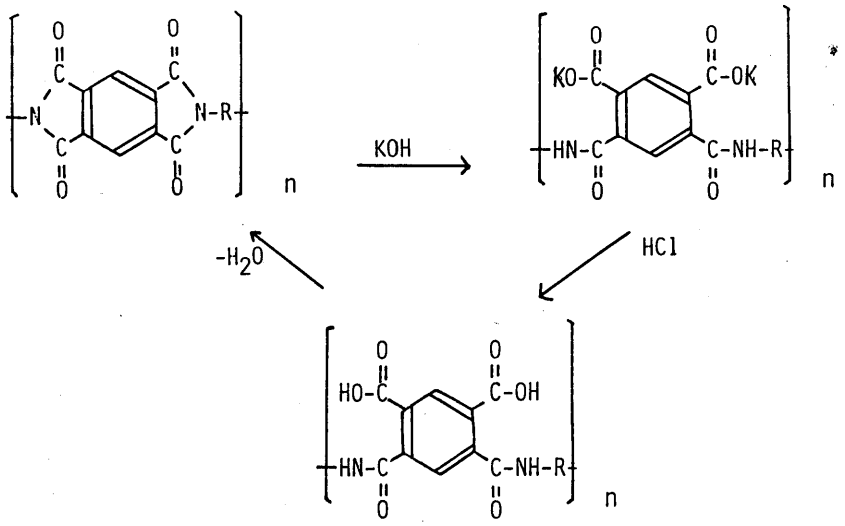

Fig.3.4. Hydrolytic reaction of polyimide.

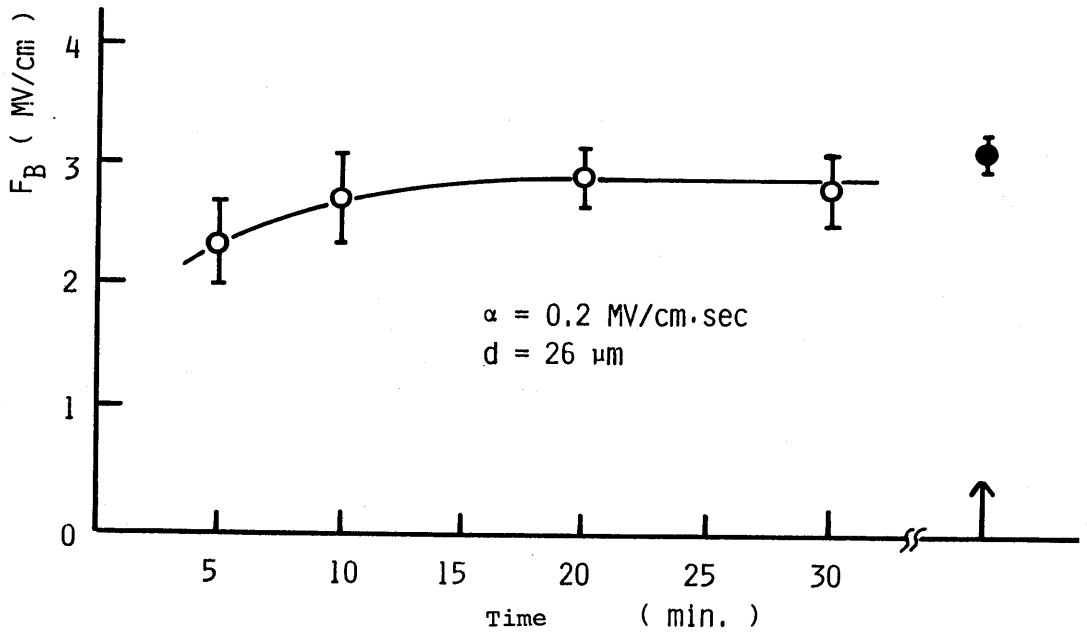

Fig.3.5. Variation of F_B of 18 hr hydrolyzed PI with heat treatment period. The heat treatment was made at 200°C in silicone oil and the breakdown measurement is at 200°C.

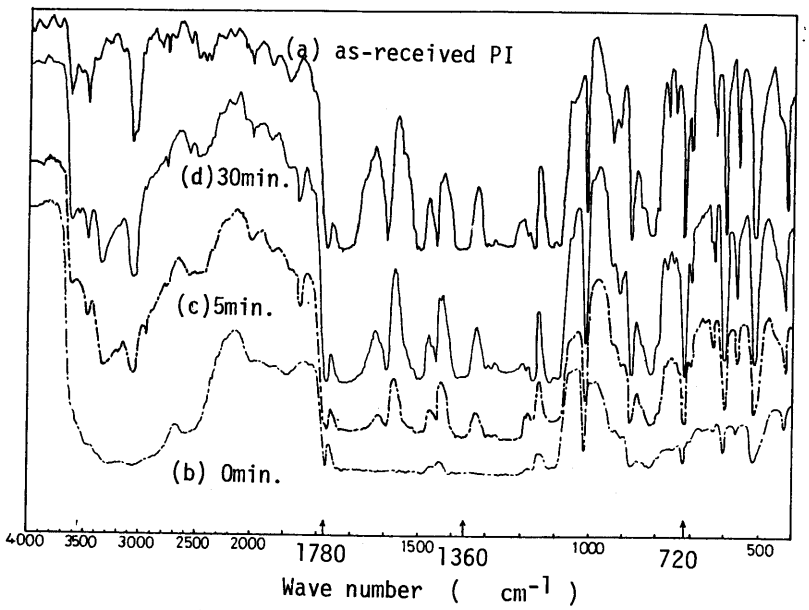

Fig.3.6. Effect of heat treatment in silicone oil (200°C) on IR spectrum of 18 hr hydrolyzed PI.

re-imidization process with heat treatment in silicone oil kept at 200°C.

Next, the temperature dependence of F_B for PI samples hydrolyzed for 12 hr. with KOH is shown in Fig.3.7. Immersion time in silicone oil at each temperature was 5 min.. In this figure unfilled and filled triangles represent electric strength for the sample dried in vacuum for 24 and 48 hr., respectively, after the hydrolytic treatment. The electric strength F_B for as-received film (unfilled circle) is also shown to make a direct comparison. It is seen that F_B for the sample followed by 24 hr. drying in vacuum is lower than that for as-received one below 200°C. But above 200°C, it closely agrees with that for the as-received one and decreases with increasing temperature. Seeing carefully below 200°C, F_B for the hydrolyzed sample decreases with increasing temperature between room temperature and 100°C, but it increases with temperature between 100 and 200°C.

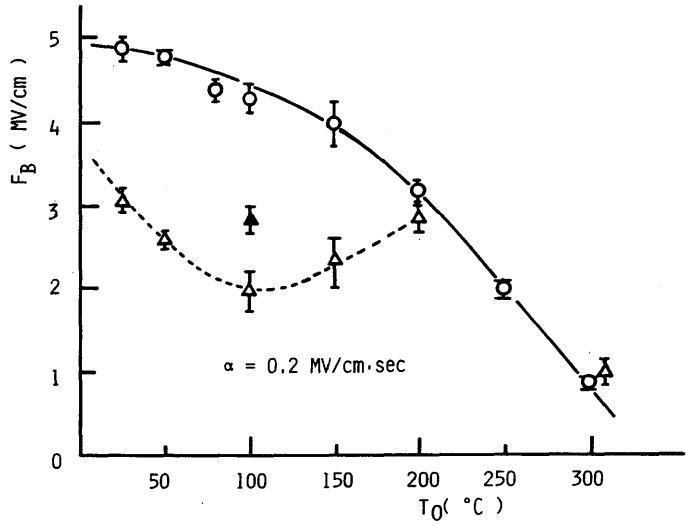

Fig.3.7. Temperature dependence of electric strength of hydrolyzed PI. Unfilled circle represents F_B of as-received film, and unfilled and filled triangle represent F_B of 12 hr hydrolyzed film followed by drying in vacuum for 24 hr and 48 hr, respectively.

The variation of infra-red spectrum intensity of imide bonds, with hydrolyric treatment and succeeding heat treatment at various temperatures before breakdown test, was investigated. Firstly, as an internal standard, the absorption at 1600 cm^{-1} of C=C bond in benzene ring was taken, which is considered to scarcely change with the hydrolitic treatment. Secondly, the relative value of the absorption intensity of each imide bond was calculated by the base line method. Non-breakdown part in the sample after the breakdown test was used for the measurement of infra-red (IR) spectrum. It was difficult, as can be seen from the shape of IR spectrum in Fig.3.6, to obtain the absorption intensity at 1780 cm^{-1} because of the sample thickness. Therefore, the results for the absorption band at 1360 and 720 cm^{-1} only are given in Table 3.2. The figures in the table show the relative values with absorption intensity of imide bonds for as-received sample taken as 100%, with compensation by the absorption at 1600 cm^{-1}.

Table 3.2. IR spectrum intensity (%) of imide bands of hydrolyzed PI after heat treatment in silicone oil for about 5 min..

wave number (cm^{-1})	1360	720
as-received	100 (%)	100 (%)
hydrolyzed		
heat treatment temperature		
T_0 = 25°C	89	74
50	89	63
100	89	74
150	92	81
200	96	77
300	103	103

The data in the table suggest that imide bonds in PI film reduce firstly with the hydrolytic treatment, and the degree of re-imidization is nearly constant with temperature below 100°C. Re-imidization process starts above 100°C, but is not complete during 5 min. of heat treatment. Further heat treatment at 300°C would cause complete imidization, leading to a conversion of the hydrolyzed PI film to the as-received one. An increase in imide bonds is considered to be inversely related to an increase in polyamic acid and vice versa. By comparing the above result with that in Fig.3.7, it is implied, therefore, that an increase in polyamic acid contributes to the lowering of F_B.

It was observed that absorbed water also results in lowering of F_B. This can be seen from results in Fig.3.7 where filled triangle represents F_B for the sample dried in vacuum for 48 hr. after the hydrolytic treatment for 12 hr.. This value is higher than that for the sample dried in vacuum for 24 hr. after the hydrolytic treatment, which is represented by unfilled triangle. This indicates that the treatment for the hydrolysis includes the water absorption process.

Therefore, the influence of water absorption on F_B for PI film was examined in order to seperate the contribution of the generation of polyamic acids and the contribution of water absorption to the lowering of F_B. This result is given in the next section.

3-7 Effect of Water Absorption on Breakdown Characteristics

Breakdown measurements were made with the samples immersed in distilled boling water at 100°C for 5 days followed by drying in air for a day or in vacuum for 14 days. F_B measured at 100°C for the sample obtained after the above procedure is shown in Fig.3.8. This figure also shows the result with the hydrolytic treatment which will be described later and the result of the as-received sample dried in vacuum for 4 days. The reason why the measuring temperature for breakdown test was selected to be 100°C is to overcome re-imidization before voltage application as far as possible. It can be seen that

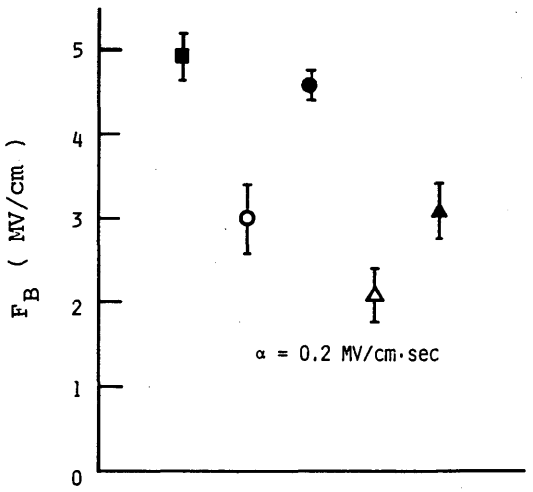

Fig.3.8. Effects of absorbed water on F_B of PI. Filled square represents F_B of non-treatment sample with drying in vacuum for 96 hr, unfilled and filled circle : aquous treatment in boiling water for 5 days followed by drying in air (24 hr) and in vacuum (14 days), respectively. Unfilled and filled triangle represent F_B of 12 hr hydrolyzed sample followed by drying in vacuum for 24 hr and about 3 weeks, respectively.

the electric strength F_B is lowered with the aqueous treatment at 100 °C, as indicated by unfilled circle. But it is also almost recovered to the value for the as-received sample provided the water content is fully removed from the sample by drying it in vacuum. The lowering of F_B is considered to be caused by a decrease in dissociation energy of ion due to water absorption, leading to an increase in mobile ions. However, further investigations are necessary to verify this consideration.

Next, the influence of water absorption during hydrolytic treatment on the electric strength for the hydrolyzed film is described. Unfilled and filled triangles in Fig.3.8 represent F_B for the samples dried in vacuum for 1 day and 3 weeks, respectively, after the hydrolytic treatment for 12 hr.. The period of vacuum drying for the latter was made longer by a week than that for the case of filled circle. The electric strength F_B for the hydrolyzed sample followed by sufficient vacuum drying is still considerably lower than that for the as-received one. This difference may be concerned with the contribution of the hydrolysis of polyimide to the lowering of F_B. Thus, it is confirmed that the presence of polyamic acid which is the residual non-reacted material affects the breakdown characteristics of PI film.

3-8 Conclusion

It was reported that the dielectric breakdown mechanism of polyimide in high temperature region was considered to be thermal breakdown, and an increase in the electric strength was attained with heat treatment. No direct evidence for further imidization, however, could be obtained with infra-red spectroscopy.

In this chapter, therefore, the effect of hydrolysis, which increases the concentration of polyamic acid with a process opposite to

the imidization, was studied. The treatment for the hydrolysis includes the water absorption process. In addition, a re-imidization process starts above 100°C. Therefore, it may be included in the breakdown measurement procedure for high temperatrues. After the influence of these processes was examined, it was indicated that a presence of polyamic acid affects the breakdown characteristics. Thus, the further imidization is possibly one of the factors which contribute to the improvement of the high temperature electric strength with the heat treatment. However, it is required in a practical application to examine a variation of chemical and mechanical properties with the heat treatment and to establish the best condition of the treatment.

References

[1] N.W.Todd: Engineering 1026 (1964).

[2] H.Yoshioka: J. Inst. Elect. Engrs. Japan 87 829 (1967) in Japanese.

[3] C.E.Sroog, A.L.Engrey, S.V.Abramo, C.E.Berr, W.M.Edwards, and K.L.Olivier: Journal of Polymer Science Part A 3 1373 (1965).

[4] Y.Imai, K.Uno, and Y.Iwakura: Die Makromolekulare Chemie 94 114 (1966).

[5] S.L.Cooper, A.D.Mair, and A.V.Tobolsky: Textile Research Journal 1110 (1965).

[6] G.A.Bernier and D.E.Klein: Journal of Appl. Poly. Scie. 12 593 (1968).

[7] E.Butta, S.D.Petris and M.Pasquini: J. Appl. Poly. Scie. 13 1073 (1969).

[8] L.E.Amborski: Ind. Eng. Chem. 2 189 (1963).

[9] E.Sacher: IEEE Trans. Elect. Insulation EI-13 94 (1978).

[10] M.Nagao, G.Sawa and M.Ieda: Trans. Inst. Elect. Engrs. Japan 97-A 279 (1977).

[11] M.Nagao, G.Sawa, M.Fukui and M.Ieda: Japan. J. Appl. Phys. 15 1813 (1976).

[12] M.Nagao: Ph.D thesis, Nagoya University (1978) in Japanese.

[13] S.D.Bruck: Polymer 6 49 (1965).

[14] E.Sacher and D.G.Sedor: Journal of Poly. Scie. : Poly. Phys. Edit. 12 629 (1974).

[15] E.Sacher: 1976 Annual Rept. Conf. on Elect. Ins. and Dielect. Pheno., NAS, 33 (1976).

[16] S.Isobe: OHM 60 53 (1973). in Japanese.

[17] Kanesashi: OHM 60 58 (1973). in Japanese.

[18] Murakami: Industrial Material 21 (1963). in Japanese.

[19] E.Sacher: IEEE Trans. Electr. Insulation EI-14 85 (1979).

[20] J.P.Crine, D.L.Riron and A.Yelon: Conf. on Electrical Insulation and Dielectric Phenomena, NSA-NRC 226 (1977).

[21] G.Sawa, S.Nakamura, K.Iida and M.Ieda: Japan. J. Appl. Phys. 19 453 (1980).

[22] J.Nishizaki: J. Chem. Soc. Japan, Ind. Chem. Sec. 69 1393 (1966) in Japanese.

Chapter IV Electrical Breakdown of Poly(vinylidene-fluoride)

4-1 Introduction

Poly(vinylidene-fluoride) (PVDF) is expected to have many interesting practical applications, owing to its piezoelectric[1,2] and pyroelectric[3,4,5] properties. Recently, PVDF was also proposed as a dielectric material for high energy density capacitors[6] because of its high dielectric constant as compared with the other polymeric materials.

The dielectric properties[7], piezoelectricity[1,2], and pyroelectricity[3,4,5] have been extensively studied by many authors. However, much remains unknown about the electrical insulating properties which are necessary for its application as an insulator. Especially, the dielectric breakdown of PVDF has not been understood sufficiently.

In this chapter, the dielectric breakdown of PVDF is studied over the temperature range from room temperature to 150°C. The breakdown mechanism is discussed in detail in the high temperature region above 50°C. In addition, the theoretical impulse thermal breakdown strength is calculated, assuming ionic conduction. An estimation of the conduction parameters is made by fitting the calculated theoretical values of breakdown strength to the experimental characteristics.

Next, the influence of ionic conduction parameters on the electric strength of PVDF at high temperatrues is investigated including Poole-Frenkel effect in dissociation process of ionic charge. Lastly, the relation between its crystalline phase and the breakdown characteristics is discussed.

4-2 Experimental Details

PVDF is a polar and highly crystallized polymer, with chemical

structure of $(-CH_2-CF_2-)_n$. It has two representative stable crystalline phases; α-phase and β-phase[8]. The β-phase is mainly obtained by uniaxial stretching, and electrets manufactured from the film involving β-phase show strong piezoelectricity[9]. The β-phase has a planer zigzag type conformation with large dipole moment of CF perpendicular to the main chain. Its lattice constants are reported to be as follows: a=8.58 Å, b=4.91 Å, and c=2.56 Å. On the other hand, the α-phase with helical conformation is non-polar, since dipoles are cancelled out in a unit cell, and its lattice constants are such that a=4.96 Å, b=9.64 Å, and c=4.62 Å.

Specimen for breakdown measurements is a biaxially stretched PVDF film (KF polymer, Kureha Chemical Industry Co. Ltd.) of 12 to 25 μm in thickness, whose crystallinity is about 50%. Samples sandwiched with sphere-plain electrodes were immersed in silicone oil (KF-965, 100 cs, Shin-etsu Chemical Industry Co. Ltd.) which is kept at a given temperature T_0 between room temperatrue and 150°C. After the sample was immersed for about 5 min., a linearly rising voltage was applied to the sample at various rates from 100 V/sec to 1 kV/sec until a breakdown occurred.

4-3 Fundamental Breakdown Characteristics

The temperatrue dependence of the electric strength F_B of 12 μm thick PVDF film at field rising rate of about 0.2 MV/cm·sec is shown in Fig.4.1. Each point an corresponding bars represent an average of about 14 tests and standard deviation, respectively. As can be seen in Fig.4.1, F_B at room temperature is more than 8 MV/cm, but falls rapidly with increasing temperature T_0 above 50°C.

Figure 4.2 shows relation between the electric strength and the rate of rise of the applied electric field in a 12 μm thick film at various temperatures. At room temperature, F_B is almost independent

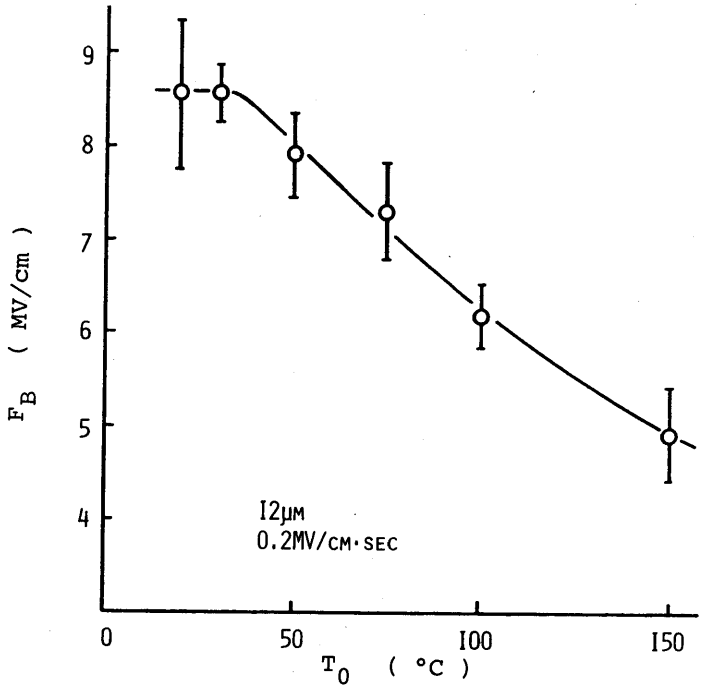

Fig.4.1. Temperature dependence of electric strength.

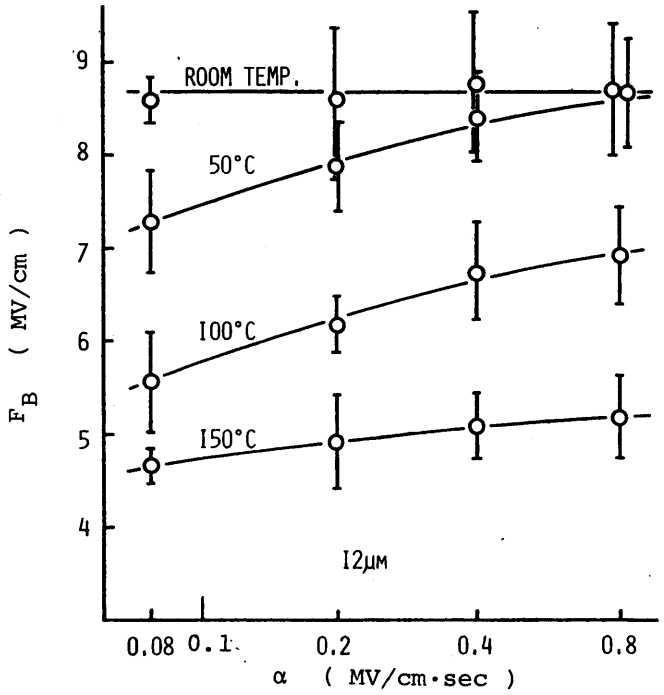

Fig.4.2. Relation between electric strength and rising rate of applied electric field.

of the field rising rate within the experimental limit, but increases with the field rising rate above 50°C.

The thickness dependence of F_B at field rising rate of about 0.2 MV/cm·sec at various temperatures was measured using 12 and 25 μm thick films. The results are shown in Fig.4.3. At room temperature, F_B decreases with increasing sample thickness. In contrast, above 50°C, F_B is almost independent of the thickness.

4-4 Discussion

4-4-1 Breakdown mechanism

The breakdown characteristics obtained above are summarized in Table 4.1. According to the temperature dependence of F_B, the temperature range can be divided into two regions, I (room temperature to 50°C) and II (50 to 150°C). Little variation of F_B with temperature in Region I ($\partial F_B/\partial T_0 \simeq 0$) indicates that the breakdown is

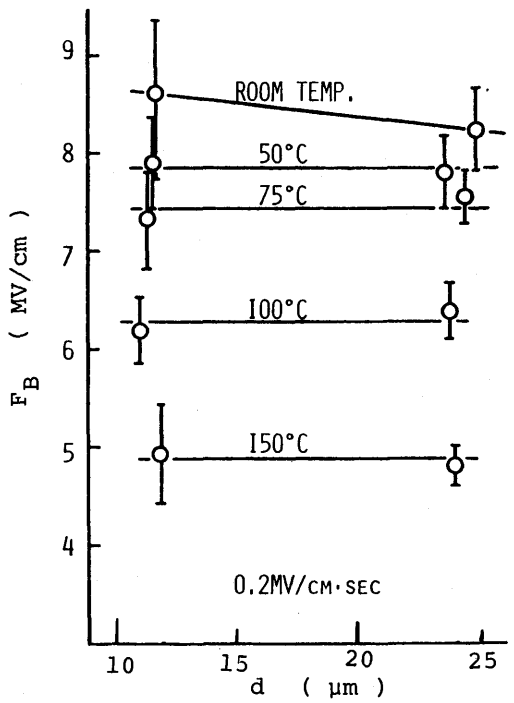

Fig.4.3. Thickness dependence of electric strength.

Table 4.1. Breakdown characteristics of PVDF.

Region I		Region II	
25°C	------- 50°C	---------	150°C
$\partial F_B/\partial T_0 \simeq 0$		$\partial F_B/\partial T_0 < 0$	
$\partial F_B/\partial \alpha \simeq 0$		$\partial F_B/\partial \alpha > 0$	
$\partial F_B/\partial d < 0$		$\partial F_B/\partial d \simeq 0$	

possibly due to an electronic process[10], but further details will not be discussed here, as attention is focussed on high temperature region. There are three possible mechanisms to explain the decrease in F_B with increasing temperature in Region II; the thermal breakdown, the electromechanical breakdown, and the electronic breakdown in amorphous materials presented by Fröhlich[10]. Thermal breakdown can be considered as a probable mechanism in Region II from the following considerations. From the electromechanical deformation model[11], the theoretical value of electric strength is estimated as 15 to 30 MV/cm for the mechanical instability taking Young's modulus to be 0.8 to 1.9 x 10^{-9} N/m^2 and the dielectric constant as 9.4 to 13.8 in the temperature range from 20 to 100°C (H.Kakutani, private communication). These estimated values are about three times as large as the experimental values of 8.6 to 6.2 MV/cm. Fröhlich's amorphous theory also cannot explain the observed dependence of F_B on the rising rate of applied electric field in Region II, as shown in Fig.4.2, because each stress duration is much longer than 10^{-7} - 10^{-8} sec which is accepted as the upper limit of the time lag to breakdown in Fröhlich's theory[12].

The thermal breakdown is treated according to the equation

$$C_v \left(\partial T/\partial t \right) - \mathrm{div} \left(\kappa \, \mathrm{grad} \, T \right) = j F, \qquad (4.1)$$

where C_v is the specific heat at constant volume, t the time, κ the thermal conductivity, j the conduction current density and T the temperature during the breakdown process. The initial or ambient temperature is disignated T_0 to avoid confusion. Since the heat conduction term can be neglected, eq.(4.1) becomes

$$C_v \left(dT/dt \right) = j F, \tag{4.2}$$

for the impulse thermal breakdown. Therefore, the impulse thermal critical field strength is obviously independent of the sample thickness. The present experimental results in Region II are consistent with this expectation[13].

4-4-2 Estimation of Ionic Conduction Parameters from Breakdown Characteristics

i) Case I: Neglecting Poole-Frenkel Effect

The electrical conduction is assumed to be ionic in nature because of the high temperature. The ionic current density j can be expressed as

$$j = 2 q n_i \nu_0 (2\lambda_i) \exp(-U/kT) \sinh(q\lambda_i F/kT), \tag{4.3}$$

where q is the ionic charge, n_i the density of ions, $2\lambda_i$ the ionic jump distance, k the Boltzmann constant, ν_0 the vibration frequency of ions, and U the potential barrier.

Neglecting the influence of the electric field, the density of ions is given by

$$n_i = A_i N_i^{1/2} \exp \left(-W/2kT \right), \tag{4.4}$$

where A_i is a constant, N_i is the density of source of thermally dissociated ions and W is the dissociation energy. Equation (4.3)

therefore becomes as follows:

$$j = j_0 \exp (-\phi/kT) \sinh (q\lambda_i F/kT), \qquad (4.5)$$

where $j_0 = 2\, q\, A_i\, N_i^{1/2}\, \nu_0\, (2\lambda_i)$ and $\phi = U + W/2$. When the electric field rises linearly with time, i.e. $F = \alpha t$, where α is the rising rate of the applied electric field, eq.(4.2) can be transformed to

$$dT/dF = j\, F/C_v \alpha. \qquad (4.6)$$

For PVDF, C_v is 2.43×10^6 J/K·m^3[14]. Equation (4.6) can be solved for constant α numerically by using eq.(4.5), if the ionic conduction parameters j_0, ϕ and $2\lambda_i$ are given. The temperature and current density of the specimen as a function of the electic field were computed by the Runge-Kutta-Gill method[15].

A typical example of numerically calculated values of T and j for different values of j_0 is shown in Fig.4.4 when ϕ =0.85 eV and $2\lambda_i$=9 Å. As can be seen from the figure, initially the temperature of the specimen rises slowly with the electric field, and then very steeply. This sudden rise of specimen temperature strongly depends on ϕ. For a large value of ϕ, therefore, the electric strength can be well determined without defining exactly the critical temperature required for breakdown. In this numerical calculation, the critical temperature T_m required for breakdown was taken as 180°C, the melting point for PVDF, for convenience, and the electric field at which the specimen temperature reaches T_m was regarded as the theoretical electric strength.

The conduction parameters are evaluated by fitting the theoretical results to the experimental ones. The theoretical relation between F_B and α at 100°C was calculated for different values of $2\lambda_i$, keeping ϕ constant and varying j_0 so that F_B (α = 0.2 MV/cm·sec at

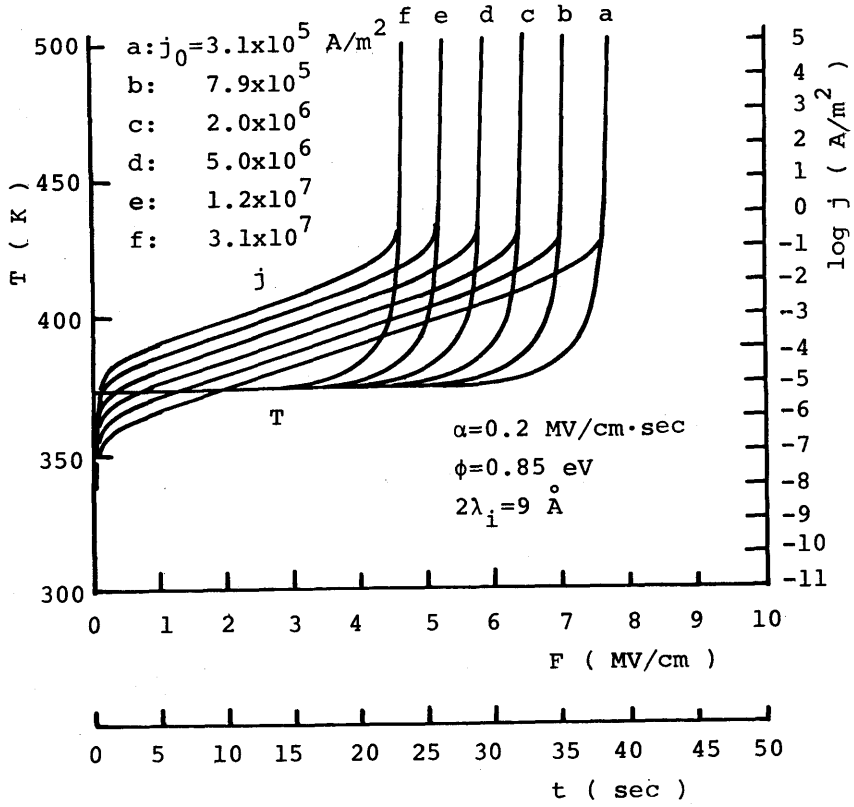

Fig.4.4. Examples of numerically calculated values of T and j for different values of j_0.

100°C) obtained by the calculation coincides with that obtained experimentally for each value of $2\lambda_i$. This calculation was carried out for some different values of ϕ. Figure 4.5 shows one typical example of the results for ϕ = 0.9 eV, which gives the best fit to the breakdown data. The experimental results are indicated by filled circles in Fig.4.5. The dependence of F_B on the initial temperature of the sample T_0 was calculated for different values of ϕ, keeping $2\lambda_i$ constant and varying j_0 as a parameter in the same way as mentioned above. Figure 4.6 shows the results when $2\lambda_i$ = 9 Å. It can be seen from Figs.4.5 and 4.6 that the best fit of the experimental plot to the theoretical curve is attained when $2\lambda_i$ = 9 Å, ϕ = 0.9 eV, and j_0 =

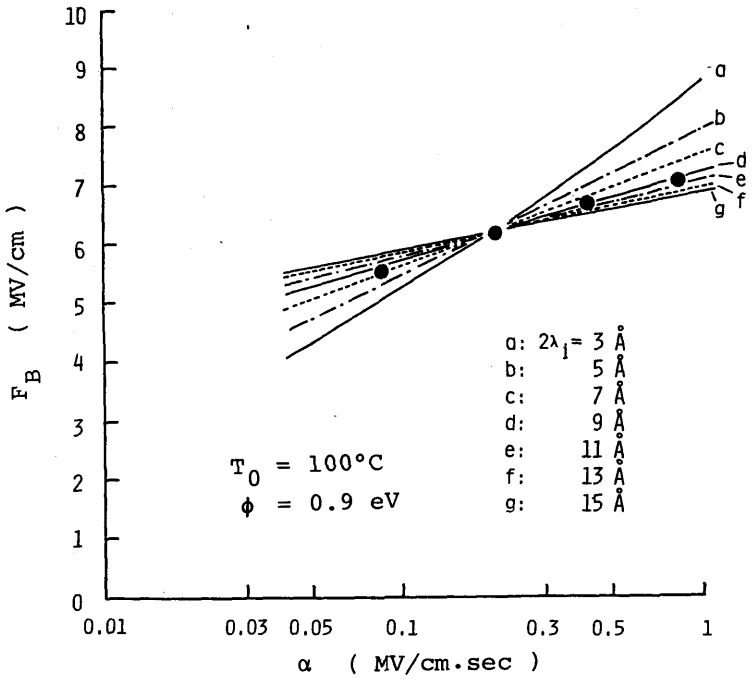

Fig.4.5. Examples of calculated values of F_B as a function of α with a parameter of $2\lambda_i$ without Poole-Frenkel effect.

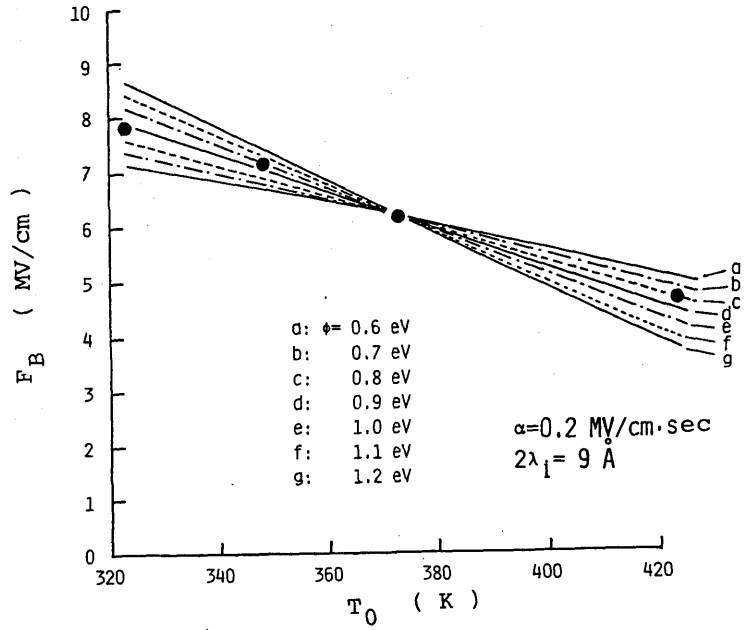

Fig.4.6. Examples of calculated values of F_B as a function of T_0 with a parameter of ϕ without Poole-Frenkel effect.

1.2×10^7 A/m^2.

The conduction current measurements were made by applying a step voltage. However, the current decayed over a long period and showed a considerable spread of results from sample to sample. Due to these uncertainties, the estimation of the parameters j_0, ϕ and $2\lambda_i$ from the conduction data on polymers usually presents various practical difficulties. Theoretically, $2\lambda_i$ can be obtained from the j-F curve by using eq.(4.5), and j_0 can be evaluated from an extrapolation of the ln j-1/T curve, knowing $2\lambda_i$. However, the calculated value of j_0 varies by many orders of magnitude with a small change in slope of the ln j-1/T curve, from which ϕ can be obtained. Therefore, the ionic conduction parameters estimated from the breakdown data will be compared with the experimental conduction data in the magnitude of the current density at a given temperature and electric field. The theoretical current density at 100°C and 1 MV/cm was calculated to be 1.7×10^{-5} A/m^2 from the values quoted above for $2\lambda_i$, ϕ, and j_0. On the other hand, the measured current density at 100°C and 1 MV/cm was about 2×10^{-4} A/m^2 10 min. after a step voltage was applied. This time of 10 min. exceeds any of the times to breakdown. Nevertheless, the calculated value is lower by an order of magnitude than the measured value. This is probably due to a residual absorption current which may mask the ionic conduction current at low fields. The field dependence of the former current component is smaller than that of the latter. Thus, ionic conduction current must predominate over such a weak field-dependent component in the breakdown field region.

ii) Case II: Including Poole-Frenkel Effect

In the previous treatment, the effect of the electric field upon the density of ions was not considered. Hereafter, the case of including Poole-Frenkel effect in a dissociation process of ionic

charges will be discussed. The density of the thermally dissociated ions at thermal equilibrium is given in place of eq.(4.4) by the following equation:

$$n = A_i N_i^{1/2} \exp\left(- \frac{W - \beta_{PF} F^{1/2}}{2kT} \right), \qquad (4.7)$$

where $\beta_{PF} = (q^3/\pi \varepsilon_0 \varepsilon_r)^{1/2}$, ε_0 is the permittivity of the free space, ε_r the relative permittivity of the material, and q is assumed to correspond to a monovalent ion. The current density then is written in the form

$$j = j_0 \exp\left[- \frac{\phi - (\beta_{PF}/2) F^{1/2}}{k T} \right] \sinh (qF\lambda_i/kT). \qquad (4.8)$$

Using eq.(4.8), eq.(4.6) is solved numerically in almost the same way as mentioned in the previous subsection.

In general, the high frequency limiting value of the relative permittivity is used for ε_r appearing in the expression for β_{PF}. However, if the dissociation is accompanied with hopping over a large number of potential barriers, the influence of orientation polarization of dipoles can not be ignored. Therefore, different values of ε_r which contain different type of dipole polarizations were considered for the calculation. At low temperature, ε_r of PVDF was about 3.0 at 1 kHz. Above -25°C, which is identified with the glass transition temperature, its value is about 10, since the contribution of the orientation polarization of dipoles in the amorphous region is added. Above 80°C, the contribution from the crystalline region is also included, leading to further increase of ε_r to about 14. Using the values of $\beta_{PF} = 2.03 \times 10^{-5}$, 2.40×10^{-5} and 4.38×10^{-5} eV $m^{1/2}/V^{1/2}$ which correspond to 14, 10, and 3 for ε_r, respectively, the numerical calculation was carried out.

Figures 4.7 and 4.8 show typical examples of the theoretical

relation between F_B and α, and the temperature dependence of F_B for $\varepsilon_r = 14$, respectively. By fitting the calculated values to the experimental ones indicated by filled circles, the parameters were estimated as follows: $2\lambda_i = 4$ Å, $\phi = 0.9$ eV, and $j_0 = 6.5 \times 10^5$ A/m^2. Almost the same values of the parameters $2\lambda_i$, ϕ, and j_0 were obtained for $\varepsilon_r = 14$ and 10. However, when $\varepsilon_r = 3$, the estimation led to the result that $2\lambda_i < 1$ Å, which would be unreasonable physically from a view of the solid structure. Therefore, it is not allowed to use the value of β_{PF} evaluated from $\varepsilon_r = 3$. It seems appropriate, therefore, that the value of ε_r involving the contribution of dipole polarization for the purpose of the evaluation of β_{PF} should be selected.

Then, whether relaxation of dipole orientation can occur within the time during which ions are dissociated or not were examined. When the Poole-Frenkel effect is considered, the distance from a neutral state of ion to a maximum potential barrier, r_{max}, is given by

$$r_{max} = [\, q/(\, 4\pi\, \varepsilon_0 \varepsilon_r\, F\,)\,]^{1/2}, \qquad (4.9)$$

which varies with the applied electric field[16]. For the case when $\varepsilon_r = 14$, the values of r_{max} for different values of F are given in Table 4.2. At high fields near the breakdown field, r_{max} is the same order of magnitude as previous estimated value of $2\lambda_i$.

Next, the vibrating frequency of ions ν_i can be expressed in terms of the theory of rate process[17] as follows:

$$\nu_i = (kT/h) \exp(-\Delta F^*/kT), \qquad (4.10)$$

where
$$\Delta F^* = \Delta H^* - T\,\Delta S^*, \qquad (4.11)$$

h is Planck's constant, ΔF^* the free energy of the activation, ΔH^* the activation enthalpy, and ΔS^* the activation entropy. ν_i is also

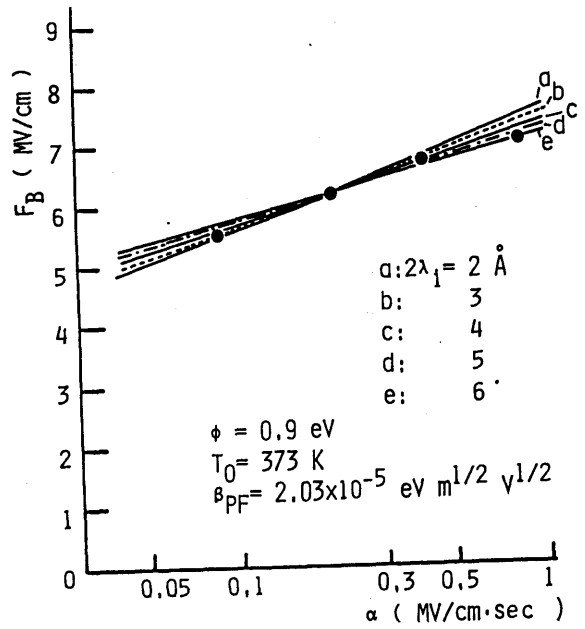

Fig.4.7. Examples of calculated values of F_B as a function of α with a parameter of $2\lambda_i$ with Poole-Frenkel effect.

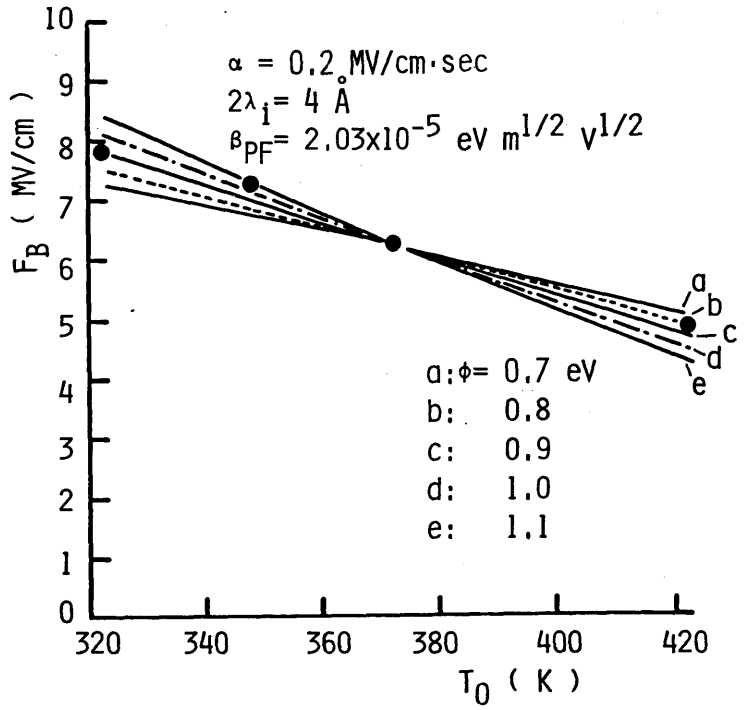

Fig.4.8. Examples of calculated values of F_B as a function of T_0 with a parameter of φ with Poole-Frenkel effect.

Table 4.2. Values of r_{max}.

F (MV/cm)	0.01	0.1	1	6
r_{max} (Å)	101	32	10	4.1

($\varepsilon_r = 14$)

Table 4.3. Relation between ΔS^* and ν_i.

ΔS^* (cal/mol·K)	0	10.3	19.5	60	300
ν_i (1/sec)	5.42	10^3	10^5	7.54×10^{13}	2.81×10^{66}

$U = 0.9$ eV, $T_0 = 373$ K

connected to eq.(4.3) by the relationship

$$\nu_i = \nu_0 \exp (-U/kT). \tag{4.12}$$

Comparing eqs.(4.10), (4.11) and (4.12), the following relations are obtained:

$$\begin{aligned} \nu_0 &= (kT/h) \exp (\Delta S^*/k), \\ U &= \Delta H^*. \end{aligned} \tag{4.13}$$

Since ϕ generally contains W, the value of U is unknown, but provided $\phi = U$, it may give a minimum estimation to the term of exp (-U/kT). Table 4.3 shows the relation between ΔS^* and ν_i, for $U = 0.9$ eV and $T_0 = 373$ K. Now, as a rough approximation, ions are assumed to reach the top of potential barrier for dissociation after they hop many times over potential mountains, which are $2\lambda_i$ apart from each other. Therefore, the time taken for ions to be dissociated is obviously $r_{max}/2\lambda_i\nu_i$, and is required to be longer than at least the relaxation time of dipole orientation. In the vicinity of the breakdown field, the jump distance becomes almost eqaul to r_{max}, meaning that the

number of hopping of ion requied for dissociation is less than one time, so that it is difficult to apply the above consideration. The concept mentioned above, however, may be applied at a little lower fields than the breakdown field.

Relaxation time of dipole orientation decreases with increasing temperature. Suppose the relaxation time of the order of millisecond corresponding to the value at the frequency of 1 kHz, as an estimation of the limiting value in the longest time region. In this case, in order that the time required for dissociation ($r_{max}/2\lambda_i\nu_i$) is larger than that for dipole orientation, ΔS^* must be 10.3 cal/mol·K as shown in Table 4.3. It is quite difficult at present to understand the physical meaning of this value of ΔS^*. For instance, the value of ΔS^* for the dipole relaxation of ice has been reported to be 17.6 cal/mol·K, with which the above estimated value of ΔS^* appears to be comparable.

As shown above, the estimated values of jump distance are 4 and 9 Å for the two cases with and without Poole-Frenkel effect, respectively, by taking ε_r in the range 10 to 14. An explicit decision as to which is appropriate as the jump distance, 4 or 9 Å, cannot be made, even though these values are compared with the lattice constants for PVDF. By using the estimated conduction parameters including Poole-Frenkel effect, the current density at 100°C and 1 MV/cm was calculated as 7.1×10^{-6} A/m^2, which is smaller than that without Poole-Frenkel effect, and also lower by about two orders than the experimental result. For the case which includes Poole-Frenkel effect, it is not certain whether the dielectric breakdown proceeds keeping an equilibrium of dissociation according to eq.(4.7), in addition to the problem at high fields near the breakdown field mentioned earlier. From the above consideration, the influence of the electric field on the thermal dissociation in a real breakdown process cannot be

expressed in such a simple form as eq.(4.7). Thus, at present, it seems to be very difficult to conclude which analysis, including or neglecting Poole-Frenkel effect, is valid, so in the following subsection the discussion placing the two cases in parallel will be proceeded.

4-4-3 Influence of Ionic Conduction Parameters on Electric Strength

Impulse thermal breakdown was found to be the dominant mechanism of dielectric breakdown of PVDF at high temperatures as discussed in subsection 4-4-1. On the basis of this result, the condcution parameters were estimated by comparing the theoretical characteristics of the dielectric breakdown with the experimental ones. In this subsection, the influence of these parameters on the electric strength is examined.

Firstly, consider the case in which the density of ions is independent of the electric field. The parameter j_0 is separated into two components, i.e. the density of ions and the jump distance. Substituting eq.(4.5) into eq.(4.6), the following equation is obtained.

$$dT/dF = (J_1/C_v) 2\lambda_i \exp (-\phi/kT) \sinh(q\lambda_i F/kT), \quad (4.14)$$

where $J_1 = j_0/2\lambda_i\alpha = 2 q A_i N_i^{1/2} \nu_0/\alpha$.

F_B was numerically calculated from the above equation by varying one of three parameters ϕ, $2\lambda_i$, and J_1 at a time and using the fixed values: ϕ = 0.9 eV, $2\lambda_i$ = 9 Å , and $J_1 = 6.7 \times 10^8$ A·sec/V·m^2 (α = 0.2 MV/cm.sec), which were obtained in the previous subsection.

Figure 4.9 shows the variation of F_B with the ionic conduction parameters, neglecting Poole-Frenkel effect at 373 K. The parameter varied is shown in bracket along with each curve. Filled circle

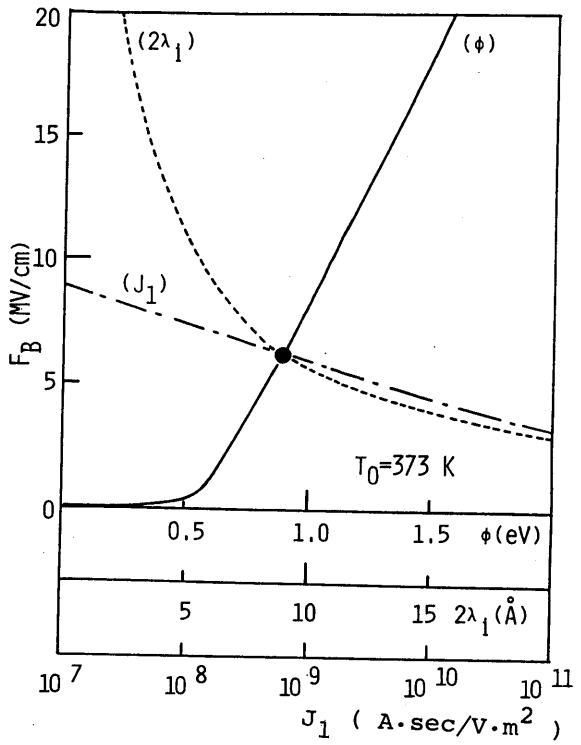

Fig.4.9. Variation of electric strength with the ionic conduction parameters J_1, $2\lambda_i$ and ϕ without Poole-Frenkel effect. Unfilled circle represents the experimental value of F_B.

indicates the experimental value of F_B. It is seen that F_B at high temperatures is expected to be improved provided J_1 and $2\lambda_i$ can be reduced and ϕ can be raised. Table 4.4 shows the changes $\Delta\phi$, $\Delta 2\lambda_i$ and ΔJ_1 required in ionic conduction parameters for increasing F_B by 1 MV/cm at 323 and 373 K .

Next, the calculated results after taking into account Poole--Frenkel effect are given in Table 4.5, where $\beta_{PF} = 2.03 \times 10^{-5}$ eV·m$^{1/2}$/V$^{1/2}$, ϕ = 0.9 eV, $2\lambda_i$ = 4 Å, and $J_1 = 8.1 \times 10^7$ A·sec/V·m^2 which have been already obtained by fitting the theoretical values to the experiments. The same result is obtained for both cases that Poole-Frenkel effect is taken into consideration or not, as shown in

Table 4.4. The changes $\Delta\phi$, $\Delta 2\lambda_i$ and ΔJ_1 in ionic conduction parameters required for increasing F_B by 1 MV/cm without Poole-Frenkel effect.

	$\Delta\phi$	$\Delta 2\lambda_i$	$(J_1+\Delta J_1)/J_1$
323 K	0.05 eV	-1 Å	0.15
373 K	0.05 eV	-1.5 Å	0.15

Table 4.5. The changes $\Delta\phi$, $\Delta 2\lambda_i$ and ΔJ_1 in ionic conduction parameters required for increasing F_B by 1 MV/cm with Poole-Frenkel effect.

	$\Delta\phi$	$\Delta 2\lambda_i$	$(J_1+\Delta J_1)/J_1$
323 K	0.05 eV	-1 Å	0.15
373 K	0.05 eV	-1.2 Å	0.15

($\varepsilon_r = 14$)

Tables 4.4 and 4.5. It is found that the density of supplying source of thermal dissociated ions is required to be decreased by about two orders of magnitude for improving F_B by 1 MV/cm, since J_1 is proportional to $N_i^{1/2}$ with constant α, as shown in eq.(4.14). It is also found that an equivalent increase in F_B is obtained for either decreasing $2\lambda_i$ by 1 to 1.5 Å or increasing ϕ by 0.05 eV.

It is generally suggested that removal of impurities and stabilization of material containing thermal dissociated ions are the powerful means for a reduction of the density of ions, which would result in the improvement of F_B in high temperature region. However, besides these ways, the change of the solid structure, which would lead to a change in $2\lambda_i$ and ϕ, is expected to give a great contribution to the improvement of F_B for PVDF at high temperatures. In order to realize such improvement, it is strongly required that the microscopic physical meaning of the parameters $2\lambda_i$ and ϕ, which are closely related to the solid structure, should be elucidated. The relation

between solid structure and breakdown characteristics of PVDF is discussed in the next subsection.

4-4-4 Solid Structure and Breakdown Characteristics

As has been mentioned, PVDF has two different types of crystalline phases, i.e. α-phase and β-phase. It has also been suggested that the breakdown characteristics are expected to be altered by any change in the conduction parameters connected with solid structure, provided the thermal breakdown due to ionic conduction is operative. In this subsection, the relation between the solid structure and breakdown characteristics for PVDF with different types of crystalline structure is discussed.

Specimen with almost same degree of crystallinity but different ratio of α-phase and β-phase were used for breakdown measurements. Physical properties of these specimen are given in Table 4.6 along with those of a biaxially stretched film. The ratio of the two types of crystalline phases was decided from D_α/D_β which is the ratio of the absorption at 530 cm^{-1} at which the specific peak for α-phase in the low frequency region appears, to that at 510 cm^{-1} which is the specific peak for β-phase (D is the magnitude of absorption). Measurements for breakdown were made in the same manner as in Section 4-1.

Table 4.6. Physical parameters of the specimen.

sample type	infra-red obsorption ratio D_α/D_β	thickness
unstretched	-	35 μm
biaxially stretched	1.5	12
uniaxially stretched A	1.1	15
uniaxially stretched B	<0.05	15

The temperature dependence of the electric strength for various types of films listed in Table 4.6 was investigated at a field rising rate of 0.2 MV/cm·sec in the temperature range, room temperature to 150°C. The result is shown in Fig.4.10. In Section 4-2, it was shown that F_B for biaxially stretched film above 50°C was independent of the sample thickness between 25 and 50 μm. Sample thickness for various PVDF films investigated here was not equal to each other as shown in Table 4.6. Nevertheless, if the assumption is made that F_B is independent of the sample thickness in all cases, it is inferred from Fig.4.10 that as the ratio of α-phase increases, F_B is lowered, except for an uniaxially stretched film B in the temperature range above 100°C. F_B for the uniaxially stretched film steeply decreases above 100°C, which could be possibly due to larger residual internal strain compared to the other films as this film was made by low temperature stretching.

Next, F_B for various types of films was obtained at 100°C by varying α from 0.03 to 0.8 NV/cm·sec. The typical result for unstretched film is shown with filled circles in Fig.4.11. It was found that in each type of film, F_B increases with increasing α. From the above results as well as the negative temperature dependence of F_B, the thermal breakdown is considered to be dominant for both uniaxially stretched and unstretched films above room temperature by following the same arguments as for the biaxially stretched film. Therefore, assuming possible breakdown mechanism to be the impulse thermal breakdown, the same analysis as the biaxially stretched film was made with using the numerical calculation. The typical results for unstretched film are shown in Fig.4.11 and 4.12. The ionic conduction parameters were obtained by fitting the theoretical curves to the experimental data. These estimated parameters are summarized in Table 4.7. It is found that both, the jump distance and the

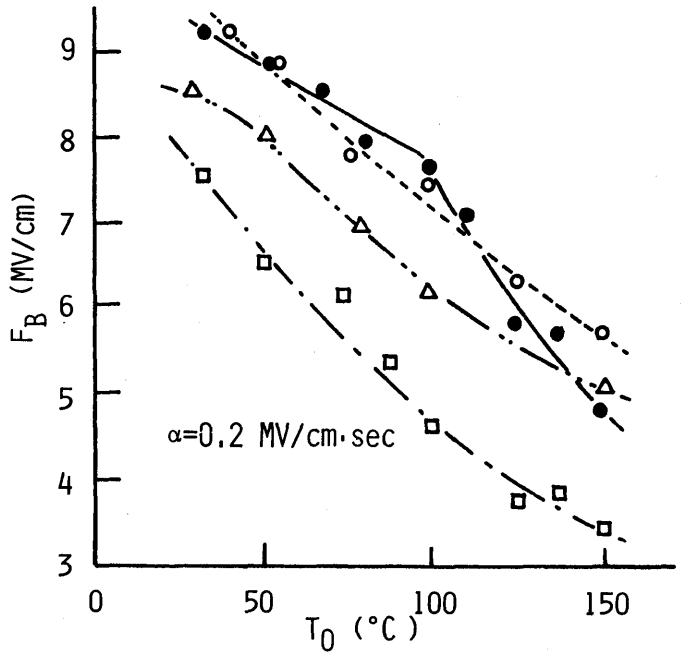

Fig.4.10. Temperature dependence of F_B for various types of PVDF . Unfilled square: unstretched, unfilled traiangle: biaxially stretched, unfilled and filled circle: uniaxially stretched A and uniaxially stretched B, respectively.

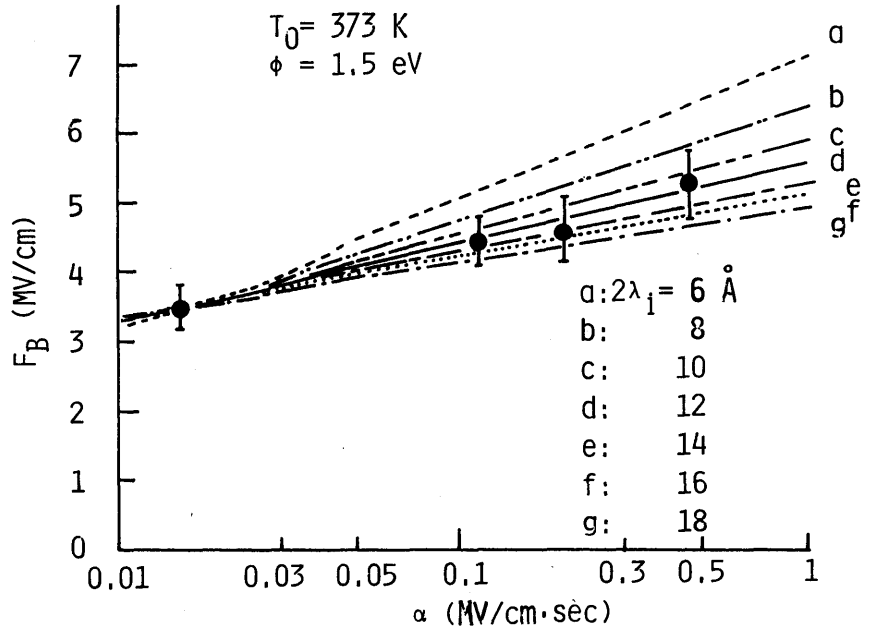

Fig.4.11. Examples of calculated values of F_B as a function of α with a parameter of $2\lambda_i$ for unstretched film.

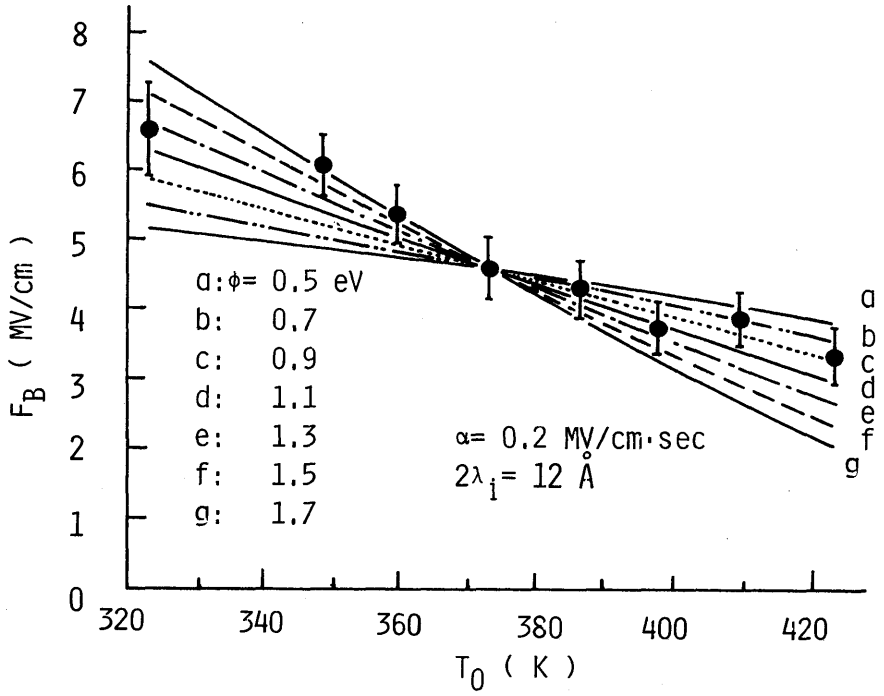

Fig.4.12. Examples of calculated values of F_B as a function of T_0 with a parameter of ϕ for unstretched film.

Table 4.7. Fitting ionic conduction parameters.

	unstretched	biaxially stretched	uniaxially stretched A	uniaxially stretched B
ionic jump distance(Å)	1.2	9	9	6
activation energy(eV)	1.1	0.9	0.9	0.5 (RT--100°C) 0.9 (100°C --)
pre-exponential factor (A/m^2)	9.3×10^9	1.2×10^7	1.8×10^6	2.5×10^2 3.1×10^7

activation energy, increase with apparent increase in the ratio of α-phase. It is concluded, therefore, that the change in the crystalline structure for PVDF would be associated with the change in the

ionic conduction parameters as estimated from the breakdown data. However, at present, the physical meaning of these results is still not well understood, so that further investigation must be attempted.

4-5 Conclusion

The electric strength of PVDF above 50°C was found to decrease with increasing temperature and to depend on the rising rate of applied field but not on the sample thickness. From these results, the impulse thermal breakdown process was considered to be operative in the temperature region investigated. Assuming ionic type of conduction, the electric strength was calculated numerically. The values of $2\lambda_i$, ϕ, and j_0 were estimated to be 9 Å, 0.9 eV, and 1.2×10^7 A/m^2, respectively, by fitting the theoretical values to the experimental electric strengths.

The discussion was extended to include Poole-Frenkel effect in a dissociation process of ionic charge. For ε_r = 10 to 14, the estimated parameters were $2\lambda_i$ = 4 Å, ϕ = 0.9 eV, and $j_0 = 6.5 \times 10^5$ A/m^2. Further, in order to get an information to improve F_B of PVDF in high temperature region, the influence of the changes in ionic conduction parameters on F_B was studied quantitatively. In order to improve F_B by 1 MV/cm, for example, the density of supplying source of thermally dissociated ions was required to be decreased by about two orders of magnitude, whether Poole-Frenkel effect is taken into account or not. It was also shown that an equivalent increase in F_B was acheived either by decreasing $2\lambda_i$ by 1 to 1.5 Å or increasing ϕ by 0.05 eV.

Further, the relation between the crystalline structure and breakdown characteristics by using sample with different ratios of the different crystalline phases was discussed. As a consequence, it was indicated that the change in the crystalline structure would be associated with the change in the ionic conduction parameters

estimated from the breakdown data.

References

[1] Matsuyama, Sasaki, Daito and Kitagawa: The Japan Society of Appl. Phys. 46 705 (1977).

[2] M.G.Broadhurst, G.T.Davins and J.E.Mckinnery: J. Appl. Phys. 49 4992 (1978).

[3] G.Pfister, M.Abkowitz and R.G.Crystal: J. Appl. Phys. 44 2064 (1973).

[4] K.Takahashi, H.Lee, R.E.Salomon, and M.M.Labes: J. Appl. Phys. 48 4694 (1977).

[5] D.K.Das-Gupta and J.S.Duffy : J. Appl. Phys. 50 561 (1979).

[6] R.Parker: Report of NASA, No. NASA CR. 124926 (1976).

[7] S.Osaki, S.Uemura and Y.Ishida: J.Polymer Sci. Part A-2 9 585 (1971).

[8] R.Hasegawa, M.Kobayashi and H.Tadokoro: Polymer J. 3 591 (1972).

[9] Y.Wada and R.Hayakawa: Japan. J. Appl. Phys. 15 2041 (1976).

[10] J.J.O'Dwyer:"The Theory of Electrical Conduction and Breakdown in Solid Dielectrics " (1973) Clarenden Press, Oxford.

[11] K.Stark and C.G.Garton: Nature 176 1225 (1955).

[12] J.Artbauer, C.Sc and J.Griac: Proc. Inst. Elect. Engrs. 112 818 (1965).

[13] M.Nagao, G.Sawa and M.Ieda: Trans. I.E.E.Japan 97-A, 279 (1977).

[14] Satogawa, Yonetani, Yamada, and Koizumi: "Fusso-jushi" Nikan-Kogyo Shinbunsha (1979). in Japanese.

[15] Ozaki and Hagiwara: "Denkishugaku III" OHM-sha (1965). in Japanese.

[16] J.Frenckel: Phys. Rev. 54 674 (1938).

[17] S.Glasstone, K.J.Laidler and H.Erying : "The Theory of Rate Process" (1941) McGrow Hill.

Chapter V Theoretical Analysis of Approximation Required for Using Impulse Thermal Breakdown

5-1 Introduction

In general, the equaition of thermal breakdown is given as follows:

$$C_v \left(\partial T/\partial t \right) - \mathrm{div} \left(\kappa \, \mathrm{grad} \, T \right) = j F, \tag{5.1}$$

where C_v is the heat capacity of the material per unit volume, κ the thermal conductivity, j the current density, and F the electric field. Consider the case when the heat conduction from the dielectric surface to the surroundings is ideally complete. Provided the voltage duration to breakdown t_B is sufficiently shorter than the thermal time constant of dielectric t_{th}, that is

$$t_B << t_{th}, \tag{5.2}$$

the second term of the left-hand side in eq.(5.1), which is the heat conduction term, can be ignored. In such a case, the impulse thermal assumption can be expected to be valid[1,2].

In Chapter IV, it was concluded that the dielectric breakdown for poly(vinylidene-fluoride) (PVDF) in high temperature region was considered as the thermal breakdown when a ramp voltage at field rising rate between 0.1 and 0.8 MV/cm·sec was applied. The impulse thermal breakdown theory was applied to the data obtained above 50°C. Assuming ionic conduction, the numerical calculation of the basic equation was carried out, and the conduction parameters were estimated by fitting the theoretical results to the experimental ones. Vermeer[3] solved approximately the equation of the impulse thermal breakdown by using the conduction data of glass. He concluded that

the impulse thermal breakdown was dominant in the glass at high temperatures. Further, Miyairi et al.[4] analyzed the dielectric breakdown of impurity doped polyethylene in high temperature region by making use of the equation of the impulse thermal breakdown. For all above cases, the thermal time constant t_{th} was shorter than the voltage duration to breakdown t_B within their experimental conditions, so that inequality (5.2) is not satisfied. However, the electric strength F_B was found to be almost independent of the sample thickness, which is one of the features expected for the impulse thermal theory. These facts indicate that provided an insufficient heat conduction from the dielectric material is taken into account, the impulse thermal breakdown form is possibly established even though inequality (5.2) is not fulfilled. A quantitative examination on this relationship has not been done. In this chapter, the fundamental equation (5.1) is numerically solved under the boundary condition which obeys Newton's law of cooling for various values of heat transfer coefficient λ from the dielectric surface to the surroundings. The theoretical electric strength is presented as a function of λ for PVDF. The calculation is made by using the ionic conduction parameters estimated in Chapter IV. From these results, the validity of approximation to the impulse thermal theory is examined quantitatively. The influence of λ on various kinds of breakdown characteristics, such as the thickness and field rising rate dependence of F_B is also discussed.

5-2 Thermal Breakdown and Heat Transfer Coefficient in Insulators

5-2-1 Procedure of Numerical Calculation

In eq.(5.1), C_v and κ are assumed to be independent of temperature. Let X axis be in the direction of the sample thickness.

Then, taking into consideration the heat conduction only along X axis, eq.(5.1) becomes

$$C_v \left(\partial T/\partial t \right) - \kappa \left(\partial^2 T/\partial^2 X \right) = j F. \tag{5.3}$$

In order to reduce the number of parameters and facilitate the numerical calculation, the variables in the above equation are transformed into non-dimensional variables

$$u = \left(T - T_0 \right) / T_0 \tag{5.4}$$

$$x = X/d \tag{5.5}$$

$$z = \left(\kappa / d^2 C_v \right) t, \tag{5.6}$$

where T_0 and d are the ambient temperature and the sample thickness, respectively. Equation (5.3) then becomes

$$\left(\partial u/\partial z \right) - \left(\partial^2 u/\partial^2 x \right) = d^2 j F/\kappa T_0. \tag{5.7}$$

Equation (5.7) is a partial differential equation with respect to x and z, and cannot be solved analytically. Therefore, replacing the differential terms by finite differences, the resulting finite difference equation is numerically solved. By taking forward finite differences for x and z, eq.(5.7) becomes

$$(u_{i,j+1} - u_{i,j})/\delta z - (u_{i+1,j} - 2u_{i,j} + u_{i-1,j})/(\delta x)^2 = d^2 jF/\kappa T_0, \tag{5.8}$$

where the subscripts i and j represent the numbers of infinitely small division for x and z, respectively. This equation can be rearranged as follows:

$$u_{i,j+1} = r\,(u_{i+1,j} + u_{i-1,j}) + r_1\,u_{i,j} + r_2\,j\,F, \qquad (5.9)$$

where $r = \delta z/(\delta x)^2$, $r_1 = 1 - 2r$ and $r_2 = (\delta z)\,d^2/T_0\kappa$. (5.9)

Next, the way of giving the boundary condition in solving eq.(5.8) is described. It is assumed that the heat dissipation from the dielectric surface to the surroundings obeys Newton's law of cooling. Now, consider an infinitely small fraction of volume which consists of a rectangular prism with base of unit area and height of δX. Then, from the condition of heat balance in the fraction at volume δX, the following equation can be deduced:

$$\delta X\,C_v\,(\partial T/\partial t)_{X=\delta X} - \kappa\,(\partial T/\partial X)_{X=\delta X} + \lambda\,(T - T_0) = jF\delta X, \qquad (5.11)$$

where λ is the heat transfer coefficient from the dielectric surface to the part which is kept at constant temperature T_0 in the ambient medium. Figure 5.1 shows heat balance in the infinitely small fractional volume. In eq.(5.11), the first term of the left-hand side represents the temperature rise in the volume δX, the second term the heat flow from the element in the bulk adjacent to this small volume element, and the third term the heat dissipation from the dielectric surface. The term on the right-hand side represents Joule's heat generated in this volume element. By similar transformation and replacement of differentials by forward finite differences as in eq.(5.3), eq.(5.11) can be led to the following equation:

$$u_{i,j+1} = r_3\,u_{i,j} + r\,u_{i+1,j} + r_2\,j\,F, \qquad (5.12)$$

where $r_3 = 1 - r - \delta x\,d\,\lambda\,r/\kappa$. (5.13)

On the basis of eqs.(5.9) and (5.12), exchanged temperature rise $u_{i,j}$ in arbitrary time and space can be obtained through the following

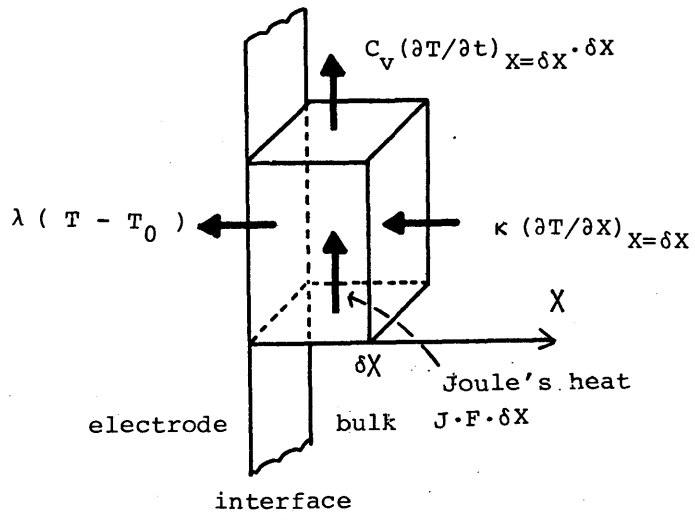

Fig.5.1. Heat balance in the fraction at the specimen surface.

calculation procedure;

i) set up the initial condition: $u_{i,j} = 0$ for $j = 0$.

ii) calculate $u_{2,j+1}$ by using eq.(5.9).

iii) calculate $u_{1,j+1}$ by using eq.(5.12), which is applicable only for i=1, since eq.(5.12) is applied only at the surface.

iv) return to ii) and replace j by j+1.

The calculation procedure is illustrated schematically in Fig.5.2. Numerical calculation was carried out according to this schedule. The electric field at which the temperature in the central part of the bulk reaches a critical temperature T_c was regarded as the theoretical electric strength F_B.

5-2-2 Results of Calculation

In this subsection, F_B as a function of λ, will be presented, assuming ionic conduction. In general, the ionic conduction current density j is expressed as

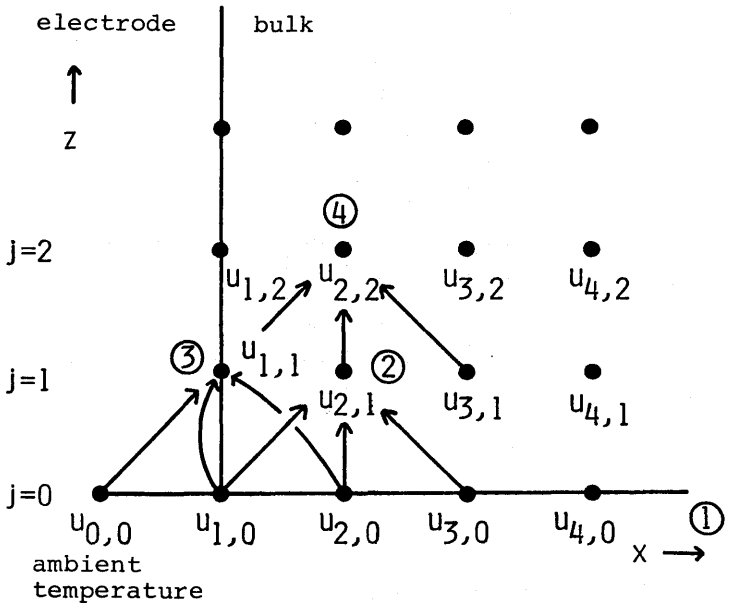

Fig.5.2. Procedure of numerical calculation.

$$j = j_0 \exp (-\phi/kT) \sinh (q\lambda_i F/kT), \qquad (5.14)$$

where j_0 is a constant, ϕ the activation energy, $2\lambda_i$ the ionic jump distance, q the ionic charge, and k the Boltzmann constant. Substituting eq.(5.14) into eqs.(5.9) and (5.12), the numerical calculation was carried out. In this case, the values of ionic conduction parameters for PVDF estimated in Chapter IV were used as j_0, ϕ, and $2\lambda_i$ in eq.(5.14). The values of various parameters used in this calculation are summarized in Table 5.1. Figure 5.3 shows the electric strength F_B calculated as a function of λ when the sample thickness d = 12.5 μm, the ambient temperature T_0 = 373 K and voltage rising rate dV/dt = 250 V/sec. A filled circle in the figure indicates the numerical solution from the impulse thermal theory under the same conditions. The features observed from Fig.5.3 are as follows:

i) When $\lambda \leq 1$ W/m^2·K, theoretical electric strength F_B is

Table 5.1. Values of physical parameters of PVDF used for numerical calculation.

j_0	1.2×10^7 A/m^2	κ	0.126 W/m·K
ϕ	0.9 eV	C_v	2.0×10^6 J/K·m^3
$2\lambda_i$	9 Å	T_c	453 K

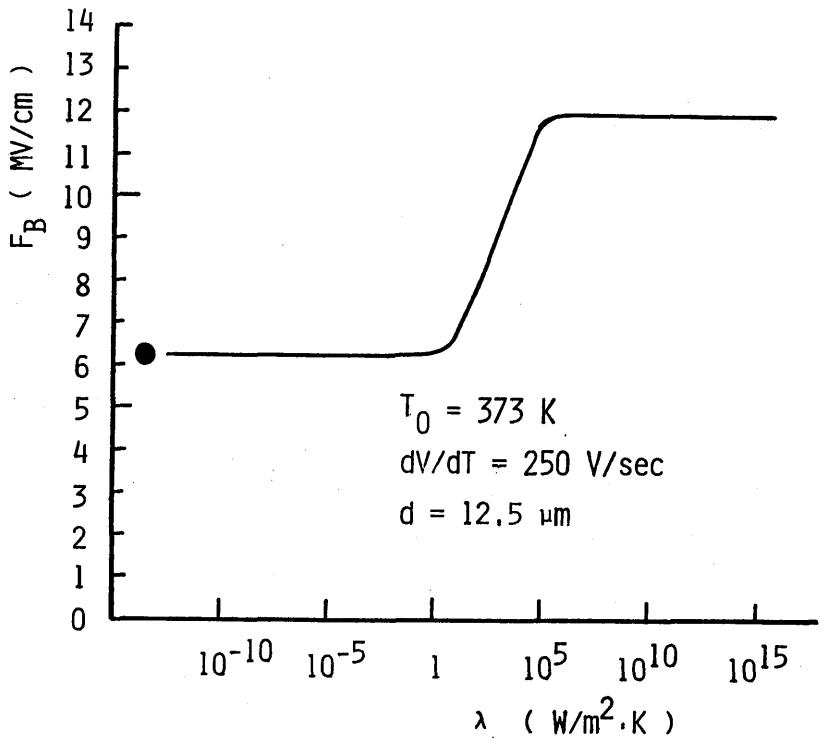

Fig.5.3. Theoretical relationship between heat transfer coefficient and electric strength F_B. Filled circle represents theoretical electric strength for the impulse thermal theory under the same conditions.

almost independent of λ and equal to that obtained from the impulse thermal theory.

ii) When $1 \leq \lambda \leq 10^5$ W/m^2·K, F_B varies from 6.2 to 11.9 MV/cm with increasing λ.

iii) When $\lambda \geq 10^5$ W/m^2·K, F_B does not depend on λ and closely approaches the curve in the limit when heat dissipation from the surface is ideally complete, which means λ is infinite.

5-2-3 Discussion

For the case of plane sample with thickness d, the thermal time constant of the material t_{th} is written in the form[1]

$$t_{th} = C_v d^2/\kappa . \tag{5.15}$$

In the case of PVDF, for example, t_{th} equals 62.8 μsec when d = 12.5 μm. For field rising rate α of about 0.2 MV/cm·sec, which was the standard experimental condition for the results in Chapter IV, the voltage duration to breakdown t_B is about 30 sec. This means that $t_B >> t_{th}$, so that inequality (5.2) does not hold. Thus, the impulse thermal assumption cannot be applicable, provided ideally complete heat dissipation from the dielectric surface is assumed. The second term of left-hand side (heat conduction term) in eq.(5.1) should be included in the calculation. However, it is found that the theoretical electric strength is nearly the same as that estimated on the impulse thermal assumption provided $\lambda \leq 1$ W/m^2·K. Till now, only a few reports have appeared in which heat dissipation from the dielectric surface and the heat conduction term in eq.(5.1) were taken into consideration. Copple et al.[5] solved the one-dimensional form of eq.(5.1) and obtained the transient temperature distribution and temperature rise in a dielectric. They consequently showed that the time variation of temperature in the bulk under alternating field can be explained by assuming an exponential variation of heat generation with temperature. Shousha et al.[6] proposed a breakdown model in which the generation of sufficient heat in a narrow channel resulting

from electron avalanche raises the electrical conductivity of the channel to a level at which thermal runaway could start, thus leading to destructive breakdown in a narrow region of the dielectric. They assumed as an approximation that the film has no temperature gradient in the direction of sample thickness. It was also assumed that the film is cylindrical with hot channel and the heat loss from the surface obeys Newton's law of cooling.

In this chapter, by choosing one value for each kind of parameter present in eqs.(5.4), (5.5) and (5.12), F_B as a function of λ was obtained. By using electrodes system which has a constant thermal property, breakdown characteristics such as the temperature, thickness and field rising rate dependences of F_B are obtained by varying one of these parameters. It is considered that within a certain range of variation of these parameters, apparent dielectric breakdown form for a constant λ can transform from the impulse thermal to the steady state. This behavior of the variation of breakdown process is very interesting in investigation the dielectric breakdown mechanism. This point shall be discussed in more detail in the next subsection.

There have been only a few reports on the heat transfer coefficient from the surface owing to difficulties in a direct measurement of λ. Moon[7] measured directly λ by using hot plate and obtained the value of λ as 5.1×10^2 W/m^2·K for glass-copper interface and 1.3×10 W/m^2·K for copper-air surface. He reported that by measuring the temperature difference between inner and outer glass walls with a thermo-couple, λ from the surface between glass and $NaNO_3$ solution was about 4.0×10^2 W/m^2·K. It was also reported that λ between metals which would offer the least thermal resistance in actual contacts was of the order of 10^5 W/m^2·K[8]. Above experimental values of λ, however, are considered to change largely with the surface

condition[7].

In the report, the sphere-plane electrodes were made of brass in measuring breakdown characteristics of PVDF. It could not be clarified how large λ was under present experimental condition. It was found, however, that the impulse thermal assumption is valid even if $t_{th} < t_B$ provided λ is smaller than 1 $W/m^2 \cdot K$. Thereafter, it is required to examine the heat transfer coefficient from sample surface to the ambient medium in an experimental situation.

5-3 Effect of Heat Transfer Coefficient on Breakdown Characteristics

In this section, the effect of transfer coefficient on the breakdown characteristics will be presented. Basic equations and the procedure of numerical calculation are the same as in the previous section. Various parameters in ionic conduction estimated for PVDF are employed.

Figure 5.4 shows the theoretical electric strength F_B as a function of field rising rate α with λ as a parameter, when d = 12.5 μm and T_0 = 373 K. It is seen that for $\lambda = 10^6$ $W/m^2 \cdot K$, nearly corresponding to the ideally complete heat dissipation, F_B is almost constant up to α about 10^2 MV/cm·sec. But it gradually increases with α and finally approaches the curve obtained for λ = 1 $W/m^2 \cdot K$. This fact is possibly due to the reason that in the region of α beyond 10^3 MV/cm·sec, t_B is of the same order or less than t_{th}, and so the impulse thermal breakdown is dominant whether heat dissipation from the dielectric surface to the surroundings is taken into account or not. Figure 5.5 shows the theoretical thickness dependence of F_B for various values of λ when α = 0.2 MV/cm·sec and T_0 = 373 K. As can be seen, F_B for λ = 1 $W/m^2 \cdot K$ is almost independent of sample thickness, being consistent with the impulse thermal breakdown form. On the other hand, as λ increases, the degree of dependence of F_B on

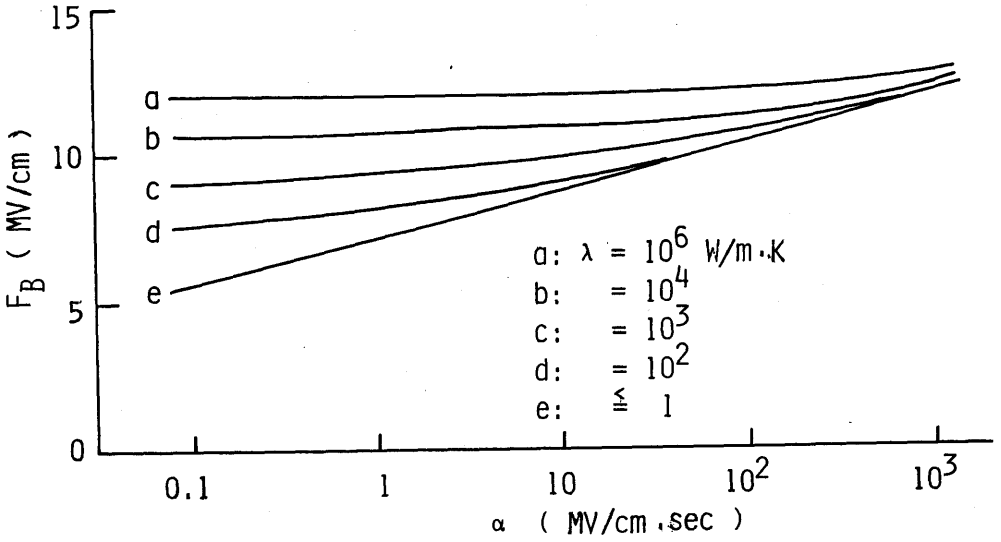

Fig.5.4. Theoretical electric strength F_B as a function of field rising rate α with λ as a parameter when d = 12.5 μm and T_0 = 373 K.

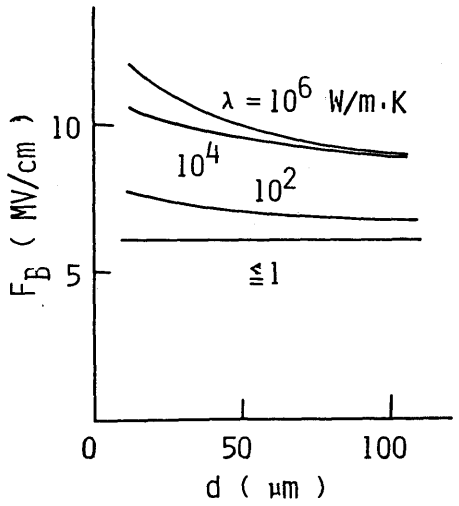

Fig.5.5. Theoretical thickness dependence of F_B for various values of λ when α = 0.2 MV/cm·sec and T_0 = 373 K.

thickness remarkably increases. The theoretical electric strength as a function of d and α was also computed with a constant λ and varying T_0. Figures 5.6 and 5.7 show the theoretical relation between F_B and α, and that between F_B and d, for $\lambda = 10^2$ W/m^2·K with T_0 as a parameter, respectively. It is found that the shape of the curves is almost insensitive to the ambient temperature.

From above numerical calculations, a qualitative knowledge can be obtained about the theoretical feature of thermal breakdown characteristics involving heat transfer coefficient. Namely, provided λ is so small that the heat loss from the surface is negligible, F_B increases with the field rising rate but is almost independent of thickness. This is consistent with the expectation from the impulse thermal breakdown, in spite of the relation between t_B and t_{th}. On the other hand, for the case of the other limit of λ, i.e. ideally complete heat dissipation, F_B scarcely depends on α in the region of α which corresponds to $t_B \geq t_{th}$. F_B is remarkably dependent on thickness especially in a small thickness region. For the medium with λ between above two limiting cases, the breakdown characteristics also show an intermediate feature between them.

Provided electrical conduction mechanism, heat transfer coefficient and the values of the other parameters involved are known for a given material, the theoretical breakdown characteristics can be calculated in the same way. This method is, therefore, expected to be a powerful mean to elucidate the dielectric breakdown mechanism. However, there remains some problems to be discussed in this model. It is supposed that an actual breakdown could be caused by local filamentary heat generation rather than heat generation from whole area in the sample as assumed in this model. Also, the method of determining λ is a problem. Further examinations on these aspects will be required.

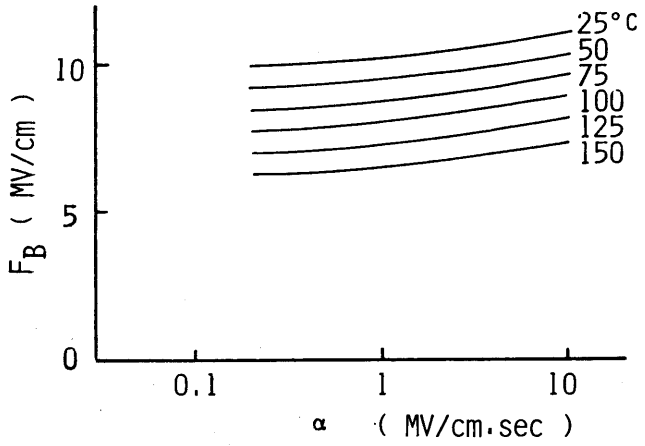

Fig.5.6. Theoretical relation between F_B and α for $\lambda = 10^2$ W/m^2·K with T_0 as a parameter.

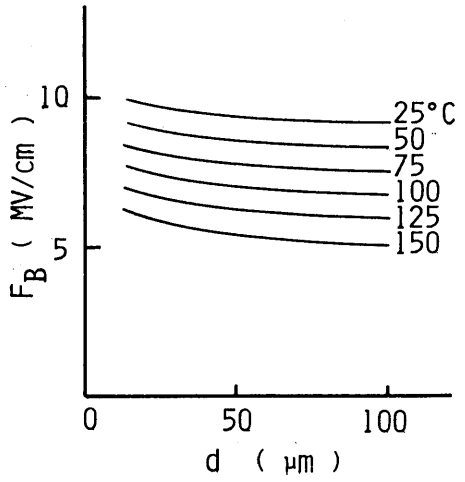

Fig.5.7. Theoretical thickness dependence of F_B for $\lambda = 10^2$ W/m^2·K with T_0 as a parameter.

5-4 Conclusion

The fundamental equation of thermal breakdown was numerically solved under the boundary condition which obeys Newton's law of cooling for various values of heat transfer coefficient λ from the dielectric surface to the ambient. As a result, it was found that the impulse thermal assumption is valid even if the thermal time constant of dielectric, t_{th}, is shorter than the time to breakdown, t_B, provided λ is smaller than a critical value. The theoretical electric strength was presented as a function of λ for poly(vinylidene-fluoride). The calculation was carried out by using the ionic conduction parameters estimated in Chapter IV, and the published data for the thermal conductivity and specific heat. In the case of a 12.5 μm thick sheet at 100°C, the calculated electric strength is nearly the same as that estimated on the impulse thermal assumption provided $\lambda \leq 1$ W/m^2·K. The effect of transfer coefficient on the breakdown characteristics was also discussed.

References

[1] J.J.O'Dwyer:"The Theory of Electrical Conduction and Breakdown in Solid Dielectrics" p. 202 (1973) Oxford: Clarenden Press.

[2] M.Hikita, M.Nagao, G.Sawa and M.Ieda: J.Phys. D: Appl. Phys. 13 661 (1980).

[3] J.Vermeer: Physica. 22 1269 (1956).

[4] K.Miyairi, G.Sawa and M.Ieda: Trans. I.E.E.J. 92-A 531 (1972). in Japanese.

[5] C.Coople, D.R.Hartree, A.Poter and H.Tyson: Proc. Inst. Elect. Engrs. 85 561 (1939).

[6] A.H.M.Shousha,D.L.Pulfrey and L.Young: J.Appl. Phys. 43 15 (1972).

[7] P.H.Moon: Trans. Inst. Elect. Engrs. 1008 (1931).

[8] Centinkale and Fishenden: Gen. Disc. on Heat Transfer. p.271 Inst. of Mech. Engin. London ' (1951).

Chapter VI Electrical Breakdown of Plasma Polymerized Styrene Thin Films

6-1 Introduction

Thin polymer films are made by various techniques such as glow discharge polymerization[1], electron beam irradiation[2], ultra-violet irradiation[3], and evaporation[4]. Among them, the films produced by the glow discharge method, which are also referred to as plasma polymerized thin films, have many advantages such as a small number of pinholes and a high temperature resistance resulting from the highly cross-linked structure compared with those of conventional polymers, etc.. In addition to these merits, due to the ease of preparation, such films are expected to have practical applications in thin film capacitors, thin film insulator for field effect transistors[5], switching elements[6,7], etc.. Extensive studies have been carried out on dielectric behaviors[8,9,10], electrical conduction at high fields, electrical breakdown[11-15], and surface properties.

However, there are many problems remaining unknown about the electrical insulation properties of these films, a fundamental understanding of which is necessary for the application as insulating material. Especially, the mechanism of dielectric breakdown has not sufficiently been clarified. Thin films, in general, have an advantage of self-healing breakdown, where localized weak spots can be eliminated. Moreover, this self-healing allows a large number of experiments on one sample. Klein et al.[16,17,18] discussed the self-healing breakdown for MOS and silicon dioxide capacitors deposited on glass slides. Previously, Sawa et al.[15] established the most favourable conditions for attaining a complete self-healing and for obtaining the electric strength free from the complication of the preexisting breakdown damage on plasma polymerized styrene thin films. Further, they also

discussed the relation between the breakdown pattern and the test condition in view of the energy dissipation associated with the breakdown[15]. The aim of this chapter is to clarify the electric breakdown characteristics of plasma polymerized styrene thin films. The electric strength F_B is obtained with varying temperature T_0, voltage rising rate dV/dt, prestress, ambient atmosphere, and electrode metal. Some measurements are also made on time lag, and under X-ray irradiation and photo illumination. The dielectric breakdown mechanism is also discussed from these experimental results.

6-2 Experiments

6-2-1 Sample Preperation

A gold electrode 4 mm wide with diffused edge was evaporated in vacuum onto a glass slide (10 mm x 25 mm, Corning 7059 glass). The thickness of the electrode was about 100 Å which was evaluated from the resistance of a monitor being placed in parallel 10 mm apart in a reaction tube. Degassed and predistilled styrene monomer (Katayama Chemical Co. Ltd.) was introduced into the reaction tube at a fixed pressure of 0.5 torr. The glow discharge was initiated and maintained for a given period at a current density about 1 mA/cm^2 and frequency 5 kHz. An upper gold or aluminum electrode 4 mm wide was then evaporated onto the polymer film at a right angle to the base electrode. The configuration of the sample prepared in this way is shown in Fig.6.1. The polymer thickness was estimated from the capacitance measurement, assuming a value of 3 for the dielectric constant[15] and ranged from 2000 to 4500 Å. The thickness could be controlled by the period of glow discharge.

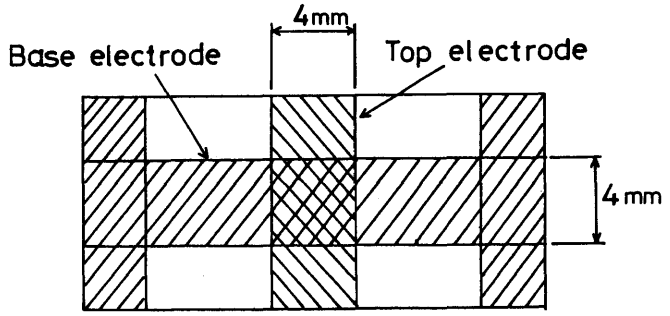

Fig.6.1.Schematic diagram of a sample.

6-2-2 Breakdown Measurements

Prior to all the experiments, several hundreds of self-healing breakdown were performed in dry nitrogen gas at 1 atm and room temperature by applying a ramp voltage at a voltage rising rate of 250 kV/sec, until the breakdown voltage reached almost a constant value. Breakdown measurements were mainly carried out in the dry N_2 gas, but some in vacuum (10^{-3} torr) and oxygen gas (1 atm) at room temperature, and also under X-ray irradiation or photo illumination. The circuit used in the breakdown measurements is shown in Fig.6.2. The voltage rising rate was widely varied from 10 V/sec to 1 MV/sec. When a breakdown occurred, a positive pulse was generated across a resistor of 2 kΩ. This positive signal triggered a thyratron connected to the resistor, and the applied voltage was immediately removed. Therefore only one breakdown event could occur for a ramp. The voltage across the sample was recorded with an oscilloscope. The breakdown voltage was determined by the crest voltage. Every fifty times of experiments, the capacitance of the sample was measured with a LCR meter (YHP 4247A Multi-Frequency LCR Meter) so as to ensure whether complete self-healing had been attained.

The breakdown measurements under X-ray irradiation or photo illumination were carried out in vacuum. X-rays were produced at anode

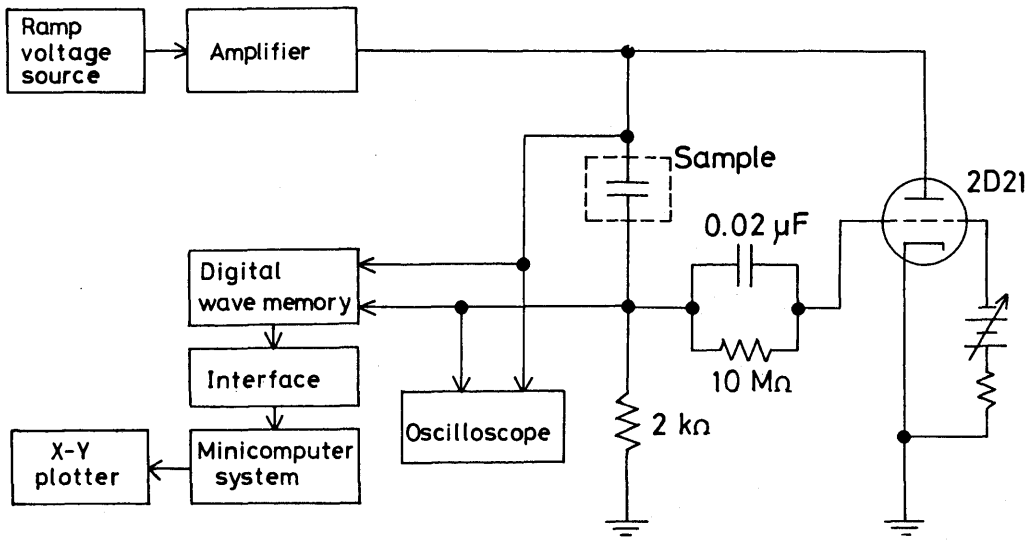

Fig.6.2. Circuit for measuring breakdown voltage with a ramp voltage.

voltage of 35 kV and at anode current of 20 mA. Firstly, the sample was shortcircuited and irradiated with X-rays for 20 min.. After that, breakdown measurements were made keeping X-ray irradiation. The sample was again shortcircuited without X-rays for 30 min.. This procedure was repeated. The breakdown measurements under photo illumination by using Xe lamp of white light were made in the same way as that under X-ray irradiation.

Some measurements were also made on time lag by applying a step voltage. The schematic diagram of the test circuit is shown in Fig.6.3. A rectangular pulse generator has a protection circuit to remove the applied voltage automatically when breakdown occurs. Time lag was determined by the pulse width measured with an aid of a counter (IWATSU Universal Counter type UC-7641). Rise time of the step voltage was about 10 μsec when connecting the sample.

Experiments on the effect of prestress were also made for which the prestress control circuit was added to the circuit shown in

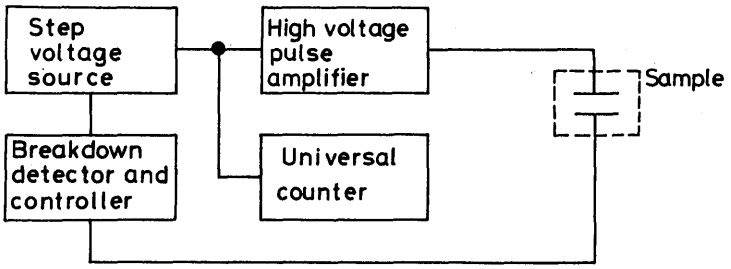

Fig.6.3. Circuit for measuring time lag.

Fig.6.1. The prestress voltage was varied from 0 to 150 V and the prestress time ranged from about 500 μsec to 3 min..

6-3 Experimental Results

6-3-1 Electric Strength of Plasma Polymerized Styrene Thin Films

The temperature dependence of the electric strength F_B of a 3800 Å thick plasma polymerized styrene thin film sandwiched between the gold electrodes (Au-PPS-Au) at a voltage rising rate, dV/dt, of 250 kV/sec is shown in Fig.6.4. Here, "Au-PPS-Au" represents the sample structure of top electrode - plasma polymerized styrene thin film - base electrode. Each point and corresponding bars represent an average of about 10 tests and the standard deviation, respectively. As can be seen in Fig.6.4, F_B for Au-PPS(3800Å)-Au is almost independent of temperature in the range -196 to 100°C. It is found from another experiment for Au-PPS(2300Å)-Au that F_B scarcely changes with temperature over -196 to 200°C. Oakes[19] measured F_B of conventional polystyrene film of 10 to 70 μm thickness by applying a ramp voltage (dV/dt = 500 V/sec) over a temperature range from 0 to 110°C. He showed that F_B of the conventional film fell steeply with temperature

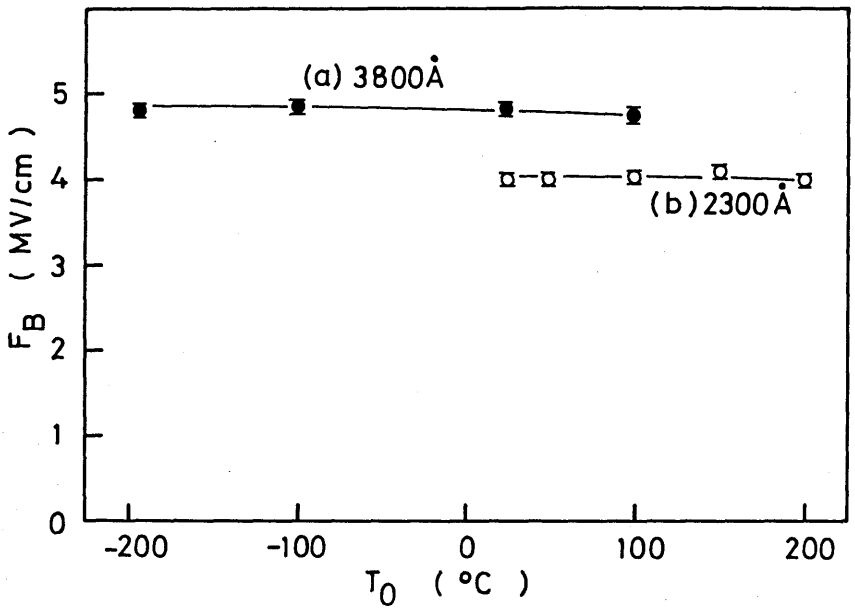

Fig.6.4. Temperature dependence of electric strength for Au-PPS-Au.

above about 80°C, which is the softening temperature of the polymer. This is a feature of the breakdown characteristics at high temperatures for usual linear polymer films. Therefore, it can be confirmed from the breakdown data that PPS has a much higher temperature resistance due to its highly cross-linked structure than the conventional polystyrene film.

Figure 6.5 shows the relation between the electric strength and the voltage rising rate for Au-PPS(2600Å)-Au at room temperature. F_B depends strongly on dV/dt over a wide range from 10 V/sec to 1 MV/sec.

6-3-2 Time Lag to Breakdown

In general, time lag to breakdown can be formally expressed as [20]

$$N_t/N = \exp [- (t - t_f)/t_s], \qquad (6.1)$$

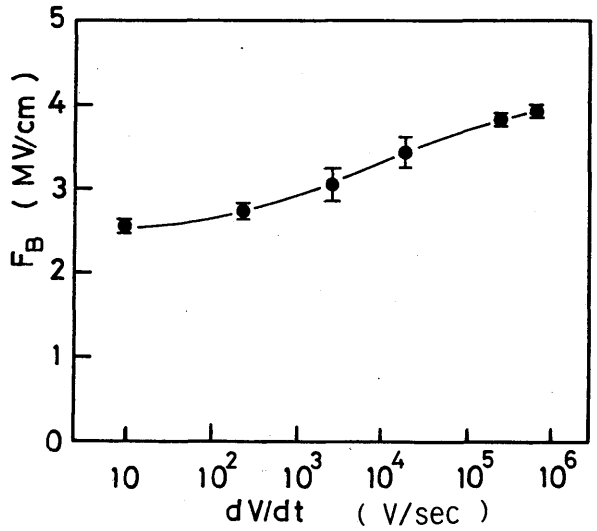

Fig.6.5. Relation between electric strength and voltage rising rate for Au-PPS(2600Å)-Au.

where N is the total number, N_t is the number of tests in which no breakdown takes place before the time t in a series of N tests under identical conditions, t_s is the mean statistical time lag (this is also called the statistical time lag), and t_f is the formative time lag, being assumed to be constant for a given electric field.

Figure 6.6 shows the Laue plots of the time lag (ln (N_t/N) vs. t) for the dielectric breakdown of Au-PPS(2600Å)-Au at various electric fields. If the Laue plots are regarded approximately to be linear, the slope gives t_s and the point at 100% for N_t/N gives t_f. It was found that both t_f and t_s decreased with electric field, and an apparent value of t_f estimated from the Laue plots was more than a few tens microseconds. The rise time of the step voltage was about 10 μsec. Therefore, the detailed discussion on the formative time lag cannot be given. However, it can be said that the formative time lag is of the order of ten μsec under the present condition, being

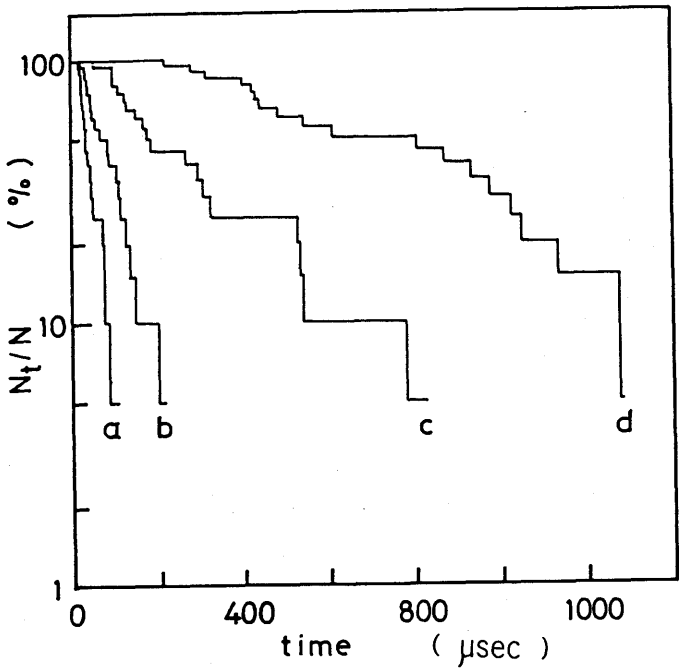

Fig.6.6. Laue plots of time lag for various electric field with Au-PPS(2600Å)-Au. (a) 3.88, (b) 3.70, (c) 3.51 and (d) 3.33 MV/cm.

considerably long compared with 10^{-9} - 10^{-12} sec, which is generally accepted for electronic breakdown process in solid dielectrics[21-24].

Solomon[25] found that the mean time lag t_{BS} obtained with a step voltage is closely related to the mean time lag t_{BR} obtained with a ramp voltage as follows:

$$t_{BR}/t_{BS} \simeq 0.56\ \beta\ F, \tag{6.2}$$

where F is the applied electric field, and $-\beta$ is the slope of ln t_{BS} vs. F. Figure 6.7 shows the mean time to breakdown as a function of electric field for Au-PPS(2600Å)-Au at room temperature, both by step and ramp voltages. Figure 6.7 shows also the theoretical relation between t_{BR} and F obtained from eq.(6.2) using experimental value of

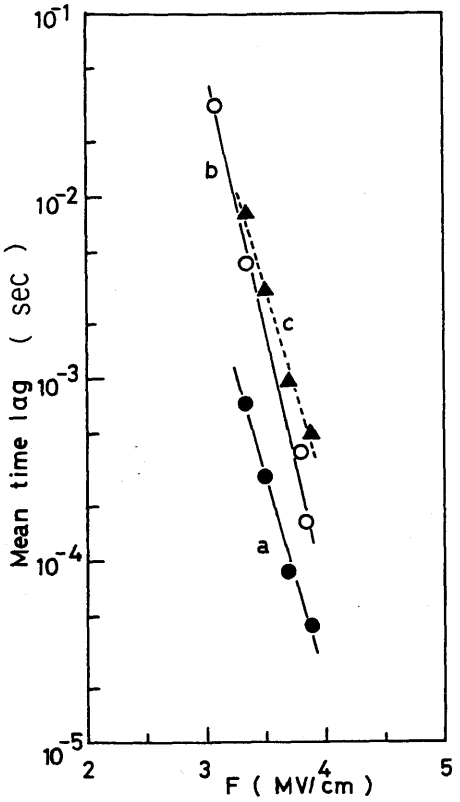

Fig.6.7. Mean time to breakdown as a function of electric field for Au-PPS(2600Å)-Au. Filled (a) and unfilled (b) circles represent experimental values measured with a step voltage and those with a ramp voltage , and filled triangles represent calculated values by using Solomon's equation.

t_{BS}. Since the present experiments show quite good agreement with the eq.(6.2), such a considerably long time lag containing a long formative time lag is qualitatively consistent with the experimental result on the dependence of F_B on dV/dt[25].

Figure 6.8 shows the temperature dependence of t_f and t_s for Au--PPS(3500Å)-Au over a temperature range from -196 to 100°C. Above room temperature, both t_f and t_s scarcely depend on temperature, being consistent with the temperature dependence of F_B for PPS. On the other hand, below room temperature, both t_f and t_s decrease as temperature increases. The reason for this is not yet clear.

From these results, the following arguments can be drawn for the breakdown of PPS: Firstly, the fact that F_B is almost independent of temperature indicates that the conduction process directly related to breakdown should be temperature independent. Secondly, F_B

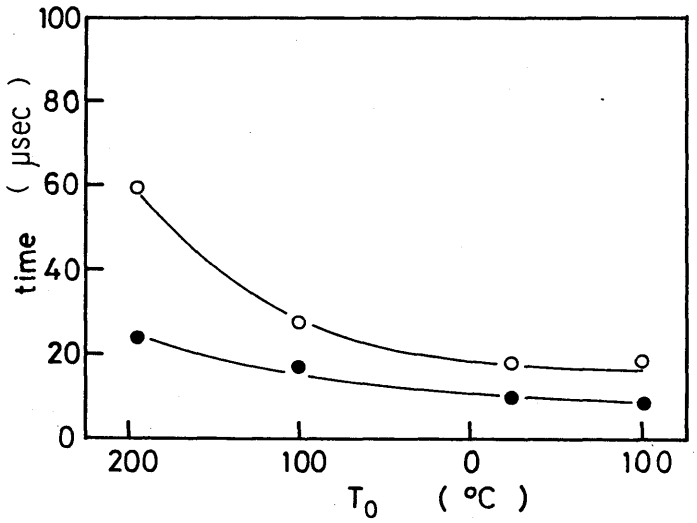

Fig.6.8. Temperature dependence of statistical time lag (unfilled circle) and formative time lag (filled circle) for Au-PPS(3500Å)-Au.

strongly depends on dV/dt even for a slow rate. The mean time lag is about 10^{-4} - 10^{-5} sec, which is considerably long as already mentioned, even though the time lag to breakdown decreased sensitively with the electric field. Such a relatively long time lag implies that a thermal process play an important role in the breakdown of PPS.

In order to get further information about the breakdown mechanism, it was investigated how the electric strength and time lag for PPS are affected by electrode metal, X-ray irradiation or photo illumination, and ambient atmosphere. These results will be discussed in the following subsections.

6-3-3 Effect of Electrode Metal on the Breakdown Characteristics

Figure 6.9 shows the effect of electrode metal on the breakdown voltage V_B of Au-PPS(3300Å)-Al in N_2 gas (1 atm, room temperature) by applying a ramp voltage at 250 kV/sec. The polarity reversal of applied voltage was carried out by exchanging the connection to the sample electrodes. As shown in Fig.6.9, when Au electrode is the cathode, F_B is almost equal to that when Al electrode is the cathode. This difference is too small to indicate the existence of the metal electrode effect.

Then, experiments were carried out on time lag for Al-PPS-Au and Au-PPS-Al structures by applying a step voltage. The Laue plots are shown in Figs.6.10 and 6.11 for Al-PPS(3200Å)-Au and for Au-PPS(3300Å)-Al, respectively. In both cases, a longer time lag is observed with the Au cathode than with the Al cathode. This means that the effective contact barrier height Φ_D at the metal-insulator interface possibly affects the breakdown cahracteristics. Let W_m be the work function of metal, and χ the electron affinity of the insulator, then Φ_D can be written in the form

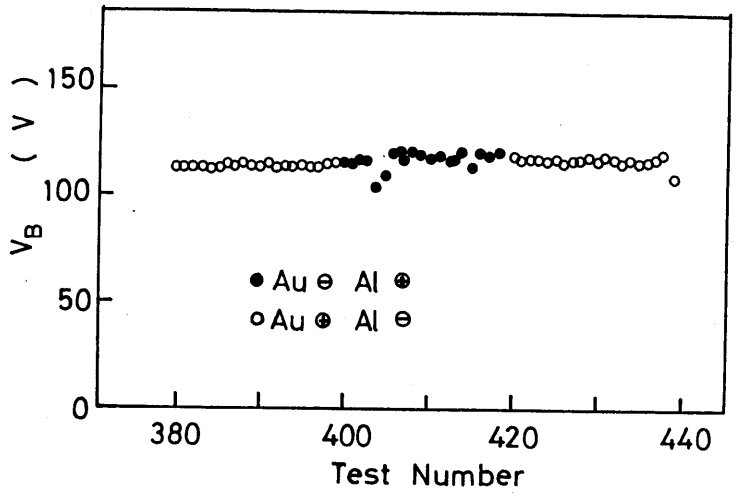

Fig.6.9. Effect of electrode metal on breakdown voltage for Au-PPS(3300Å)-Al. Unfilled circles represent breakdown voltage when Au is the anode and Al the cathode. Filled circles represent breakdown voltage when Al is the anode and Au the cathode.

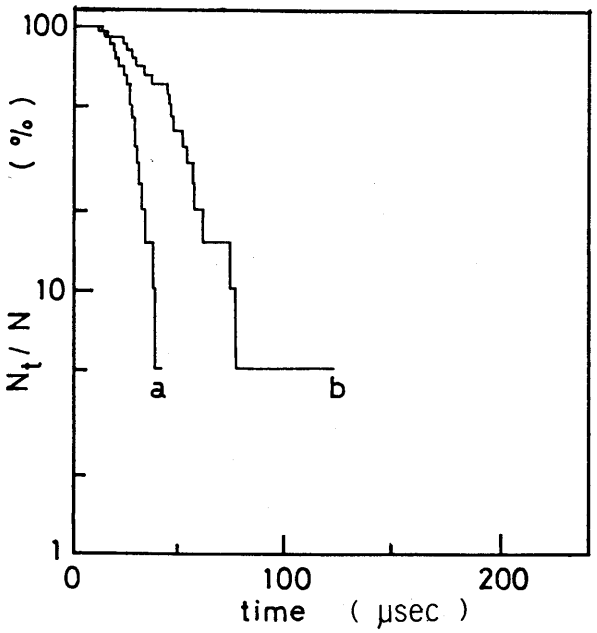

Fig.6.10. Effect of electrode metal on time lag by applying a step voltage of 5.0 MV/cm for Al-PPS(3200Å)-Au. (a) Au as the anode and Al as the cathode, and (b) Au as the cathode and Al as the anode.

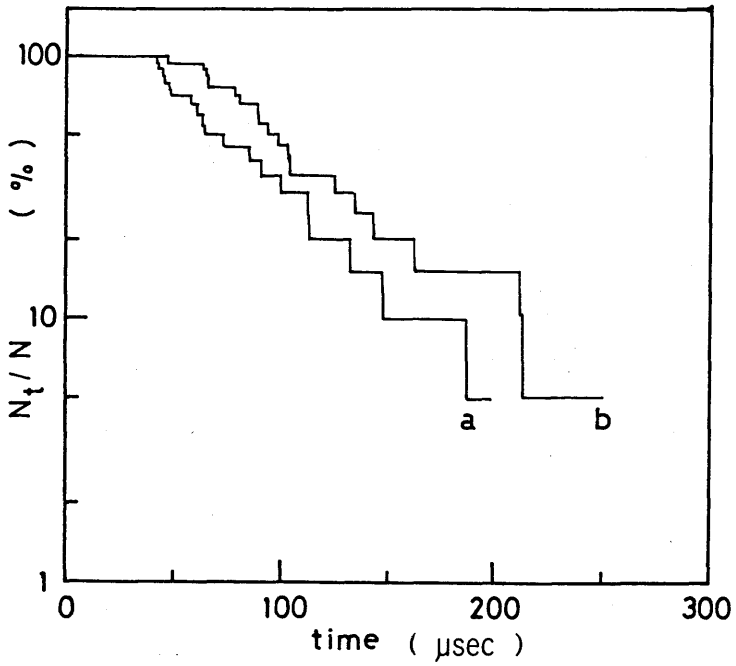

Fig.6.11. Effect of electrode metal on time lag by applying a step voltage of 3.79 MV/cm for Au-PPS(3300Å)-Al. (a) Au as the anode and Al as the cathode, and (b) Au as the cathode and Al as the anode.

$$\Phi_D = W_m - \chi . \qquad (6.3)$$

Values of W_m for Au and Al are 4.6 and 3.8 eV, respectively, so that the Al cathode injects more electrons into the polymer than the Au cathode. Therefore, taking the electrode metal effect on F_B into consideration, it is concluded that the carrier injection process cooperates on the breakdown process of PPS.

6-3-4 Effect of Ambient Atmosphere on F_B and Time Lag

Figure 6.12 shows V_B as a function of test number for Au-PPS(3330Å)-Au with a ramp voltage (dV/dt = 250 kV/sec) for various ambient atmosphere gases at room temperature. Values of F_B measured in both, vacuum and N_2, are almost equivalent, but are higher by about 10% in O_2. Figures 6.13 and 6.14 show the Laue plots of time lag

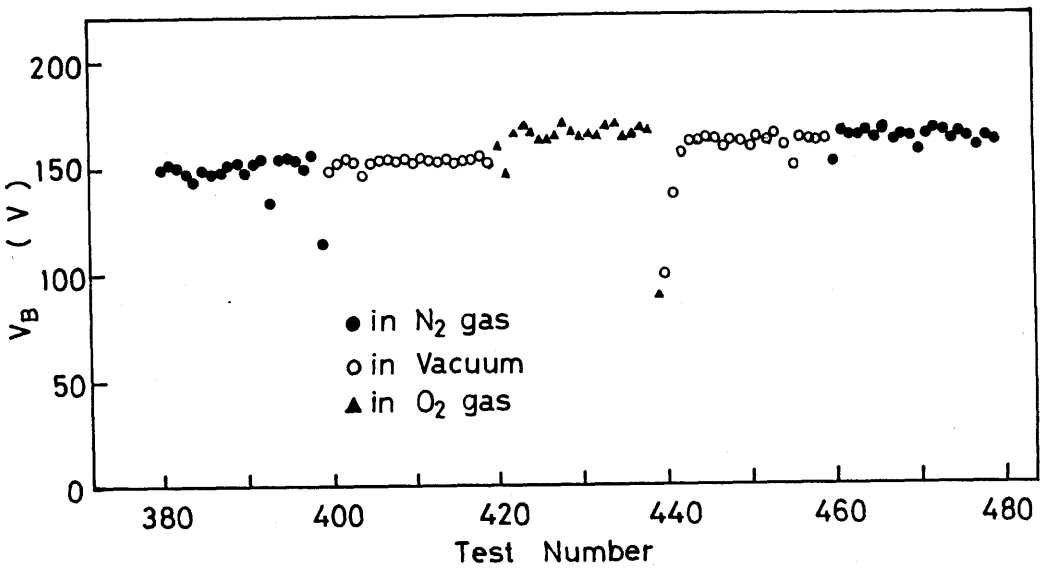

Fig 6.12. Effect of ambient atmosphere on breakdown voltage for Au-PPS(3330Å)-Au. Filled circles, unfilled circles and filled triangles represent breakdwon voltages obtained in N_2 gas, in vacuum, and in O_2 gas, respectively.

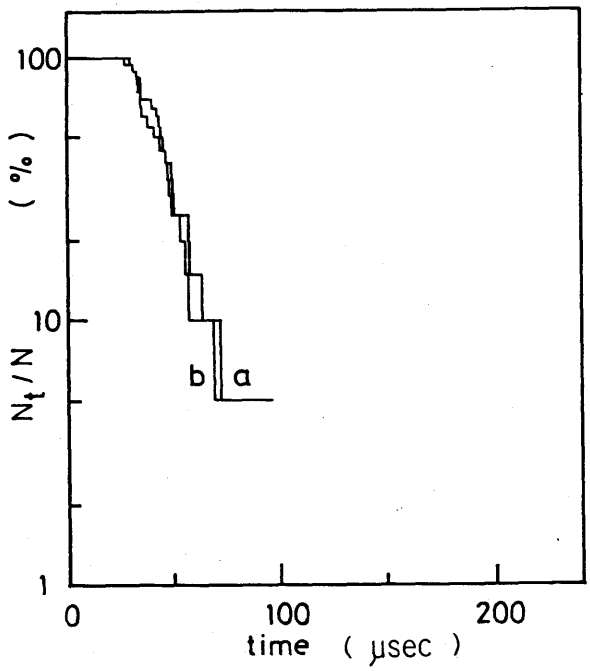

Fig.6.13. Effect of ambient atmosphere on time lag with a step voltage of 4.98 MV/cm for Au-PPS(3300Å)-Au. (a) Laue plots of time lag observed in N_2 gas, and (b) in vacuum.

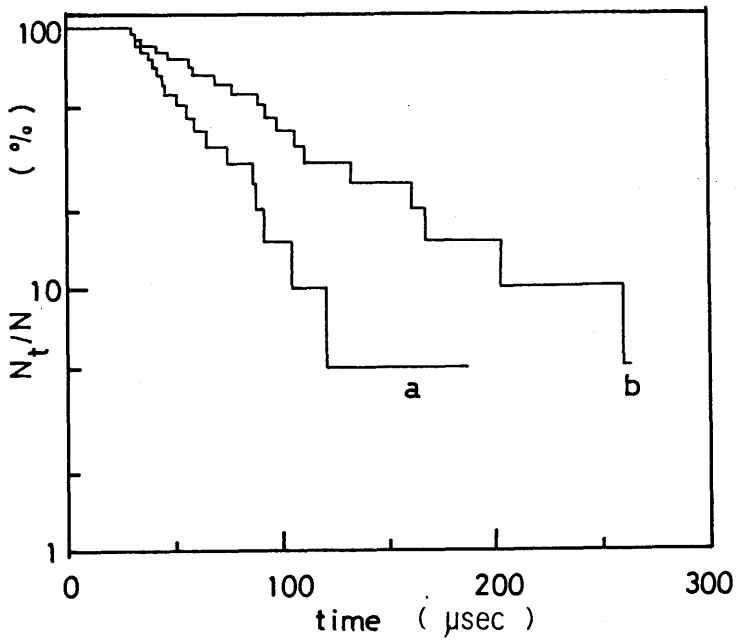

Fig.6.14. Effect of ambient atmosphere on time lag with a step voltage of 5.44 MV/cm for Au-PPS(3300Å)-Au. (a) Laue plots of time lag observed in N_2 gas, and (b) in O_2 gas.

obtained for Au-PPS(3300Å)-Au in N_2 and in vacuum at 4.98 MV/cm, and in O_2 and N_2 at 5.44 MV/cm, respectively. As can be seen from Fig.6.13, the time lag in N_2 gas almost equals that in vacuum. Whereas the time lag in O_2, as shown in Fig.6.14, is longer than that in N_2, and especially the longer t_s is observed in O_2. This is consistent with the result of the higher value of F_B obtained in O_2.

Mizutani et al.[26] reported from the photo conductivity measurement on polyethylene terephthalate film that O_2 molecules adhering on the metal-insulator interface would act as surface states, which would bring an increase in Φ_D at the metal -insulator contact for electron injection. From the effect of ambient atmosphere gas as well as the electrode metal effect, the contact barrier height at the metal--insulator interface can be considered to be connected with the breakdown mechanism of PPS.

6-3-5 Effect of X-ray Irradiation and Photo Illumination on F_B and Time Lag

Figures 6.15 and 6.16 show the effect on V_B of X-ray irradiation and photo illumination, respectively. Here, measurements were made on Au-PPS(3200Å)-Au at room temperature by applying a ramp voltage (dV/dt = 250 kV/sec). The time lag was also obtained under X-ray irradiation and photo illumination. The results are shown in the form of the Laue plots in Fig.6.17 and 6.18. As can be seen from these figures, both X-ray irradiation and photo illumination do not influence the breakdown characteristics of PPS within the present experimental conditions. It was reported[27] that when a polymer is irradiated by X-ray, carrier liberation from traps, carrier generation due to impurity dissociation, and increase in conduction electrons due to a direct excitation from the valence band to the conduction band could

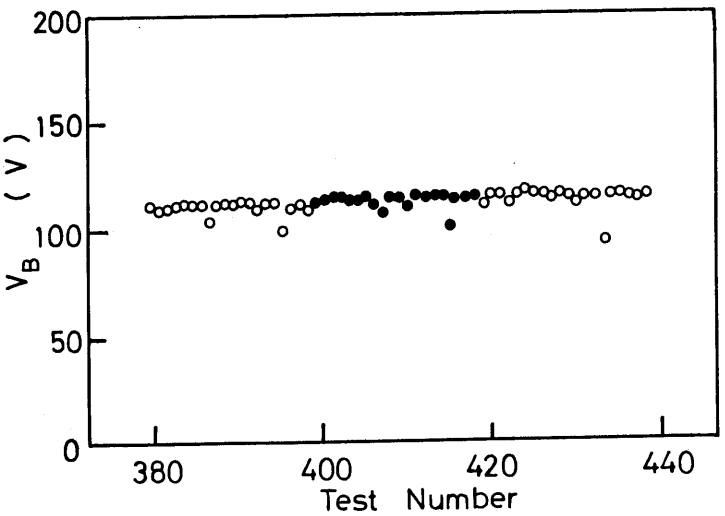

Fig.6.15. Effect of X-ray irradiation on breakdown voltage for Au-PPS(3200Å)-Au. Filled and unfilled circles indicate breakdown voltage obtained under X-ray irradiation with pre-irradiation for 20 min. and that without X-ray irradiation, respectively.

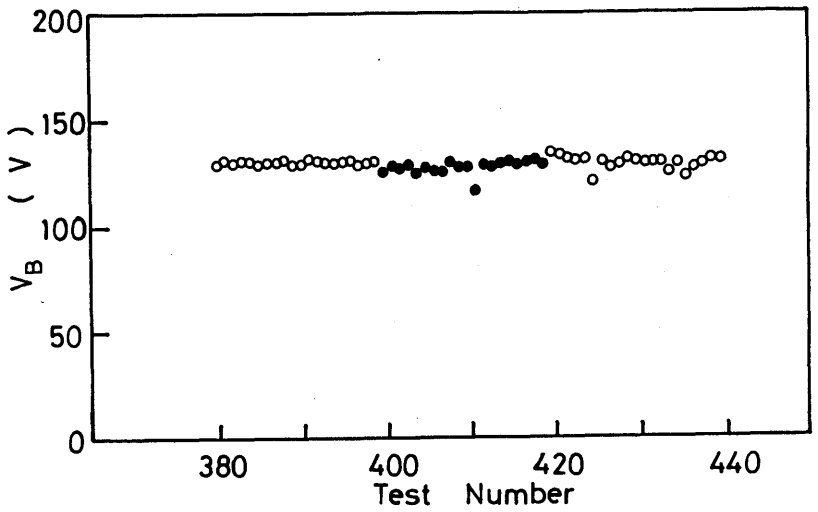

Fig.6.16. Effect of photo illumination on breakdown voltage for Au-PPS(3170Å)-Au. Filled and unfilled circles indicate breakdown voltage obtained under photo illumination with pre-illumination for 20 min. and that without photo illumination.

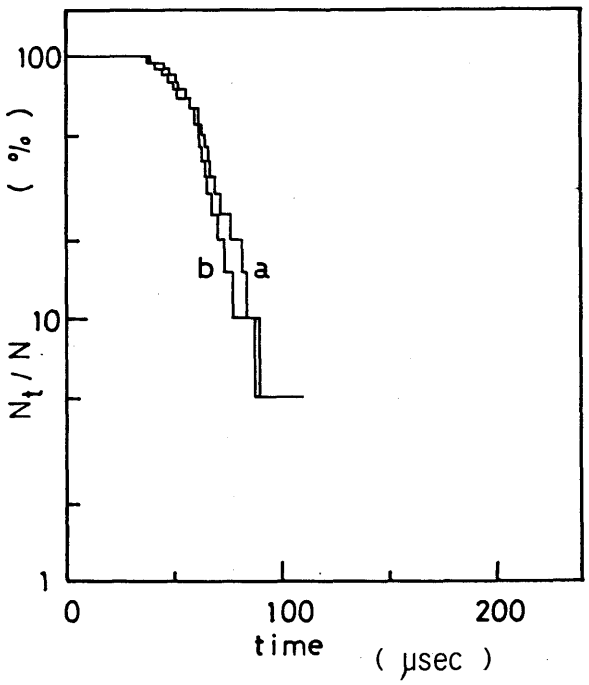

Fig.6.17. Effect of X-ray irradiation on time lag with a step voltage of 3.73 MV/cm for Au-PPS(3200Å)-Au. (a) Laue plots of time lag without X-ray irradiation, and (b) under X-ray irradiation.

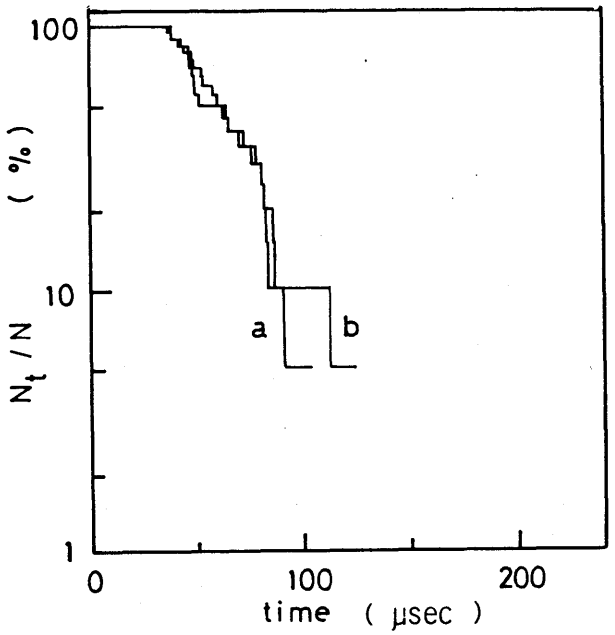

Fig.6.18. Effect of photo illumination on time lag with a step voltage of 4.23 MV/cm for Au-PPS(3170Å)-Au. (a) Laue plots of time lag without photo illumination, and (b) under photo illumination.

occur. The photo illumination is expected to cause carrier injection from electrode[28] and carrier liberation from traps[29]. Since no influence of X-ray irradiation or photo illumination on breakdown has been observed, electron injection or carrier liberation from traps does not seem to contribute to the breakdown process, within the present experimental conditions.

6-3-6 Prestress Effect on Electric Strength of PPS

To examine the secondary influence of space charge on the breakdown characteristics of PPS, the prestress effect was investigated.

Positive or negative prestress F_p in a range between 0 and 3 MV/cm was applied for a given period t_p just before a positive ramp voltage at 250 kV/sec was imposed on the sample in N_2 gas (1 atm).

Figure 6.19 shows F_B of Au-PPS(2600Å)-Au at room temperature as

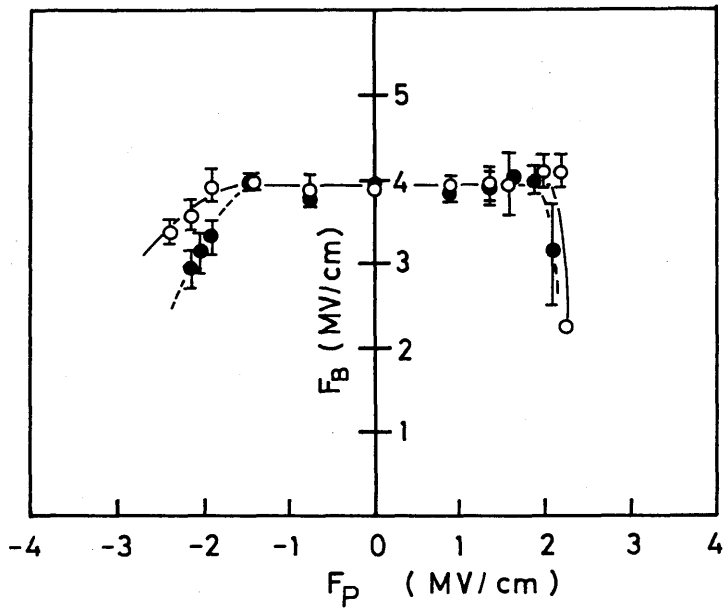

Fig.6.19. Prestress effect on electric strength at 23°C for different prestress time for Au-PPS(2600Å)-Au. Unfilled and filled circles indicate electric strength for 60 and 180 sec prestress time, respectively.

a function of F_p for t_p = 60 and 180 sec. For both polarities prestress, F_B is almost independent of F_p up to about 2 MV/cm, but decreases steeply at higher values. The slope of the curve in the region $|F_p| > 2$ MV/cm in which F_B decreases with F_p is steeper for t_p = 180 sec than that for t_p = 60 sec. Further, the similar experiments were carried out varying ambient temperature from -196 to about 100°C. The temperature dependence of the prestress effect was found to be scarcely observed.

The decrease in F_B with the prestress of opposite polarity to the applied ramp voltage has been interpreted as being due to the hetero space charge effect[30]. For thin films, injected carriers might reach the counter electrode. In this case, the hetero space charge would manifest itself and a decrease in F_B is expected, for both the

same and reverse polarity prestress. The result $\partial F_B/\partial(dV/dt) > 0$ can be consistently interpreted in terms of hetero space charge. However, the experimental results can be also understood with an alternative process as Joule's heat produced during prestress. This point will be discussed further in the following section.

6-4 Discussion

The results of breakdown experiments on PPS are summarized in Table 6.1. In this section, the breakdown mechanism of PPS is discussed comparing with various existing theories.

Firstly, if we consider intrinsic breakdown[31] to be dominant, it might be impossible to explain such a considerably long time lag to breakdown as the order of 10^{-4} to 10^{-5} sec. Further, it can not be understood with this theory that F_B changed with voltage rising rate, electrode metal and ambient atmosphere. Then, the intrinsic theory is difficult to be taken as the breakdown mechanism of PPS. Zener breakdown process[32] can also be discarded by similar arguments.

Table 6.1. Breakdown characteristics of PPS.

temperature dependence	$\partial F_B/\partial T_0 \simeq 0$ (-196°C -- 200°C)
field rising rate dependence	$\partial F_B/\partial \alpha > 0$
electrode metal effect	F_B(Au cathode) $\gtrsim$ F_B(Al catode)
ambient atmosphere effect	F_B (in O_2) $\gtrsim$ F_B (in N_2, vacuum)
prestress effect	F_B decreases with both polarity of prestress field

F_B : electric strength , T_0: ambient temperature,
α : field rising rate .

A single avalanche breakdown theory can explain the temperature dependence of F_B, and the influence of electrode metal, and ambient atmosphere on the statistical time lag. An initial electron is supplied from electrode metal or traps in the bulk. The avalanche formation is expected to be affected by electron density either injected from the cathode or released from traps in the bulk. As mentioned in subsection 6-3-5, it is possible to release carrier from traps in the bulk by X-ray or photo illumination. However, neither F_B nor t_s varied with X-ray irradiation or photo illumination. This means that the electron liberation from traps in the bulk does not take part in the breakdown process of PPS. A single avalanche mechanism cannot also explain the long statistical time lag of the order of 10^{-4} sec compared with that usually accepted for avalanche breakdown.

The strong dependence of F_B on dV/dt and the relatively long time lag of the order of 10^{-4} sec can be qualitatively understood with thermal breakdown process. The behavior that F_B decreased with F_p for both the same and the reverse polarity prestress is also interpreted as a heating effect. The change in F_B with temperature was, however, so small that the thermal theory appears not to be applied to the experimental results. Nevertheless, provied the conduction current which plays an important role in thermal breakdown is controlled by a small temperature dependent process, the thermal breakdown process is not probably unreasonable; then the results on the effects of electrode metal and ambient atmosphere shown in the subsections 6-3-3 and 6-3-4 are also consistent with this consideration, taking into accout this type of the current. Thus, all the experimental results except the temperature dependence of F_B can be explained qualitatively in terms of thermal breakdown mechanism.

As discussed, only a single breakdown mechanism could not explain the breakdown characteristics of PPS. The experimental results shall

be discussed by using the multi-step breakdown process.

Redley[33] presented a breakdown model as follows: Conduction electrons injected by a tunnelling emission produce Joule's heat, with which positive ions are dissociated. They move towards the cathode to form positive space charge resulting in an increase in electric field in front of the cathode, which in turn accelerates electron emission from that electrode. This whole sequence of events act as positive-feedback and the breakdown occurs. However, since F_B of PPS was almost independent of temperature, it can not be considered that positive ions contribute to the breakdown process.

O'Dwyer[31] proposed the multi-step breakdown process as follows: Initially substantial collision ionization begins at a certain critical field within the bulk. Then the holes produced by collision ionization drift slowly towards the cathode and their space charges enhance the field near the cathode, which causes enhanced electron emission. The injected electrons cause further collision ionization. This whole events act as positive-feedback and the breakdown occurs by the greatly enhanced field strength in the vicinity of the cathode. The experimental results will be discussed below with this model.

The relatively long time lag of the order of 10^{-4} sec observed for PPS may be interpreted as the time requied for the formation of space charge of holes produced by collision ionization due to electron. If we assume a tunnelling emission as an injection process, the present experimental results can be explained with this model, such as the temperature and the voltage rising rate dependences of F_B, and the effects of ambient atmosphere taking into account the effective contact barrier at the metal-insulator interface. The prestress effect also can be understood consistently; assuming that the positive space charge is formed sufficiently deep into the bulk, F_B is expected to decrease with F_p for both polarity prestress due to the hetero

space charge effect. However, it becomes a serious problem whether the collision ionization might develop sufficiently and the positive space charge might be formed or not, in such very thin films as about several thousand Angstroms.

As can be seen by various discussions given above, the experimental results are unaccountable consistently with various existing theories. In the following chapter, a new model for the breakdown of PPS will be presented according to the fundamental instructions derived from the present study as summarized below:

i) The effects of electrode metal and ambient atmosphere mean that an injection process plays an important role in the breakdown.

ii) As a current multiplication process, impact ionization is considered, but not the conduction electron multiplication released from traps in the bulk, since the breakdown characteristics were not affected by temperature, X-ray irradiation or photo illumination.

iii) The considerably long time lag of about 10^{-4} sec means that the thermal breakdown criterion is preferred.

6-5 Conclusion

Electric breakdown of plasma polymerized styrene thin films was studied by taking advantage of self-healing. The electric strength F_B was obtained with varying temperature T_0, voltage rising rate dV/dt, prestress, ambient atmosphere and electrode metal. Some measurements were also made on time lag and under X-ray irradiation or photo illumination. The experimental results obtained are as follows: F_B was almost independent of temperature over -196 to 200°C, and was higher at high temperature than that reported for the conventional polystyrene film. F_B also strongly depended on dV/dt even in a slow rising rate.

The breakdown characteristics were influenced by electrode metal and ambient atmosphere, but not X-ray irradiation or photo illumination.

From the experimental results, the breakdown mechanism of PPS was discussed, comparing with existing breakdown theories. Consequently, any single breakdown process was not considered as the possible breakdown process. Further, the discussion on the breakdown was made by using the multi-step breakdown processes. It was found that although O'Dwyer's model of the cathode field enhancement by the positive space charge could explain some of the experimental results, serious problems remain regarding the long time lag, the development of electron avalanche and the formation of the positive space charge, in such very thin film as about several thousand Angstroms.

From the above considerations, the instructions important to present a new breakdown model were picked up : The breakdown of PPS will be determined by thermal breakdown criterion and greatly related to a temperature independent injection process.

References

[1] T.William and M.W.Hayes: Nature 19 769 (1966).

[2] R.W.Christy: J.Appl. Phys. 31 1680 (1960).

[3] P.White: Insulation 13 52 (1967).

[4] M.White: Vacuum 15 449 (1965).

[5] D.C.Allam and C.T.H.Stoddart: Chemistry in Britain 2 410 (1965).

[6] H.Carchano, R.Iacoste and Y.Segui: Appl. Phys. Lett. 19 414 (1971).

[7] Y.Segui, B.Ai and H.Carchano: J. Appl. Phys. 47 140 (1976).

[8] M.Shen: "Plasma Chemistry of Polymers" Marcel Dekker, New York (1976).

[9] G.Sawa, O.Ito, S.Morita and M.Ieda: J. Polym. Sci. 12 1231 (1974).

[10] G.Sawa, K.Suzuki, S.Morita and M.Ieda: J.Polym. Sci. 14 173 (1976).

[11] S.Sapieha, M.Kryszewski and J.Tomczyk: Int. Microsymp. on Polarization and Conduction in Insulating Polymers (Bratislava, 1972) pp.119.

[12] M.Kryszewski, W.Jablonski and S.Sapieha: Int. Microsymp. on Polarization and Conduction in Insulating Polymers (Bratislava, 1972) pp.125.

[13] V.Ya Airazov and V.G.Kobka: Sov. Phys. Tech. Phys. 16 1782 (1972).

[14] Y.Segui, Ai Bui and H.Carchano: Thin Solid Films 22 S.15 (1974).

[15] G.Sawa, K.Arakawa, M.Nagao and M.Ieda: Thin Solid Films 59 131 (1979).

[16] N.Klein and H.Gafni: IEEE Trans. Electron Devices ED-13 281 (1966).

[17] N.Klein: IEEE Trans. Electron Devices ED-13 788 (1966).

[18] N.Klein and N.Levanon: J. Appl. Phys. 38 3721 (1967).

[19] W.G.Oakes: Proc. Inst. Elect. Engrs. 96I 37 (1949).

[20] J.M.Meek and J.D.Craggs: " Electrical Breakdown of Gases " John. Wiley & Sons, New York (1978) Chapter 7.

[21] J.Artbauer and J.Griac: Proc. IEEE 112 818 (1965).

[22] Y.Inuishi and T.Suita: J. Inst. Elect. Engrs. Japan 74 150 (1954) [in Japanese].

[23] K.Arii, I.Kitani and Y.Inuishi: Trans. Inst. Elect. Engrs. Japan 93-A 313 (1973) [in Japanese].

[24] I.Kitani and K.Arii: Trans. Inst. Elect. Engrs. Japan 94-A 251 (1974) [in Japanese].

[25] P.Solomon, N.Klein and M.Albert: Thin Solid Films 35 321 (1976).

[26] T.Mizutani, Y.Takai, T.Osawa and M.Ieda: J. Phys. D: Appl. Phys. 9 2253 (1976).

[27] J.F.Fowler: Proc. Roy. Soc. 236 A 464 (1956).

[28] Y.Takai, T.Osawa, K.C.Kao, T.Mizutani and M.Ieda: Jpn. J. Appl. Phys. 14 473 (1975).

[29] Y.Takai, T.Ina, T.Mizutani and M.Ieda: Jpn. J. Appl. Phys. 14 1251 (1975).

[30] G.Sawa and M.Ieda: OYOBUTURI 48 1177 (1979) [in Japanese].

[31] J.J.O'Dwyer: " The Theory of Electrical Conduction and Breakdown in Solid Dielectrics " Clarenden Press, Oxford (1973).

[32] C.Zener: Proc. Roy. Soc. of London A145 523 (1934).

[33] B.K.Redley: J. Appl. Phys. 46 998 (1975).

Chapter VII A Model for Dielectric Breakdown Mechanism in Plasma Polymerized Styrene Thin Films

7-1 Introduction

In the previous chapter, experimental results of breakdown of plasma polymerized styrene thin films were presented, which were difficult to understand with a single breakdown process. Models of non-thermal breakdown produced by electronic impact ionization or by other processes were reviewed by Klein[1] on thin insulators. Thermal breakdown is also considered as a cause for thermal switching and breakdown phenomena[2]. There are many reports of dielectric breakdown on inorganic thin films such as thermally grown silicon dioxide [3], aluminum oxide[4] or silver sulphide, but not so many on organic thin films.

In this chapter, a new model followed by the instructions in the previous chapter is presented, in which the current is controlled by tunnelling emission from the cathode discarding space charge and the breakdown is governed by the impulse thermal process. In the same model, additionally, a steady state electron avalanche is considered as a possible bulk conduction.

7-2 Model of Breakdown and Basic Equations

A new breakdown model involves the following two fundamental processes; the current is controlled by tunnelling emission from the cathode and the bulk breakdown is governed by the impulse thermal process. To avoid complications, it is assumed that space charge and heat conduction towards the surroundings are neglected in the first state. The electron avalanche process and space charge effect will be discussed in detail in Section 7-4.

The differential equation is given below for the impulse thermal

breakdown

$$C_v \left(dT/dt \right) = j F, \tag{7.1}$$

where C_v is the heat capacity of the material per unit volume, T the absolute temperature, t the time, j the current density, and F the electric field.

As the current density in eq.(7.1), the Fowler-Nordheim tunnel injection[6] will be used, which is written in the form

$$j = A_{FN} F^2 \exp \left(-B_{FN}/F \right), \tag{7.2}$$

where

$$A_{FN} = 2.2\, e^2/(8 \pi h \Phi_D), \tag{7.3}$$

and

$$B_{FN} = 8 \pi (2m^*)^{1/2} \Phi_D^{3/2}/(2.92\, h\, e), \tag{7.4}$$

where e is the electronic charge, h Planck's constant, Φ_D the effective barrier height for electron injection, and m^* the mass of electron.

When the electric field rises linearly with time, i.e. $F = \alpha t$, eq.(7.1) can be transformed by using eq.(7.2) to

$$dT/dF = A_{FN} F^3 \exp \left(-B_{FN}/F \right)/C_v \alpha, \tag{7.5}$$

This ordinary differential equation can be solved numerially by using various methods, for instance, the Runge-Kutta-Gill method. In the following calculation, it is assumed that $C_v = 2.0 \times 10^6$ J/K·m^3 and m^* is identified with the mass of free electron, m_0.

7-3 Results of Calculation

A typical example of the temperature of the specimen as a function of the applied electric field for different values of α is

demonstrated in Fig.7.1, solving numerially eq.(7.5) with Φ_D = 0.95 eV. It is seen that the temperature rises suddenly when the field exceeds a certain value. The similar relationship between T and F when a ramp voltage is applied was attained in Chapter IV of the thesis, and by Vermeer[7]. In these cases, the ionic conduction, which involves the thermally activated processes, was employed. In the present model, Joule's heat is produced by the Fowler-Nordheim tunnelling emission current with a strong field dependence which leads to such a sudden temperature rise in a way similar to the case of the thermal activation process. Therefore, the theoretical electric

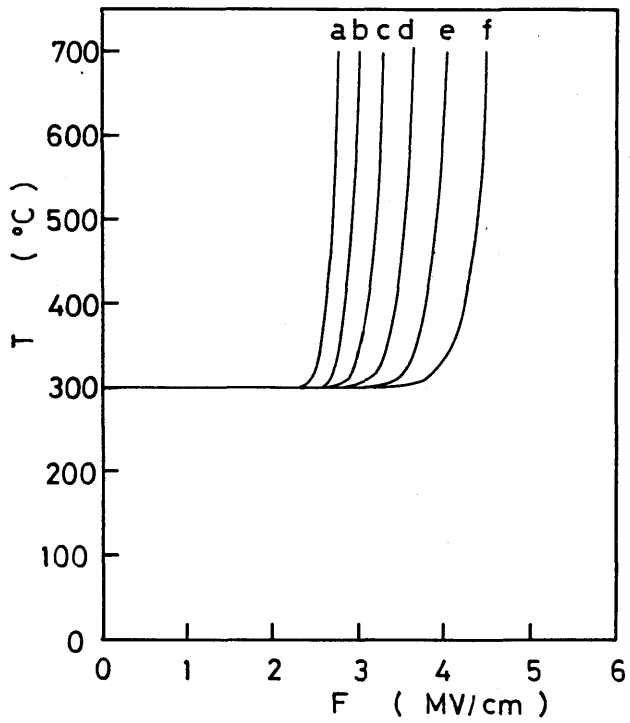

Fig.7.1. Theoretical relation between temperature T and applied field F for various field rising rate α. (a) 8.3 x 10^7 (V/m·sec) , (b) 8.3 x 10^8, (c) 8.3x10^9 ,(d) 8.3x10^{10} , (e) 8.3x10^{11}, and (f) 8.3x10^{12}.

strength can well be determined without exactly defining the critical temperature T_c required for breakdown. In the following calculation, T_c is taken as 550 K, for convenience. The effective barrier height Φ_D, which is now the only parameter, will be estimated by fitting the theoretical results to the experimental ones. The theoretical dependence of F_B on the initial temperature, designated by T_0, was calculated for different values of Φ_D at α of 8.3×10^{11} V/m·sec. The result is illustrated in Fig.7.2. The experimental values are also indicated by filled circles in this figure. In thermal breakdown, a negative temperature dependence of F_B has been generally expected. It can be seen, however, that in this model F_B is almost constant over the wide range of temperature between 0 and 200°C, being consistent with the experimental results. The reason for this is considered to

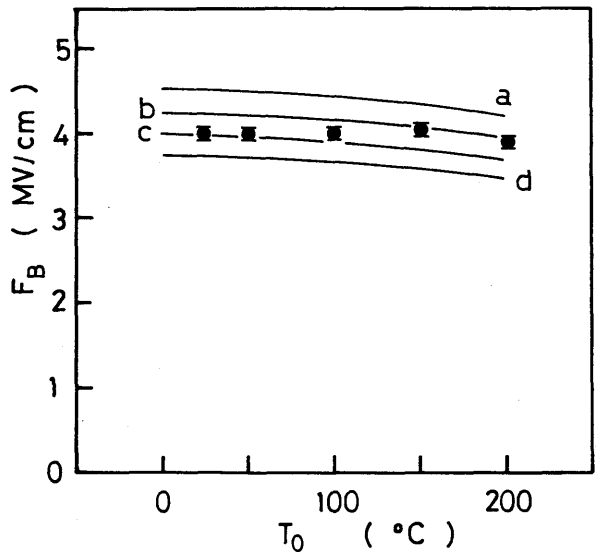

Fig.7.2 Theoretical temperature dependence of F_B with effective barrier height Φ_D as a parameter. Filled circles represent experimental values for Au-PPS(2300Å)-Au. (a) Φ_D = 1.05 eV, (b) 1.0 , (c) 0.95 , and (d) 0.9.

be the temperature independent nature of current density j in eq.(7.1). The best fit of the theoretical curve to the breakdown data for PPS sandwiched with gold electrodes is attained when Φ_D is 1.0 eV.

Figure 7.3 shows the teoretical relation between F_B and α at 300 K varying Φ_D as a parameter, together with the experimental results indicated by filled circles. This calculated relationship agrees well with the experimental one, too, provided Φ_D is 0.9 eV.

The calculation of prestress effect on F_B was also carried out, taking Φ_D as a parameter and varying the prestress time t_p. Figure 7.4 shows one of the results when t_p = 500 μsec, together with the experimental values when t_p = 520 μsec. As can be seen, this model can give a satisfactory agreement to the experimental fact, not only

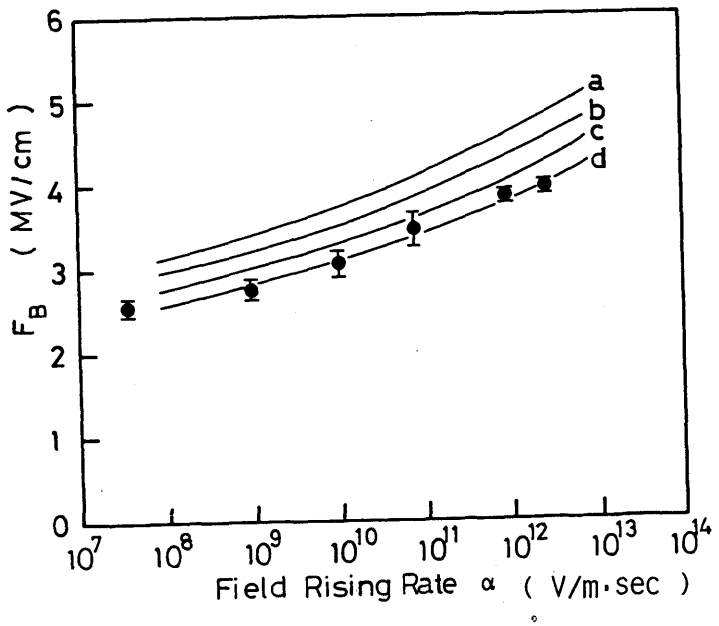

Fig.7.3. Theoretical relation between F_B and field rising rate, α, for different values of Φ_D. Filled circles represent experimental values for Au-PPS(2600Å)-Au. (a) Φ_D = 1.05 eV, (b) 1.0 , (c) 0.95, and (d) 0.9.

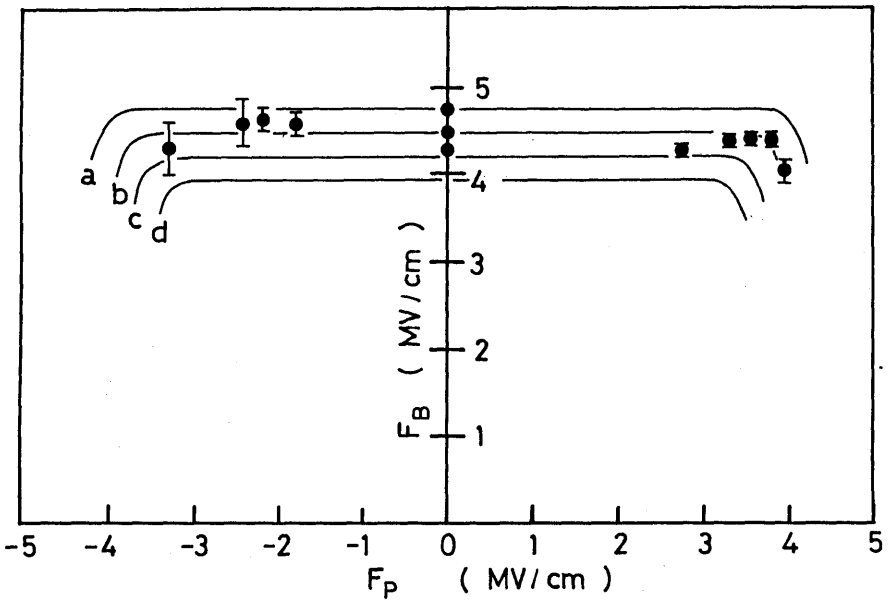

Fig.7.4. Theoretical relation between electric strength F_B and prestress field F_p for different values of effective barrier height Φ_D, and for prestress time, t_p, of 500 μsec. Filled circles represent experimental values when t_p = 520μsec for Au-PPS(3000Å)-Au. (a) Φ_D = 1.1 eV, (b) 1.05, (c) 1.0 , and (d) 0.95.

qualitatively but also quantitatively, that F_B decreases with prestress field of either polarity, when Φ_D = 1.05 eV.

The time lag to breakdown when a step voltage is applied is analysed. The theoretical time lag to breakdown t_{BS} in this model obtained by integrating eq.(7.1) with a constant electric field and using eq.(7.2) for current density is

$$t_{BS} = C_v (T_c - T_0) / A_{FN} F^3 \exp (- B_{FN}/F). \quad (7.6)$$

The theoretical dependences of t_{BS} on electric field F and initial temperature T_0 for Φ_D = 0.95 eV are shown in Figs. 7.5 and 7.6,

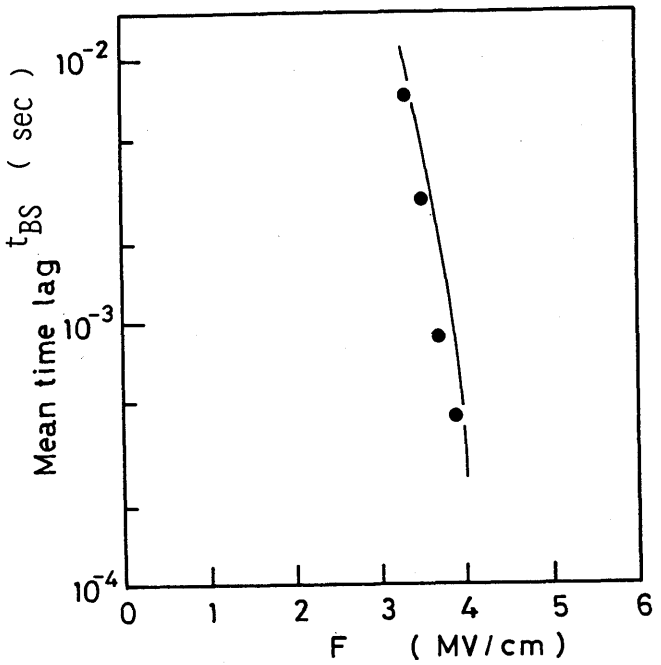

Fig.7.5. Theoretical relation between mean time lag to breakdown and applied field F for effective barrier height Φ_D of 0.95 eV. Filled circles represent experimental values for Au-PPS((2600Å)-Au.

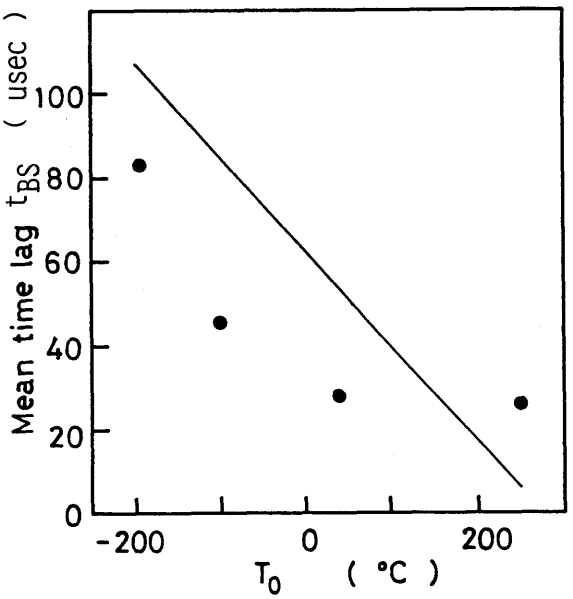

Fig.7.6. Theoretical relation between time lag and initial temperature T_0 for effective barrer height Φ_D of 0.95 eV. Filled circles represent experimental values for Au-PPS(3500Å)-Au.

respectively. The experimental values of the time lag were regarded as the sum of the statistical and formative time lags which are estimated from the Laue plots, since the statistical component is not clearly defined in the thermal breakdown. Calculated and observed relations between t_{BS} and field F agree closely. The theoretical initial temperature dependence of t_{BS} somewhat differs from the experimental one in the temperature range above room temperature.

This simple model can give a quntitative explanation to all the experimental data on PPS such as dependence of F_B on T_0, α, prestress, and time lag except initial temperature dependence of t_{BS}, provided Φ_D is about 1.0 eV which gives the best fit to the breakdown data. The cathode electrode metal and ambient atmosphere effects are consistent with this model and interpreted qualitatively in terms of the variation of Φ_D as described in the previous chapter. Namely, Φ_D for gold-polymer contact is higher than for aluminium-polymer one and thus the current injected into the bulk from the Au cathode is reduced, which leads to a decrease in Joule's heat with a consequent increase in F_B. Provided surface states introduced by oxygen gas raise Φ_D and hence depress electron emission from the cathode, F_B in O_2 gas is increased following this model.

7-4 Discussion

In the previous two sections a new model of breakdown for PPS was presented and analysed numerically. It was concluded that this simple model, consisting of the Fowler-Nordheim tunnelling emission current and the impulse thermal process, can fully explain the experimental results not only qualitatively, but also quantitatively when the effective barrier height for electron is about 1.0 eV. This simple model, however, includes some problems to be solved, which are discussed in this section.

7-4-1 Injection Process

The physical basis of the estimated value of Φ_D will be discussed. In order to know the nature of charge injection, measurements on photoconductivity were made. From Fowler Plots[8], i.e. the relationship between incident photon energy and a square root of photocurrent, the threshold energy for electron injection at zero field was estimated to be 2.93 eV by assuming a lowering of potential barrier due to Schottky effect. There is a large difference between the fitting parameter (about 1 eV) and the value obtained from the photocurrent (2.93 eV). One of the reasons for this would be in the fact that the former is valid at high fields near breakdown, while the latter at zero field. Further discussion on this difference in Φ_D is given below.

Equation (7.2) of the Fowler-Nordheim tunnelling emission current density is deduced in the exact sense by assuming a rectangular barrier and an applied voltage to be much higher than the barrier height at 0 K. Actually the tunnelling probability somewhat changes with a variation of a barrier shape due to various factors such as temperature and image force.

Simmons[9] calculated the tunnel probability for a rectangular barrier by considering image force and consequently derived an equation for the injection current density modified by this effect. The maximum potential barrier height was found to be scarcely changed with this modification.

Then, the role of the effective mass m^* in eq.(7.2) was examined. Calculations were carried out again, making Φ_D a constant of 2.93 eV and varying m^* as a parameter in this case. Consequently, m^* was estimated to be about 0.1 m_0 by curve fitting. In a polymer which consists of both amorphous and crystalline parts, electronic states are so complex that it is difficult to introduce a concept of band structure just like in a perfect crystal. Although many studies on

electronic states in polymers have been carried out, much remains unknown in its details. With regard to polyethylene, a few works on the effective mass have been reported[10,11]. Falk[10] estimated the effective mass of electron m^* of polyethylene to be 0.03 m_0 from the theoretical calculation, and McCubbin[11] also calculated m^* = 0.5 m_0. Although there is no reports on m^* for PPS and the physical meaning of m^* = 0.1 m_0 is not clarified, the value is compatible with that for polyethylene. From the above consideration, it is found that the effective barrier height Φ_D = 2.93 eV obtained from the photoconductivity measurement is not unreasonable, provided m^*=0.1m_0. However, further investigation on actual electronic states or mobility of electron for PPS will be required.

Various models for a tunnelling process in which Φ_D is lowered effectively have been presented. Riten et at.[12] discussed a multi-step tunnelling pass for current transport process of nGe-pGaAs heterojunctions on the basis of Anderson model for abrupt heterojunctions. Mahan et al.[13] proposed a model for a highly nonlinear conduction in ZnO varister. In this case, the electron tunnelling is triggered by hole creation in ZnO when the conduction band in the grain interior drops below the top of the valence band at the grain interface. If these effects are taken into account, a possible explanation may be given to the difference of Φ_D obtained from two different ways.

On the other hand, Sanchez[14] et al. have reported that the effective barrier height is about 0.9 eV for Au-PPS contact from voltage capacitance characteristics measurement. This value agrees well with that estimated theoretically in the previous section. Since at present there remain uncertainties about the estimated values of both Φ_D and m^*, further examinations on the above respects are expected to be attempted.

7-4-2 Impulse Thermal Process

As shown in Chapter II, the fundamental equation of thermal breakdown is given as follows:

$$C_v \left(\partial T/\partial t \right) - \mathrm{div} \left(\kappa \, \mathrm{grad} \, T \right) = j F, \qquad (7.7)$$

where κ is the thermal conductivity of the material. When the voltage duration t_B is sufficiently shorter than $C_v d^2/\kappa$, which is denoted by t_{th}, the second term on the left-hand side, i.e. the heat conduction term, can be ignored, and eq.(7.7) is same as eq.(7.1) approximately[15]. Here, t_{th} is referred to as the thermal time constant of the material. Substituting the values for PPS, t_{th} is evaluated to be about 1 μsec. t_B has been found to be more than a several hundreds μsec under the experimental conditions as described in Chapter VI. Since t_{th} is shorter than t_B, it appears to be unreasonable to apply the impulse thermal theory to the experimental results.

The second term of the left-hand side describes the heat conduction only in the bulk, and the necessary condition for applying impulse thermal breakdown is that $t_B << t_{th}$ when the heat dissipation to the surroundings is ideally complete. A heat transfer coefficient from the dielectric surface to the ambient must be incorporated. In Chapter V, the theoretical relation between λ and F_B was calculated by adopting one dimensional form of eq.(7.6) and ionic conduction. As a conclusion, eq.(7.1) holds to a fairly good approximation even if $t_B > t_{th}$, provided λ is smaller than a certain critical value.

7-4-3 Electronic Impact Ionization Process

In the previous section, the injection process and the impulse thermal one were only considered, so that the bulk processes such as impact ionization and recombination etc. were neglected. In this

subsection, electronic impact ionization and hole removal by drift are considered as a possible bulk conduction. O'Dwyer[16] computed the steady state conduction and showed that a region of negative resistance on V vs. j curve appears, which is referred to as the current controlled instability with dielectric breakdown. The above bulk process will be introduced into the breakdown model given in Section 7-3.

O'Dwyer's steady state conduction model, which is summarized in Chapter II, is expressed by the following set of differential equations[16]:

$$dj_n/dx = -\alpha_n j_n \exp(-H/F)/\mu_n F, \tag{7.8}$$

$$dF/dx = (j - j_n)/\varepsilon_0 \varepsilon_r \mu_p F, \tag{7.9}$$

where j_n is the electron current density, μ_n and μ_p are the effective average mobilities referring to carriers in conduction levels and traps, respectively, $\alpha_n \exp(-H/F)$ and H are the ionization coefficient and a constant field strength, respectively, j the total current density, and $\varepsilon_0\varepsilon_r$ the dielectric constant of the material. In deriving eqs.(7.8) and (7.9) following assumptions are made: The electrons are assumed to have a much greater mobility than the holes, and they alone cause impact ionization. The displacement and the diffusion currents of both types of carriers are neglected. The cathode emits electrons following the Fowler-Nordheim law, and the anode blocks the emission of holes. The conduction current and the breakdown characteristics were calculated, making $\varepsilon_0\varepsilon_r = 8.85 \times 10^{-12} \times 3$ F/m, H = 10 MV/cm and varying the other parameters. As mentioned, O'Dwyer took the appearance of negative resistance as a breakdown criterion. However, in order to explain the time dependence of F_B obtained from the experimental results, it is required to introduce the former breakdown criterion such as impulse thermal breakdown.

Figure 7.7 shows a typical example of the theoretical current density as a function of the electric field for different values of hole mobility μ_p, with the other parameters constant. The tunnelling emission current density is also shown in this figure with a broken line. Theoretical field distribution in the bulk under the same conditions as in Fig.7.7 is illustrated in Fig.7.8. As can be seen from these figures, smaller the value of μ_p, i.e. slower the rate at which holes are removed from the insulator, larger is the amount of space charge accumulated in the bulk, enhancing the cathode field.

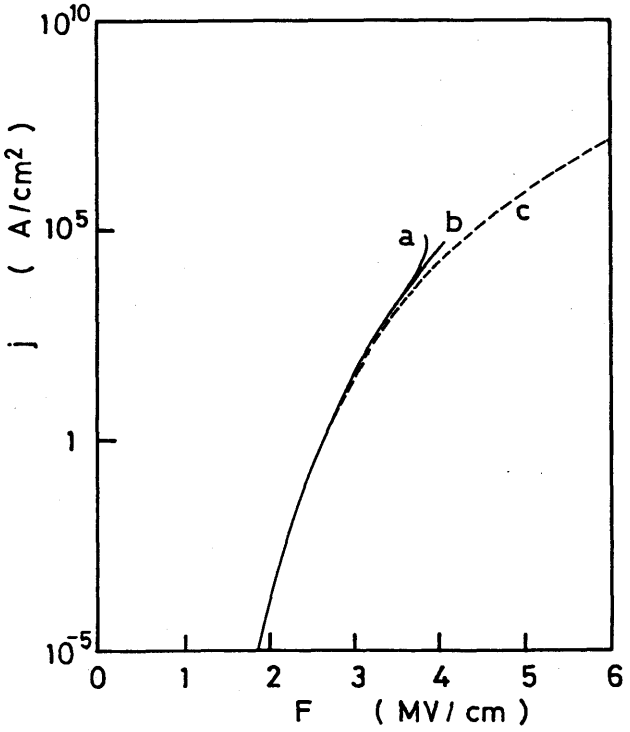

Fig.7.7. Theoretical current-field characteristics for different hole mobilities μ_p; (a) $\mu_p = 10^{-8}$ $m^2/V.sec$ and (b) 10^{-7} to 10^{-4}, for $\alpha_n/\mu_n = 10^{16}$ V/m^2 and Φ_D = 1.0 eV. (c) The broken line represents Fowler--Nordheim tunnelling emission current density.

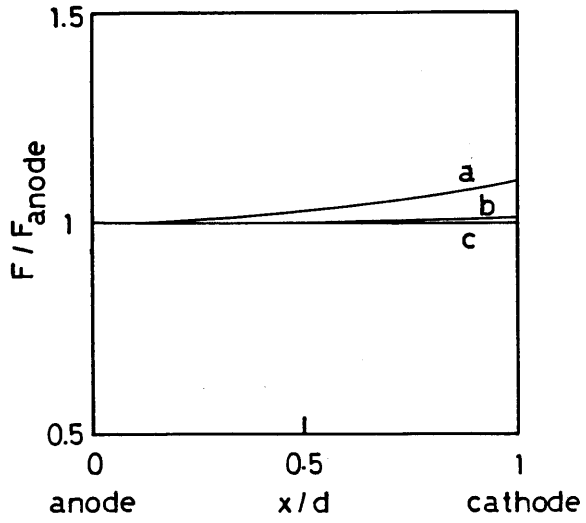

Fig.7.8. Theoretical field distribution in the bulk for different values of hole mobilities μ_p. Field is normalized by anode field, and distance from anode is also normalized by thickness of film d (3000Å): (a) μ_p = 10^{-8} m^2/V.sec, (b) 10^{-7}, and (c) 10^{-6} to 10^{-4}.

This leads to the occurrence of a negative resistance region. Using the total current density and the field distribution obtained in this way, eq.(7.5) was solved numerically. The theoretical impulse thermal breakdown strength was determined as a critical field when the maximum temperature in the bulk reaches T_c.

Figrue 7.9 shows a typical result of the calculated relation between F_B and μ_p at 300 K, where α is taken to be 8.3 x 10^{11} V/m·sec, and α_n/μ_n and Φ_D are changed widely. In the figure, broken lines represent F_B decided by the impulse thermal criterion and solid lines by a negative resistance. It is seen that the impulse thermal breakdown becomes dominant above a certain critical value of μ_p for each value of α_n/μ_n, and F_B decided by the impulse thermal breakdown is almost constant for constant Φ_D. Considering to fit the theoretical electric strength to the experimental one (4MV/cm) and to take the

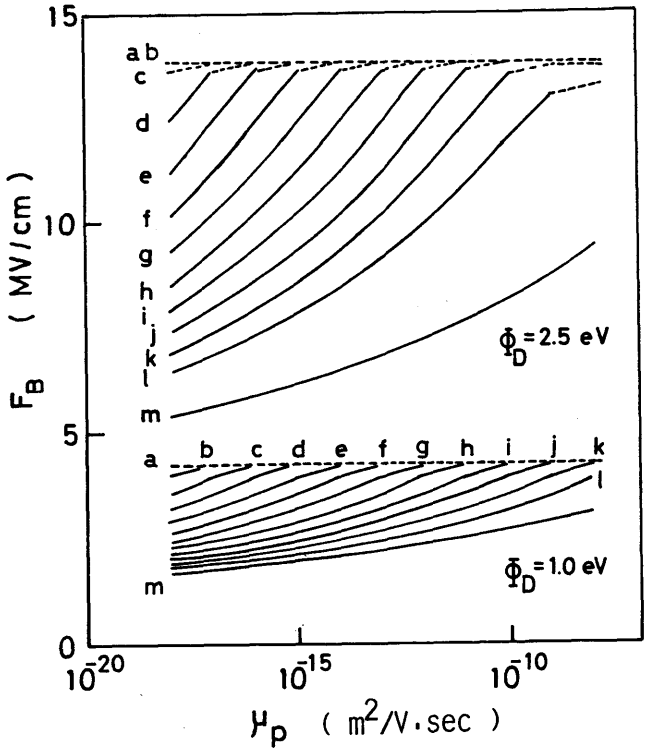

Fig.7.9. Theoretical electric strength F_B as a function of hole mobility μ_p for different values of effective contact barrier height and α_n/μ_n. Broken lines represent values of F_B decided by thermal breakdown criterion, and solid lines represent those by negative resistance criterion. (a) $\alpha_n/\mu_n = 10^5$ V/m^2, (b) 10^6, (c) 10^7 , (d) 10^8, (e) 10^9, (f) 10^{10}, (g) 10^{11}, (h) 10^{12}, (i) 10^{13}, (j) 10^{14}, (k) 10^{15}, (l) 10^{16}, and (m) 10^{17}.

impulse thermal breakdown as a breakdown criterion, Φ_D must be 1.0 eV and μ_p must be beyond a certain value for a constant α_n/μ_n.

The dependences of F_B on temperature, field rising rate and pre-stress were also calculated for different values of μ_p. It was found from these results that the best fit of the theoretical data to the experimental results is also obtained when Φ_D is 1.0 eV. This result agrees well with the simple impulse thermal breakdown model neglecting the bulk process. It follows that provided μ_p is beyond a certain

value, the space charge is scarcely formed, giving a physical basis for neglecting the space charge in the model presented in the previous section.

Other parameters μ_n, μ_p and α_n will be discussed below. Various values of μ_n have been reported[17] for polymers, inorganic materials and ionic crystals. If electrons are assumed to cause impact ionization and traverse through the extended zone in the conduction band, it may be reasonable to let μ_n be 10^{-3} $m^2/V \cdot sec$[18]. If λ_e represents the mean free path for phonon collision in the field direction, the ionization coefficient α_n can be written in the form by assuming a single electron ionization

$$\alpha_n = \mu_n F/\lambda_e. \tag{7.10}$$

Although the exact value of λ_e unknown, if it is assumed to be 400 Å, which is not unreasonable in comparison with that reported for other insulating materials[17,19], α_n/μ_n is evaluated to be 10^{16} V/m^2 using eq.(7.10) with F = 4 MV/cm.

If the above values are valid, from Fig.7.9 μ_p must be larger than 10^{-7} $m^2/V \cdot sec$, above which the impulse thermal breakdown can occur before a negative resistance appears, and a close agreement between calculated and observed values is obtained. The same α_n/μ_n was already used in the calculation of the current-field characteristics and the field distribution shown in Figs.7.7 and 7.8, respectively. Since μ_p is assumed to be much smaller than μ_n in the impact ionization model, 10^{-7} $m^2/V \cdot sec$ may be a proper value as μ_p. The parameters estimated from the impact ionization model are summarized as follows: Φ_D = 1.0 eV, $\alpha_n/\mu_n = 10^{16}$ V/m^2 and $\mu_p = 10^{-7}$ $m^2/V \cdot sec$.

7-5 Conclusion

In this chapter, a new simple breakdown model was presented on

the basis of the experimental results on plasma polymerized styrene thin films. In this model, the current is controlled by the Fowler-Nordheim tunnelling emission from the cathode and the bulk breakdown is governed by the impulse thermal process. The numerically calculated values by discarding the space charge can be fitted to the dependence of the temperature, field rising rate and prestress on the electric strength and time lag to breakdown. The value of the effective barrier height Φ_D for the electron injection was estimated to be 1.0 eV by fitting the theoretical electric strength to the experimental one. A steady state electron avalanche was considered as a possible bulk conduction. It was found that provided the mobility of positive holes is beyond a certain critical value, the space charge is scarcely established, giving a physical basis for neglecting the space charge in the breakdown model. Also, the impulse thermal breakdown can occur before a negative resistance appears. The parameters involved in the modified model were also discussed and estimated to be as follows: Φ_D = 1.0 eV, $\alpha_n/\mu_n = 10^{16}$ V/m^2 and $\mu_p = 10^{-7}$ m^2/V·sec.

References

[1] N.Klein: Thin Solid Films 50 223 (1978).

[2] L.Altcheh and N.Klein: Trans. IEEE Electron Devices 20 801 (1973).

[3] P.Solomon: J.Vac. Sci. Technol. 14 1122 (1977).

[4] H.H.de Wit, Ch.Wijenberg and C.Crevecoeur: J.Electrochem. Soc. 123 1479 (1976).

[5] S.P.Sharma and J.H.Thomas: J. Appl. Phys. 47 1808 (1976).

[6] R.H.Fowler and L.Nordheim: Proc. Roy. Soc. A119 173 (1928).

[7] J.Vermeer: Physica 12 1269 (1956).

[8] R.H.Fowler: Phys. Rev. 38 45 (1931).

[9] J.C.Simmons: J. Appl. Phys. 34 1793 (1963).

[10] J.E.Falk and R.J.Fleming: J. Phys. C: Solid Stat. Phys. 6 2954 (1973).

[11] W.L.McCubbin and R.Manne: Chem. Phys. Lett. 2 230 (1968).

[12] A.R.Riten and D.L.Feucht: Solid-State Electronics 9 1055 (1966).

[13] G.D.Mahan, Lionel M.Levinson and H.R.Philipp: J. Appl. Phys. 50 2799 (1979).

[14] D.Sanchez, M.Charchano and A.Bui: J. Appl. Phys. 45 1233 (1974).

[15] J.J.O'Dwyer: " The Theory of Electrical Conduction and Breakdown in Solid Dielectrics " Clarenden Press, Oxford (1973).

[16] J.J.O'Dwyer: Trans. IEEE Elect. Insulation EI-15 264 (1980).

[17] J.J.O'Dwyer: J. Phys. Chem. Solid 28 1137 (1967).

[18] M.Miyairi, S.Yamauchi, G.Sawa and M.Ieda: Trans. Inst. Elect. Engrs. Japan 91-A 1962 (1971) [in Japanese].

[19] P.G.LeComber and W.E.Spear: Phys. Rev. Lett. 25 509 (1970).

Chapter VIII Electrical Breakdown of Polyethylene

8-1 Introduction

Many reports on the dielectric breakdown of polyethylene (PE) have so far been published. The essential feature of the temperature dependence of the electric strength F_B of PE is schematically given in Fig.8.1[1]. The temperature range can be classified into three parts: Region I, II, and III, each of which corresponds to the different molecular states of PE.

In Region I, molecular state of PE is glass-like as microbrownian motion of molecular chains in amorphous parts is frozen. F_B scarcely varies with temperature[2-5] and increases with introducing polar group[6], and impurity with rich π electrons[7] and also with decreasing crystallinity[8,9]. From these results, as well as that on the time lag[10], the electron avalanche breakdown process is thought dominant in this region. Nagao[11] investigated the influence of the

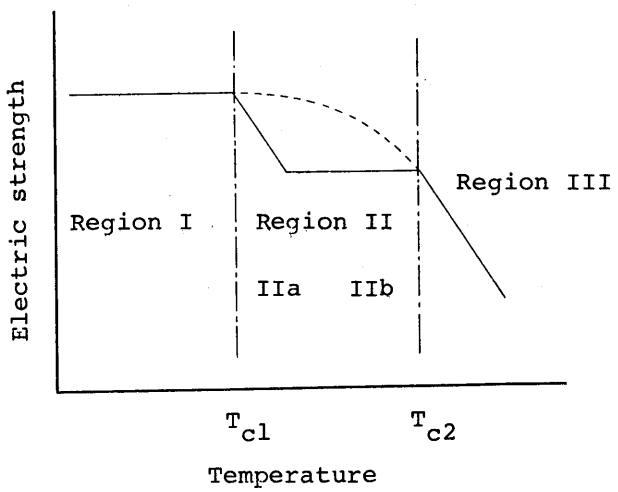

Fig.8.1. Outline of the temperature dependence of electric strength of PE.

nature of individual crystallite on the breakdown of PE with film specimens of PE and ethylene-vinyl acetate composite polymers. He suggested that at -80°C the electron avalanche develops over the region much greater than the size of individual crystallite but less than 15 μm, and the initial electron is supplied from bulk PE.

In Region II, microbrownian motion of molecular chains in amorphous parts is released, and the amorphous parts represent a rubber-like state. In this region, Fröhlich's original amorphous breakdown theory[6,12], and its modified theory[13], the electron avalanche theory[14], and the free volume breakdown theory[15-17], are suggested to be applicable. In Region IIa, a strong temperature dependence of F_B is observed related to the molecular motion in the glass-rubber transition region. In Region IIb, F_B scarcely depends on temperature and thickness[8,11,13], and decreases with increasing crystallinity[13]. A tentative model for the breakdown process was presented[11] in which the released molecular motion enhances the electron transport across the amorphous parts. In this model, the time variation of intermolecular barrier and of trap level due to molecular motion was taken into consideration. However, it was found that the dominant breakdown process in this region is varied with the wave form of the applied voltage[14] and also space charge effect cannot be neglected[18]. Further investigations are, therefore, required.

In Region III, the critical temperature T_{c2} (see Fig.8.1) for high density PE is reported to be higher than that for low density PE [11,14]. The electric strength F_B increases with cross-linking[19] due to increase of the softening point. These results suggest that electromechanical breakdown due to Maxwell stress occurs. It was also suggested from the relation between pre-breakdown current and F_B that thermal breakdown process is dominant[20]. Electronic thermal breakdown was also considered as a dominant breakdown process after

eliminating the effect of the electromechanical deformation[21].

As mentioned above, much experimental works have been made on the dielectric breakdown of PE. However, the breakdown process of PE is still not completely understood in temperature region above room temperature. This has been mainly because of its highly complex structure and a presence of unknown additives. In order to solve this problem, it is necessary to elucidate the correlation between the electric strength and the inherent nature of the polymer, such as chemical structure, molecular motion, structural irregularities, and presence of additives, etc..

In this chapter, the influence of the polymer morphology on the electric strength is investigated, focussing attention to high temperature region. The effect of the solid structures such as crystallinity and density to the electric strength is discussed firstly. Next, the relation between cross-linking by silane and F_B is discussed.

8-2 Experimental Procedure

Measurements were made on films of about 20 or 30 μm in thickness by using a ramp voltage or a rectangular pulse voltage. Detaied description of the samples is given along with experimental results. Unless otherwise noted, the direct voltage was increased at a rising rate of 500 V/sec, and the amplitude of succesive pulses with about 0.2 μsec rise time and 5 μsec width was increased by a step of 50 V/pulse at a repetition rate of 10 Hz. Gold electrodes with diffused edges were applied on both sides by vacuum deposition (Fig.8.2) to prevent occurrence of partial discharge due to a concentrated electric field. Samples were immersed in a suitable liquid, liquid nitrogen at -196°C and silicone oil at the other temperatures, kept at a constant temperature.

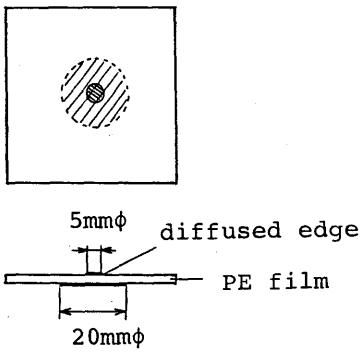

Fig.8.2. Film specimen.

8-3 Solid Structure and Electrical Breakdown

8-3-1 Results

Samples used were of approximately the same melt flow ratio related to molecular weight but with different melting point. These properties are summarized in Table 8.1.

Figure 8.3 shows the temperature dependence of electric strength F_B of these samples by applying the ramp voltage over a temperature range from room temperature to melting points. From this figure, F_B at room temperature and 95°C are replotted as a function of density and melting point in Figs.8.4 and 8.5, respectively. It is seen from Fig.8.3 that the critical temperature T_{c2}, which is defined as the temperature where the steep fall of F_B begins, shifts to a higher temperature with increasing density and melting point. On the other hand, F_B at room temperature decreases with increasing density and melting point. The behavior of F_B at 95°C is opposite. The temperature dependence of F_B under the application of rectangular pulse is shown in Fig.8.6 to 8.9. The results by ramp voltage are also included by filled circles for comparison. As can be seen, in all samples, F_B obtained by applying the pulse voltage is slightly higher or

Table 8.1. Physical parameters of PE.

	Density (g/cm^3)	Tm (°C)	M.F.R. (g/10min)
PE-1	0.917	110	1.0
PE-2	0.926	118	1.5
PE-3	0.928	128	1.0
PE-4	0.951	137	1.0
PE-5	0.920	124	1.5

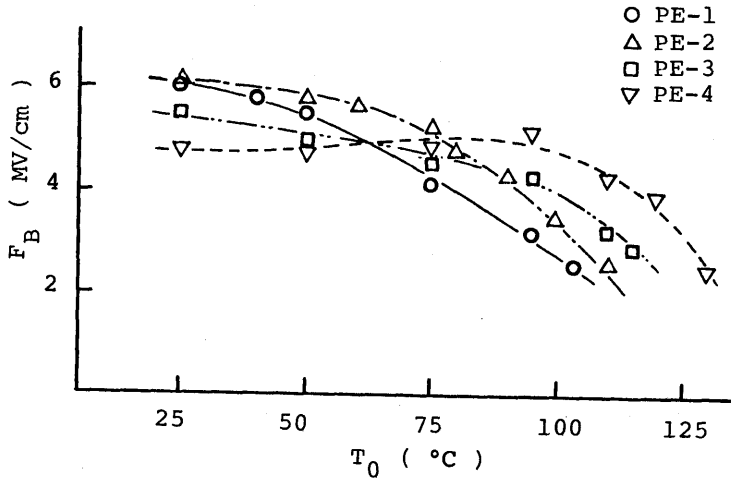

Fig.8.3. Temperature dependence of electric strength of the four kinds of films by applying a ramp voltage at voltage rising rate of 500 V/sec.

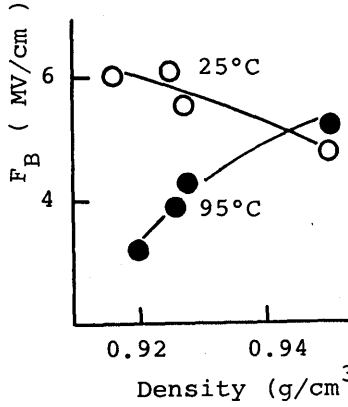

Fig.8.4. Relation between F_B and and density.

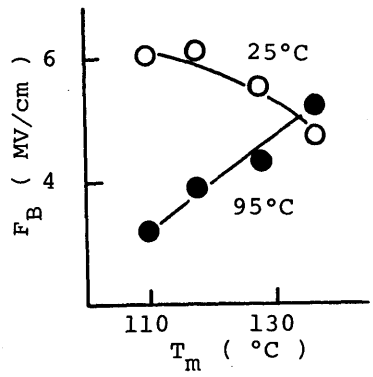

Fig.8.5 Relation between F_B melting point.

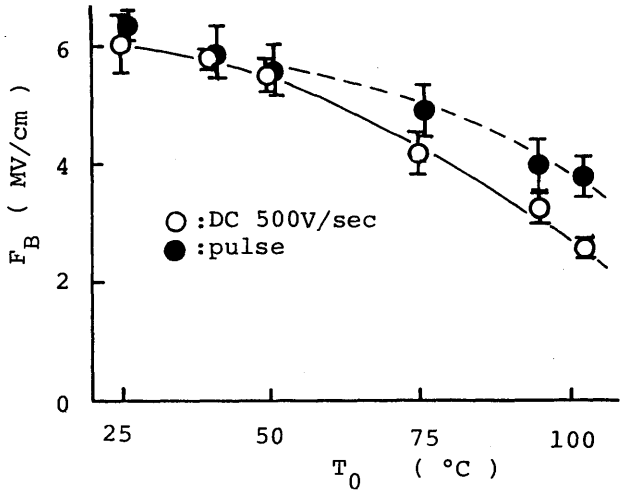

Fig.8.6 . Temperature dependence of electric strength for PE-1.

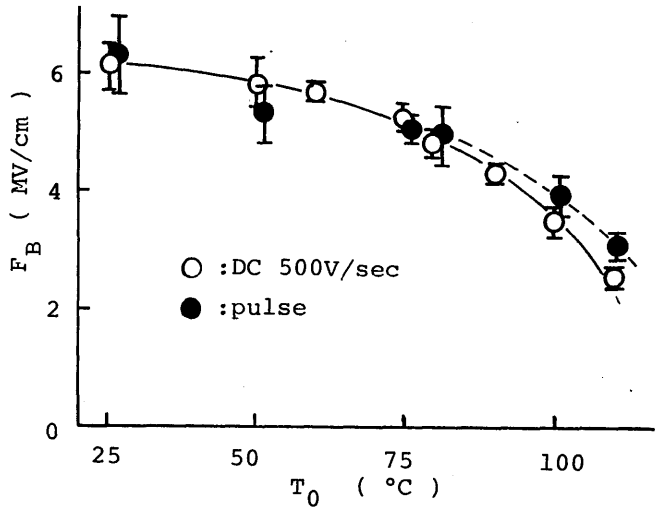

Fig.8.7. Temperature dependence of electric strength for PE-2.

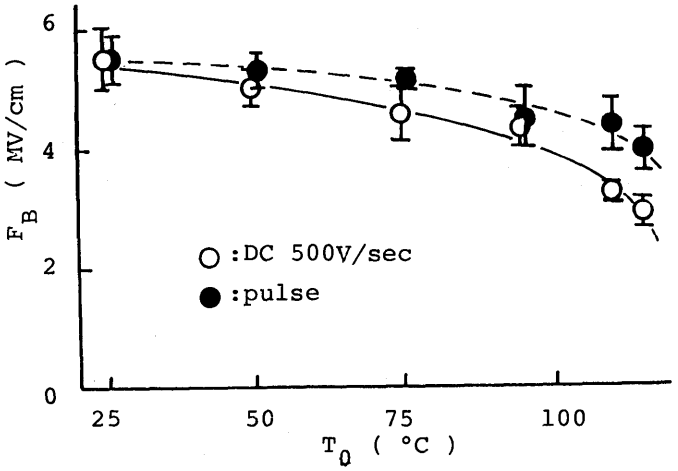

Fig.8.8. Temperature dependence of electric strength for PE-3.

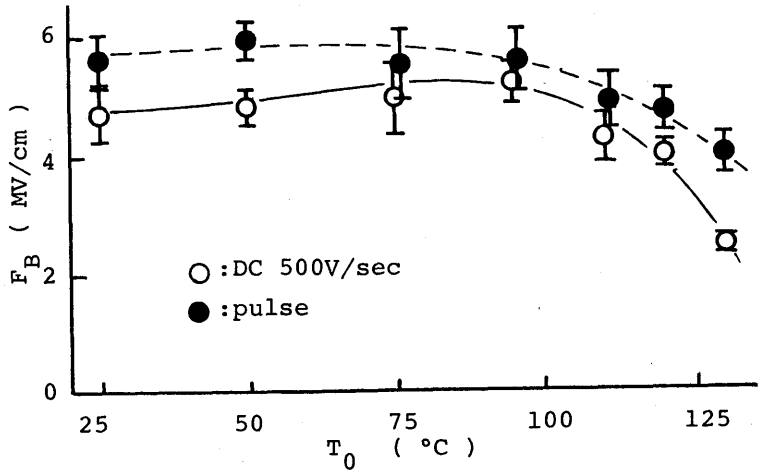

Fig.8.9. Temperature dependence of electric strength for PE-4.

nearly equal to that obtained by applying the dc ramp voltage, while this difference in the electric strength becomes larger above T_{c2}.

8-3-2 Discussion

In room temperature region, F_B decreased with increasing density. This result can be compared with the recent result[13] on the effect of the degree of crystallinity on the electric strength. In this reference[13], the degree of crystallinity was changed by varying the annealing condition on the same high density PE samples and a qualitative explanation was given employing the modified Fröhlich's electronic thermal breakdown theory. In this model, the depth of shallow trap levels for electrons was postulated to increase with crystallinity[13]. However, F_B of PE-1 varied with voltage duration over the range from 1 μsec to about few seconds as shown later. Therefore, it is difficult to understand the breakdown of PE in room temperature region simply in terms of the electronic thermal breakdown.

In a temperature range above T_{c2}, the variation of the electric strength with temperature appears to be closely related to the melting process of the crystallites, since the critical temperature T_{c2} has

been found to increase with increasing melting point, T_m. It was suggested[22] that an increase in amorphous region at high temperatures due to the melting of the crystallites causes an increase in ionic conductivity. One possibility of the breakdown mechanism at high temperatures would be thermal breakdown due to an increase in ionic conductivity. Another possibility is formation of ionic space charge near the cathode, leading to an enhancement of the field in the vicinity[23]. These two interpretations are consistent with the dependence of F_B on the duration of voltage application. On the other hand, an increase in amorphous part with temperature also introduces a lowering of Young's modulus of the sample. Electromechanical deformation of the sample caused by Maxwell stress is also, therefore, possibly responsible for the breakdown process.

In order to get a more detailed information, the electric strength of PE-1 was investigated, varying the voltage duration over a wide range from 1 μsec to few seconds. Applied voltage was obtained by transforming a rectangular pulse voltage to a ramp voltage with charging of a capacitor through a resistor which could be varied to attain different rise time. Breakdown occurred during the wave front of the impulse voltage. Voltage across the specimen after being divided by means of high voltage probe was measured with a digital voltmeter (FUJI SEIMITSU DENKI, PPV-9A) through a peak hold circuit. Time to breakdown t_{BR} was determined from the time constant of the circuit, the magnitude of the rectangular pulse, and the breakdown voltage.

Figures 8.10 to 8.13 show the electric strength of PE-1 as a function of t_{BR} for different temperatures. In each figure, tha data at t_{BR} of about 10 sec are the results obtained by applying a ramp voltage at 500 V/sec as shown earlier. At -196°C, F_B is almost independent of t_{BR}, at 30 and 60°C, F_B shows a maximum at t_{BR} of about 100

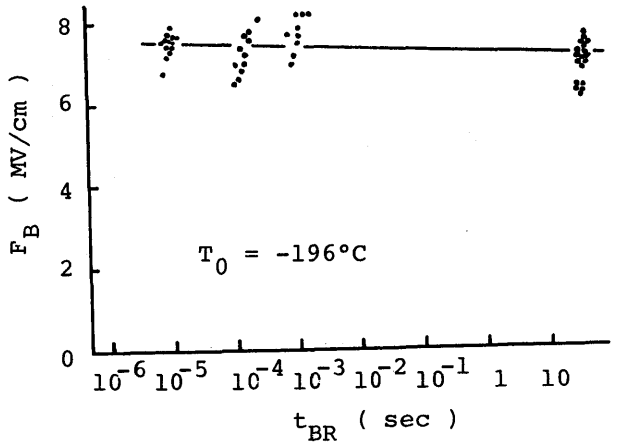

Fig.8.10. Electric strength as a function of voltage duration at -196°C.

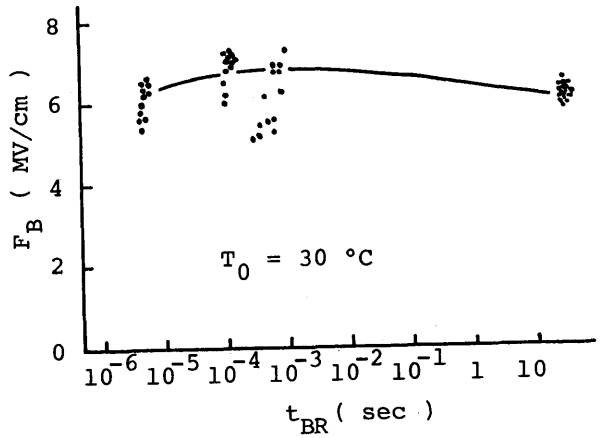

Fig.8.11. Electric strength as a function of voltage duration at 30°C.

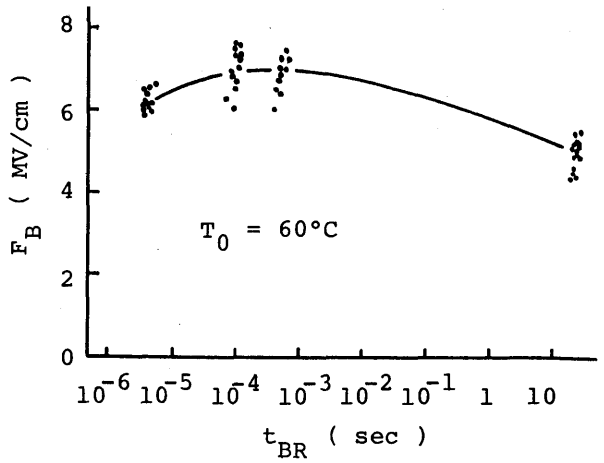

Fig.8.12. Electric strength as a function of voltage duration at 60°C.

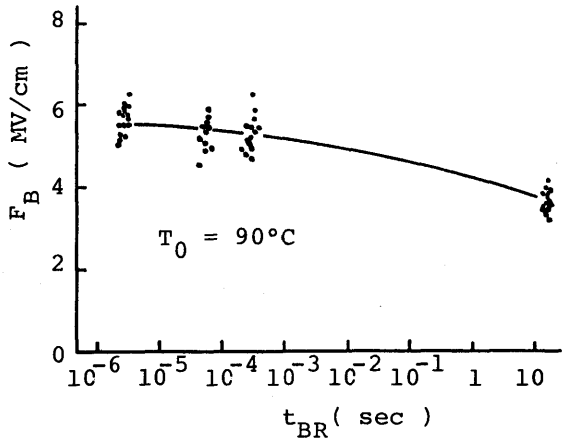

Fig.8.13. Electric strength as a function of voltage duration at 90°C.

to 1000 μsec, and at 90°C decreases slowly with increasing voltage duration.

The result at -196°C is in favour of the electronic breakdown process[2-5], since F_B scarcely changes within the experimental condition. One of the reason for the initial increase in F_B with increasing t_{BR} at 30 and 60°C is considered to be the effect of a reduction in the field stress[24]. Watson[24] interpreted that the subsequent fall in F_B with increasing voltage duration would be caused by the disappearance of the space charge in the vicinity of each electrode due to charge transport within the specimen. However, the experimental result showed that F_B in the case of applying dc ramp voltage decreases with increasing temperature in the range above room temperature. This suggests that the breakdown mechanism in this temperature range may change into thermal or electromechanical breakdown process as t_{BR} becomes longer[25,26,27]. The above consideration can explain the decrease in F_B at 90°C with increasing t_{BR} to be caused by a shift of the critical voltage duration to lower values, at which the dominating breakdown process changes from the electronic

breakdown to another process such as thermal breakdown or electromechanical breakdown. The dependence of F_B on t_{BR} at different temperatures is illustrated in Fig.8.14. The breakdown process therefore depends on the temperature and voltage duration. These results for PE-1 support the previous discussion on the breakdown process at high temperatures for different types of PE in terms of

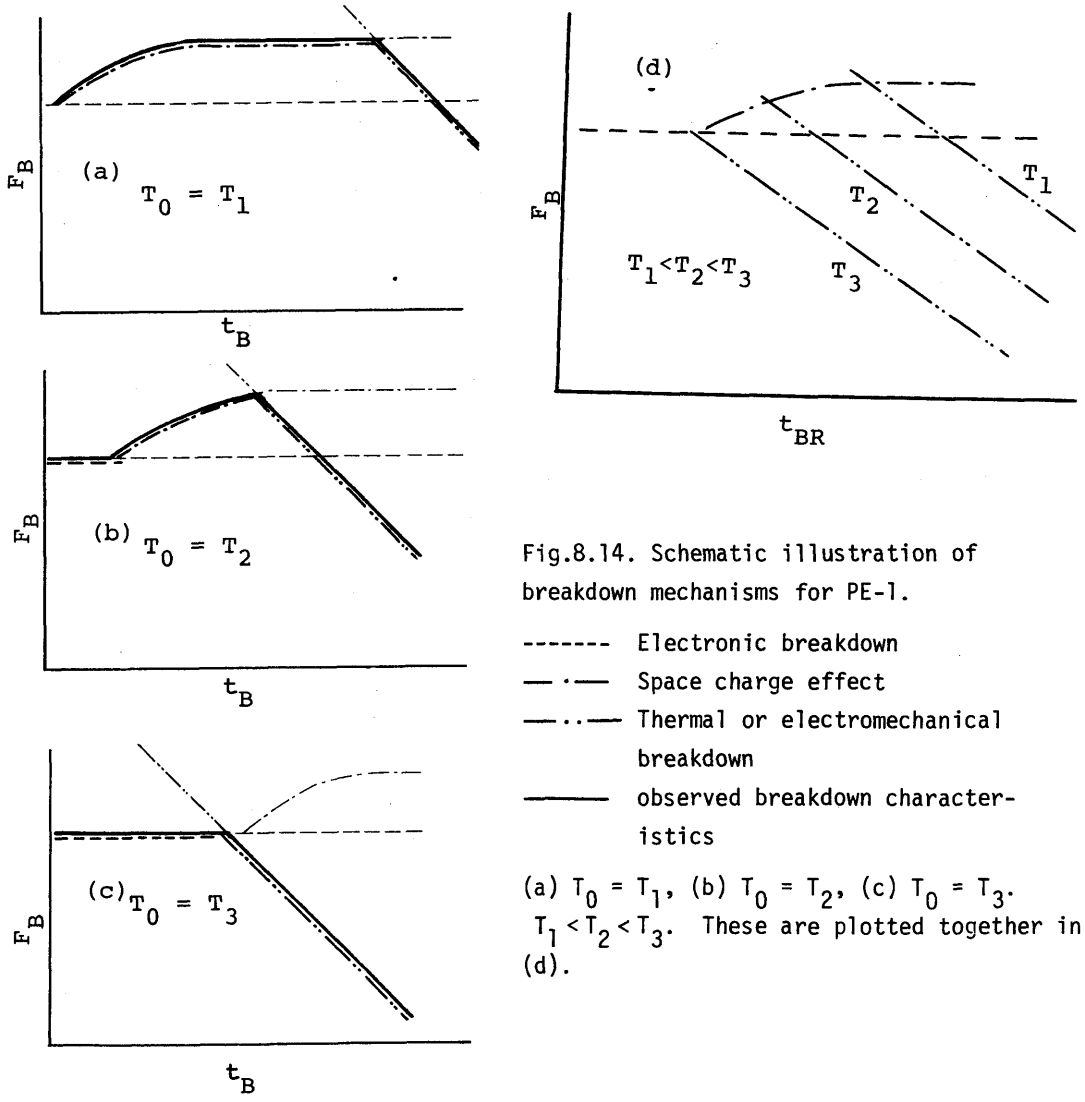

Fig.8.14. Schematic illustration of breakdown mechanisms for PE-1.

------- Electronic breakdown

— · — Space charge effect

— · · — Thermal or electromechanical breakdown

——— observed breakdown characteristics

(a) $T_0 = T_1$, (b) $T_0 = T_2$, (c) $T_0 = T_3$. $T_1 < T_2 < T_3$. These are plotted together in (d).

electromechanical breakdown or thermal breakdown in a dc voltage application.

In order to examine the effect of electromechanical deformation on the breakdown process, the relation of Young's modulus to the electric strength was examined. Measurements of electric strength and Young's modulus were made on two types of samples, PE-1 and PE-5. These samples, as shown in Table 5.1, differ in melting point but have almost the same density. The outline of the measurement of Young's modulus is as follows: A film 4 mm wide and 25.4 mm long, at a given temperature, was drawn along the direction of the film length at a drawing rate of 10 μm/sec in air. Young's modulus Y was calculated from the equation below with the simultaneously measured drawing ratio.

$$Y = \frac{y}{S} / [(l_f - l_0) / l_0], \qquad (8.1)$$

where y is the load, S is the cross-section of the film before drawing, and l_f and l_0 are the sample length after and before drawing, respectively.

The temperature dependence of Young's modulus for PE-1 and PE-5 in the temperature range from room temperature to the vicinity of the melting point is shown in Fig.8.16. Each point represents the maximum value of Young's modulus in a sample within 5% of drawing ratio. It is observed that Young's modulus at the same temperature for PE-1 and PE-5 is almost the same and the shape of the temperature dependence of Y is also similar each other.

Theoretical electric strength F_{em} determined from electromechanical breakdown process, as described in Chapter II, can be expressed as

$$F_{em} = \left(\frac{Y}{\varepsilon_0 \varepsilon_r} \right)^{1/2} \exp (-1/2), \qquad (8.2)$$

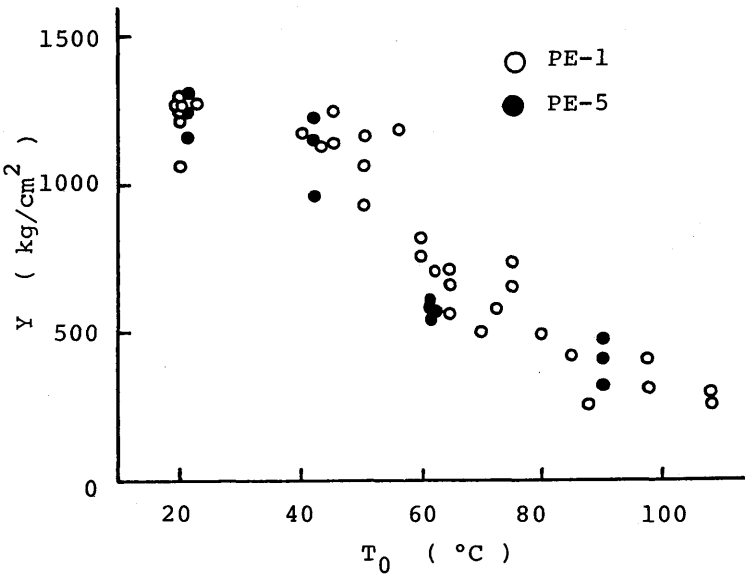

Fig.8.15. Temperature dependence of Young's modulus.

where ε_0 and ε_r are the permittivity of the free space and relative permittivity, respectively. Since PE-1 and PE-5 have the same values of Y and ε_r, the theoretical values of F_{em} in two types of samples also agree. By using the value of 2.3 for ε_r and the average Young's modulus shown in Fig.8.15, F_{em} was estimated. Figure 8.16 shows the temperature dependence of calculated F_{em}, as well as the experimental results of F_B for PE-1 and PE-5 by applying a ramp voltage at a field rising rate of 0.2 MV/cm.sec. The main features of the results shown in Figs. 8.15 and 8.16 are as follows:

(1) Below about 70°C, Young's modulus of PE-1 is almost equal to that of PE-5, but the electric strength for the former is higher than that of the latter.

(2) Above about 70°C, Young's modulus and electric strength are the same for PE-1 and PE-5.

Thus, it is considered that a lowering of Young's modulus causes a

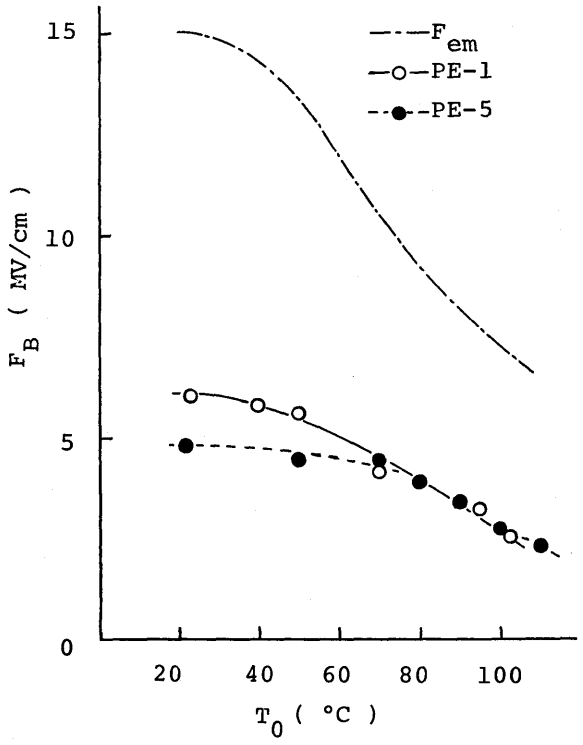

Fig.8.16. Temperature dependence of F_B for PE-1 and PE-5. Dotted dash line represents F_{em} estimated from the obtained Young's modulus.

common influence on the breakdown characteristics of both, PE-1 and PE-5, above 70°C. In this temperature region, it was also found that for both types of films, F_B obtained by applying the rectangular pulse is higher than that by applying the dc ramp voltage.

The theoretical electric strength F_{em} does not agree with the experimental results and above 70°C the former is about two times larger than the latter. Therefore, the breakdown characteristics cannot be simply understood only by the electromechanical breakdown process. It is required to investigate multi-step breakdown processes involving the effect of Maxwell stress or a local electromechanical breakdown at a weak spot in a sample as presented by Block[28].

Electrical conduction plays an important role in thermal

breakdown process. In order to discuss the breakdown characteristics obtained at high temperatures in terms of thermal breakdown process, measurements of the electrical conduction were made. Samples used were PE-1, PE-3, and PE-4, sandwiched with gold evaporated electrodes of 15 mm in diameter. The schematic procedure of the experiment is shown in Fig.8.17. A step voltage was applied to the sample for 10 min. and then shortcircuited for 10 min. at a given temperature. Next, the magnitude of voltage was increased by a given value, and this procedure was repeated at different temperatrue. Lastly, to check reproducibility , measurements were repeated for initail condition.

Figures 8.18 to 8.20 show the field-current density characteristics with temperature as a parameter for PE-1, PE-3, and PE-4, respectively. The 10 min. value of the current after the voltage

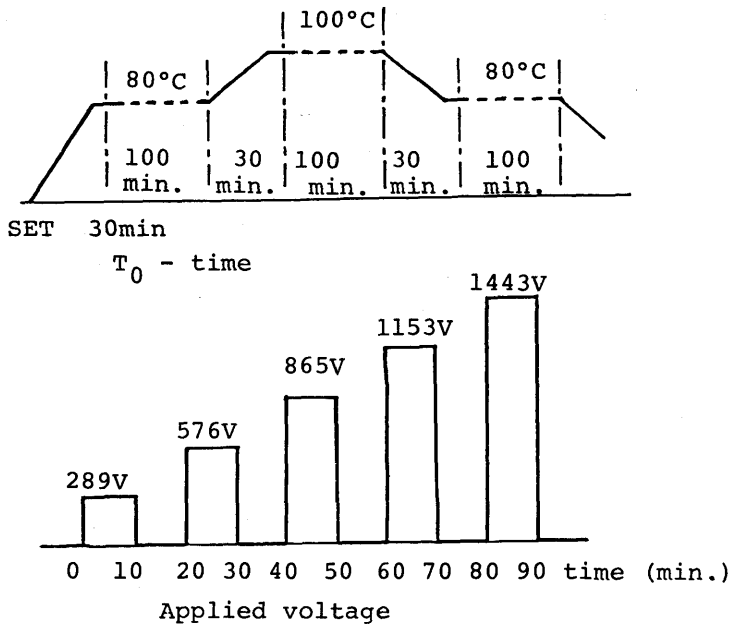

Fig.8.17. Procedure for conduction current measurement.

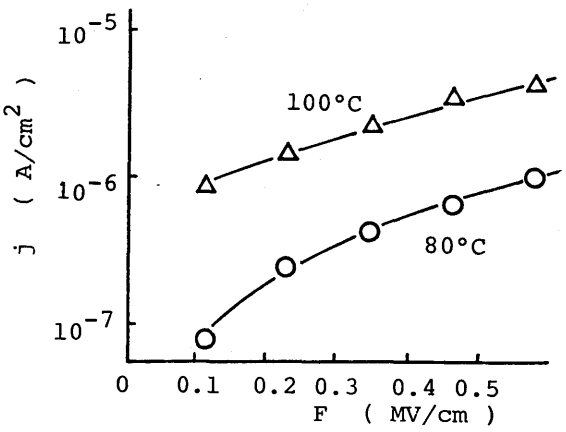

Fig. 8.18. Current density (j) - field (F) characteristics for PE-1.

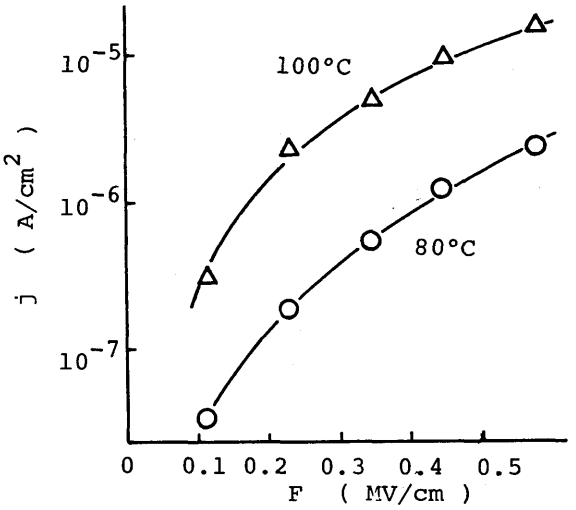

Fig. 8.19. Current density (j) - field (F) characteristics for PE-3.

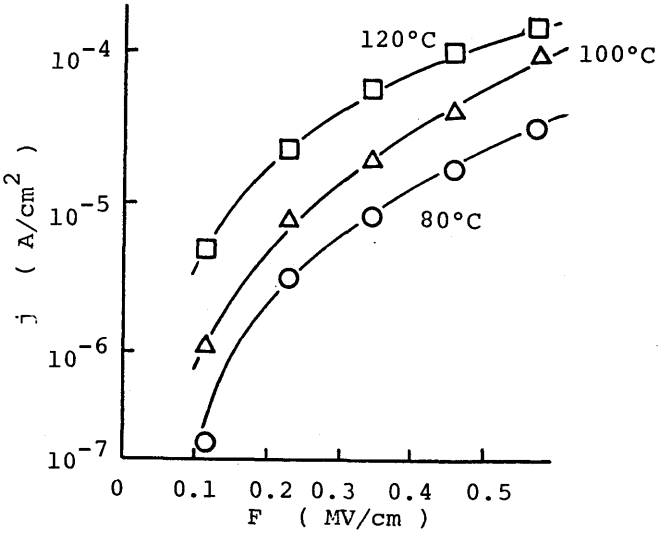

Fig. 8.20. Current density (j) - field (F) characteristics for PE-4.

application was taken to decide conduction current density in these figures. It is found that the current densities at both 80 and 100°C for PE-1 are lower by about one order of magnitude than those for PE-4. Contrary to this, F_B for PE-1 was lower than that for PE-4 in this temperature range, as already shown. In general, thermal breakdown strength decreases with increasing conductivity of the sample. The obtained result, therefore, seems to be completely opposite to the prediction from thermal breakdown process. Thus, it appears that simple interpretation in terms of thermal breakdown process cannot also give a satisfactory explanation to the breakdown of PE films at high temperatures. However, there are some unclarified points in the above discussion about the interpretation of electrical conductivity and thermal breakdown ; namely, the difference in wave form of the applied voltage in the measurement of conductivity, the determination of the current density from the value at 10 min. after voltage application and the measurement of the electrical conduction in relatively low field, etc..

8-4 Effect of Cross-linking on Electric Strength

In the previous section, the relation between the solid structure and the electrical breakdown was discussed, paying special attention to the high temperature region. It was suggested that electromechanical deformation may be partly responsible for the breakdown process. Therefore, cross-linking is expected to cause an increase in F_B in the temperature region where the mechanical deformation is effective. In this section, the effect of cross-linking on the breakdown characteristics of PE is examined. Correlation of mechanical properties to the electric strength in the high temperature region from room temperature to 160°C is mainly discussed.

8-4-1 Specimen

Specimens were two kinds of 25 μm thick silane cross-linked PE (Linkron X. Mitsubishi Petrochemical Co. Ltd.) with different gel content which gives a measure of cross-linking. The physical parameters of these films are listed in Table 8.2, as well as that of PE-1 which is the base polymer of the cross-linked PE and contains no silane cross-linking group. The method for measuring electric strength and Young's modulus has already been mentioned in Section 8-3.

8-4-2 Results and Discussion

Figrue 8.21 shows the temperature dependence of F_B for the silane cross-linked PE by applying a ramp voltage at the rate of 500 V/sec. This figure also contains the result of PE-1. It can be seen that in a temperature region from room temperature to about 90°C, F_B for Si-1 is almost the same as that for PE-1 and decreases with increasing temperature. Above 90°C, variation in F_B for Si-1 is small. On the other hand, F_B for Si-2, which has higher degree of cross-linking, is equal to that for PE-1 from room temperature to 50°C, while from 50°C to 160°C, is higher than those for PE-1 or Si-1. The effect of cross-linking due to high energy radiation on the dielectric

Table 8.2. Physical parameters of silane cross-linked PE.

	Density (g/cm^3)	M.F.R. (g/10min)	Silan content (weight %)	Gel content (weight %)
Si-1	0.921	1.2	0.5	73
Si-2	0.928	4.0	5.0	95
PE-1	0.917	1.0	—	—

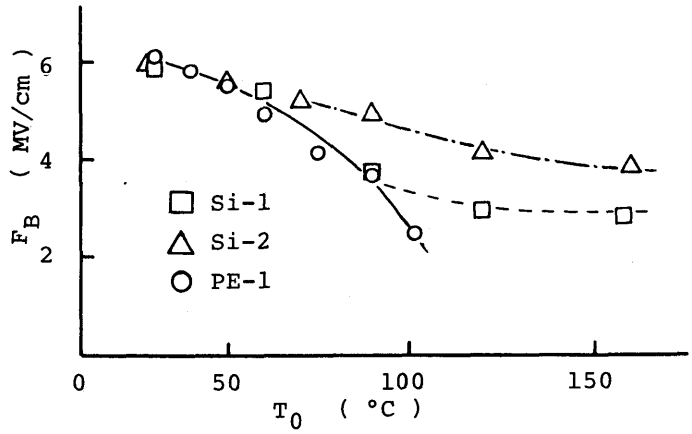

Fig. 8.21. Temperature dependence of electric strength by applying a ramp voltage at the rate of 500 V/sec for PE with a different degrees of cross-linking by silane.

breakdown of PE at high temperature has been studied by many researchers[8,19,21]. The cross-linking leads to the rise of the softening point and resulting in a marked increase in F_B. A similar behavior is also obtained for the case of the cross-linking by silane.

Young's modulus of Si-1 and Si-2 was also measured at different temperatures. The electric strength measured at the same temperature is plotted in Fig.8.22 as a function of Young's modulus for Si-1 and Si-2, as well as PE-1. The solid line in this figure represents the theoretical electric strength estimated from the electromechanical breakdown theory, using the experimental values of Young's modulus. As shown in the figure, the electric strengths for different three types of PE can be expressed as a function of Young's modulus, irrespective of temperature. As mentioned above, the dc breakdown characteristics of PE at high temperatures have been found to be closely related to the mechanical property in silane cross-linked PE also. However, the theoretical value obtained from the simple

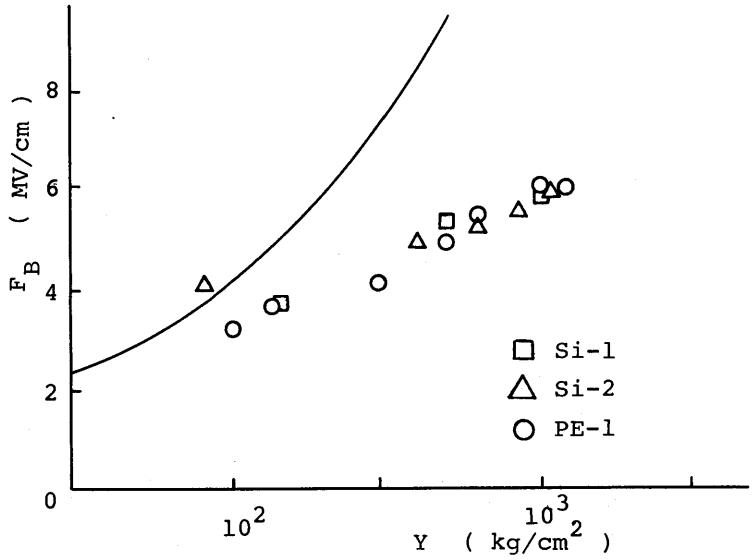

Fig.8.22. Electric strength as a function of Young's modulus.

assumption of electromechanical breakdown process is about two times higher than the experimental value, except in the region of small Young's modulus. Thus, it cannot be concluded that only the simple electromechanical breakdown assumption can be taken to explain the experimental result. Further consideration is required as mentioned in the previous section.

8-5 Conclusion

Electrical breakdown of polyethylene (PE) was studied in the high temperature region above room temperature. Firstly, the relation between the solid structure and the breakdown characteristics was examined. Various kinds of specimen with different physical parameters were prepared.

The electric strength obtained by applying dc voltage at room temperature decreased with increasing density and melting point of PE, and this behavior was reversed at 95°C. The electric strength for the case of rectangular pulse was higher than that for the case of dc

voltage application.

Further, the effect of the electromechanical deformation on the breakdown process was investigated. Young's modulus of PE-1 and PE-5, which have the same density but differ in the melting point, was measured. It was found that above 70°C both Young's modulus and the electric strength of these samples almost agreed. However, the theoretical value of electric strength calculated from the measured Young's modulus by using a simple assumption of the electromechanical breakdown theory was about two times as large as the experimental values.

The electrical conduction measurements were also made. As a result, it was difficult to understand the results of both conduction and breakdown data only in terms of thermal breakdown process.

From all the experiments, it was found that although the breakdown of PE at high temperatures is not considered as a simple electromechanical breakdown process, the breakdown is affected by the mechanical deformation due to Maxwell stress.

The influence of cross-linking by silane was also investigated. It was found that the cross-linking by silane raised the electric strength at high temperatures near the melting point of PE. Above 50°C, the electric strength increased as the degree of cross-linking became higher.

The measurements of Young's modulus were also made with the cross-linked PE. It was found that the electric strength above room temperature could be expressed as a function of Young's modulus, irrespective of the sample type or temperature. However, a good agreement between the theoretical strength and the experimental one was not obtained, although the dc breakdown characteristics of PE and silane cross-linked PE were found to be closely related to Young's modulus.

References

[1] M.Ieda: IEEE Trans. on Elect. Insulation EI-15 206 (1980).

[2] A.E.W.Austen and H.Pelzer: J. Inst. Elect. Engrs. 93-I 525 (1946).

[3] J.J.Mckeown: Proc. Inst. Elect. Engrs. 112 824 (1965).

[4] P.H.H.Fisher and K.W.Nissen: IEEE Trans. Electrical Insulation EI-11 37 (1976).

[5] W.G.Oakes: J.Inst. Elect. Engr. 95 36 (1948).

[6] W.G.Oakes: J.Inst. Elect. Engr. 96 37 (1949).

[7] K.Miyairi, T.Yamauchi, G.Sawa and M.Ieda: J. Inst. Elect. Engrs of Japan 91 1962 (1971) in Japanese.

[8] K.Amakawa, T.Moriuchi, K.Yoshino and Y.Inuishi: J. I.E.E. of Japan 84 124 (1964).

[9] M.Ieda, Y.Takai, M.Nagao and G.Sawa:I.E.E. Conference Proceedings " Dielectric Materials, Measurements and Applications" Cambridge, England (1975).

[10] I.Kitani and K.Arii: Trans. I.E.E Japan 94-A 251 (1974) in Japanese.

[11] M Nagao: Ph.D thesis , Nagoya University (1978).

[12] W.G.Lawson : Proc. Inst. Elect. Engrs. 113 197 (1966).

[13] H.Miyauchi and K.Yahagi : Trans. I.E.E. Japan 92-A 36 (1972) in Japanese.

[14] M.Ieda and G.Sawa: OYOBUTSURI 48 1177 (1979) in Japanese.

[15] J.Artbauer and J.Griac: ACTA TECHNICA CSAV 3 416 (1966).

[16] J.Artbauer and J.Griac: ACTA TECHNICA CSAV 3 429 (1966).

[17] J.Artbauer : Kolloid Z und Z. Polymere 202 15 (1965).

[18] T.Tanaka and Y.Nitta: EIM-81-62 in Japanese.

[19] K.H.Stark and C.G.Garton : Nature 176 1225 (1955).

[20] K.Miyairi and T.Yamada: Japan. J. Appl. Phys. 16 1449 (1977).

[21] K.Yahagi and A.Okinaka: CEIDP IV-2 (1981). 199.

[22] M.Yoda, G.Sawa and M.Ieda: 1979 Annual Report CEIDP NAS/NRC 356.

[23] A. von Hippel and R.S.Alger : Phys Rev. 76 127 (1949).

[24] D.B.Watson : J.Phys. D 5 410 (1972).

[25] N.Klein : Adv. in Electronics & Electron Physics 26 309 (1969).

[26] J.Vermeer: Physica 20 313 (1954).

[27] J.Vermeer: Physica 22 1257 (1956).

[28] J.Block and D.G.LeGrand: J. Appl. Phys. 40 288 (1969).

Chapter IX Conclusion

9-1 Principal Results

Lastly, overall conclusion over Chapter I to VIII will be given as follows:

(i) The research work presented in this thesis was devoted to advance the understanding of the electrical breakdown process for polymeric insulators, especially in a high temperature region. An approach was attempeted to interprete the experimental results on electrical breakdown from the standpoint of the thermal breakdown process in order to see to what extent the breakdown of polymer can be explained by the thermal breakdown theory.

Electrical Breakdown of Polyimide

(ii) The effects of hydrolysis and water absorption on the electric strength of polyimide film (PI) were investigated, based on the reports on the breakdown mechanism of polyimide and the effect of heating.

(iii) Any direct evidences for further imidization by the heat treatment could not be obtained with infra-red spectroscopy. Therefore, the effect of hydrolysis on the electric strength was studied, since the hydrolysis increases the concentration of polyamic acid contrary to the case of the imidization. After the influence of the secondary causes such as water absorption process and re-imidization process was examined, it was indicated that the presence of polyamic acid affects the breakdown characteristics. Thus, the further imidization is possibly one of the factors which contribute to the improvement of the high temperature electric strength with the heat treatment.

Electrical Breakdown of Poly(vinylidene-fluoride)

(iv) The dielectric breakdown of poly(vinylidene-fluoride) (PVDF) was studied over the temperature range from room temperature to 150°C by applying a linearly rising voltage. The electric strength was more than 8 MV/cm at room temperature, but above 50°C it fell rapidly with increasing temperature and depended on the rate of rise of the electric field but not on the sample thickness. An attempt was made to apply the impulse thermal breakdown theory to the data obtained above 50°C. Assuming ionic conduction, the temperature rise of the sample under voltage application was calculated numerically using impulse thermal breakdown theory. By fitting these theoretical electric strengths to the experimental values, the conduction parameters were estimated as follows; activation energy was 0.9 eV, ionic jump distance was 9 Å, and pre-exponential factor j_0 was 1.2×10^7 A/cm^2.

(v) The case of including Poole-Frenkel effect in a dissociation process of ionic charges was also discussed. In this case, the estimated parameters became as follows if the ralative permittivity is taken to be 10 to 14; activation energy 0.9 eV, jump distance 4 Å, and j_0 6.5×10^5 A/m^2.

(vi) In order to get an information on improvement of the electric strength of PVDF in high temperature region, the influence of the changes in ionic conduction parameters on F_B was studied quantitatively. It was found that for improving F_B by 1 MV/cm, for example, the density of supplying source of thermally dissociated ions must be decreased by two orders of magnitude, independent of whether taking into account Poole-Frenkel effect or not. It was also shown that the equivalent increase in F_B could be attained by either decreasing the jump distance by 1 to 1.5 Å or increasing the activation energy

by 0.05 eV.

(vii) The relation between the solid structure and breakdown characteristics was examined by using samples with various ratios of different crystalline phases. It was shown that the change in the crystalline structure would be accompanied by the change in the ionic conduction parameters.

Condition Required for Using Impulse Thermal Breakdown Theory

(viii) In the thermal breakdown, the impulse thermal assumption in which the heat conduction term is neglected is valid when the thermal time constant of dielectric t_{th} is greater than the time to breakdown t_B provided the heat conduction from the dielectric surface to the ambient is ideally complete. However, many reports have been published which insist the impulse thermal mechanism even under the condition $t_{th} < t_B$. In this thesis,the impulse thermal theory is shown to be successfully applied to the discussion on the breakdown process for PVDF and PPS in spite of the condition $t_{th} < t_B$. These are based on the following prediction. Provided the heat conduction from the dielectric material to the surroundings is insufficient, the impulse thermal breakdown form is expected even though $t_{th} < t_B$. Therefore, a quantitative examination on this relationship was made on the basis of the fundamental equation of thermal breakdown.

(ix) The fundamental equation of thermal breakdown was numerically solved under the boundary condition which obeys Newton's law of cooling for various values of heat transfer coefficient λ from the dielectric surface to the ambient. As a result, it was found that the impulse thermal assumption is valid even if $t_{th} < t_B$ provided λ is smaller than a critical value. The theoretical electric strength

was presented as a function of λ for poly(vinylidene-fluoride). The calculation was done using the ionic conduction parameters estimated for PVDF in Chapter IV. In the case of a 12.5 μm thick film at 100°C, the calculated electric strength is nearly the same as that estimated on the impulse thermal assumption provided $\lambda \leqq 1\ W/m^2.K$.

(x) Further, the effect of the heat transfer coefficient on the breakdown characteristics was investigated. From an example of numerical calculation assuming ionic conduction, the following qualitative result on the theoretical feature of thermal breakdown characteristics was obtained. F_B depends on the field rising rate and is almost independent of the thickness, provided λ is so small that the heat loss from the surface is negligible. On the contrary, for the case of ideally complete heat dissipation, F_B scarcely depends on the field rising rate but remarkably depends on sample thickness in the region of field rising rate which does not hold the condition for the impulse thermal assumption.

Electrical Breakdown of Plasma Polymerized Styrene Thin Films

(xi) Electrical breakdown of plasma polymerized styrene thin films (PPS) was studied by taking advantage of self-healing. The electric strength F_B was almost independent of temperature from -196 to 200°C, and strongly depended on voltage rising rate even in a slow rising rate. The breakdown characteristics were influenced by electrode metal and ambient atmosphere, but not by X-ray irradiation or photo illumination. From the experimental results, the breakdown mechanism of PPS was discussed with existing breakdown theories. Consequently, any single breakdown process could not be considered as a possible breakdown mechanism. As a result, the results important

to deduce a new breakdown model were presented: The breakdown of PPS will be determined by thermal breakdown criterion, and strongly related to a temperature independent injection process.

(xii) A new simple breakdown model was presented on the basis of the experimental results on plasma polymerized styrene thin films. In this model, the current is controlled by the Fowler-Nordheim tunnelling emission from the cathode and the breakdown is governed by the impulse thermal process. The numerically calculated values by discarding the space charge could fit the dependences of electric strength on temperature, field rising rate and prestress, and are also consistent with the other experimental results. Further, a steady state avalanche was considered as a possible bulk conduction. It was found that provided the mobility of positive charge is beyond a certain value, the space charge is scarcely formed, giving a physical basis for neglecting the space charge.

Electrical Breakdown of Polyethylene

(xiii) The electrical breakdown phenomena at high temperatures was studied on polyethylene (PE) with different physical properties. The correlation between the solid structure and breakdown characteristics of PE, and the effect of silane cross-linking on F_B were studied.

(xiv) The electric strength F_B measured by applying dc voltage at room temperature decreased with increasing both density and melting point. On the contrary, the relation at 95°C was reversed to the case at room temperature. The dependences of F_B on the electromechanical deformation due to Maxwell stress and on electrical conduction were discussed. It was found that the breakdown

characteristics of PE above room temperature cannot be understood only in terms of electromechanical breakdown process or thermal breakdown process. It was indicated, however, that the breakdown mechanism at high temperatures is possibly related to a variation of Young's modulus.

(xv) The effect of cross-linking by silane on the breakdown characteristics of PE was discussed. It was confirmed that the silane cross-linking caused an increase in F_B in a temperature region above 50°C. A correlation between Young's modulus and F_B for silane cross-linked PE was obtained. It was found that F_B above room temperature can be expressed as a function of Young's modulus, irrespective of measuring temperature. It was concluded that the dc breakdown characteristics of PE as well as silane cross-linked PE at high temperatures can be considered to be closely related to Young's modulus.

(xvi) In order to elucidate the breakdown mechanism of PE at high temperatures, it is required to invoke multi-step breakdown processes involving the effect of mechanical deformation or local electromechanical breakdown at a weak spot in a sample.

9-2 Practical Significance of the Present Work

The practical significance of present work can be summarized as follows:

(i) The electrical breakdown mechanism of polyimide in high temperature region was reported to be thermal breakdown. Thus, for an elevation of electrical insulation properties at high temperatures it is required to reduce the electrical conductivity. For this purpose, it was found to be necessary to recognize the supply source

of carriers contributing to electrical conduction and to establish a way to reduce them. One way of improvement is reported to be the heat treatment with which a prominent increase in the electric strength of commercial imide polymers could be obtained. In the thesis, in order to elucidate further the relation between polyamic acid in polyimide and the dielectric breakdown, the effect of hydrolysis was studied , which increases the concentration of polyamic acid with a process opposite to imidization. It was confirmed that the further imidization is possibly one of the factors which contribute to improvement of the high temperature electric strength with the heat treatment. However, in a practical application, variation of chemical and mechanical properties accompanied with the heat treatment should be examined to establish the best condition of the treatment.

(ii) Poly(vinylidene-fluoride) (PVDF) is expected to be applied to active devices because of its piezoelectricity and pyroelectricity. The thermal breakdown process was also considered as a dominant process of dielectric breakdown in PVDF at high temperatures. The removal of impurities and the stabilization of materials containing thermally dissociated ions may be a powerful means for a reduction of the density of ions, which would result in the improvement of the electric strength in a high temperature region. Besides these methods, the result in Chapter IV showed that the modification of the solid structure, which would lead to a change of ionic conduction parameters, especially ionic jump distance and activation energy, is expected to be a remarked way for an improvement of the electric strength. In order to realize such improvement, it is strongly needed that the microscopic physical meaning of the ionic parameters is given in the light of the solid structure.

(iii) Thin polymer films produced by a glow discharge method are expected to have practical applications to various electronic devices and electrical insulations. In this connection, the electrical breakdown of plasma polymerized styrene thin films (PPS) was studied. As a result, all the experimental results were consistently explained by a presented model: The current is controlled by the tunnelling emission from the cathode and the bulk breakdown is governed by the impulse thermal breakdown process. From the result, as well as the discussion on a steady state avalanche bulk conduction,it is expected that the electric strength is increased by the following ways:

(1) to decrease the injected conduction current, and

(2) to suppress the effect of positive space charge produced by impact ionization.

For (1), it is effective to increase the effective barrier height between the cathode metal and the polymer, or to increase the effective mass of the electron in the dielectric. For (ii), it is effective to increase hole mobility for the suppression of formation of space charge, or to decrease the electron mean free path and increase ionization energy for the suppression of impact ionization.

(iv) The electrical breakdown mechanism of polyethylene at high temperatures was not completely understood in terms of thermal breakdown process or electromechanical breakdown process. However, it was shown that the dc breakdown characteristics of PE at higher temperature than about 50°C are possibly related to Young's modulus of the measured samples, in silane cross-linked PE also. It can be said that one of good ways for an improvement of the electrical insulation properties is to improve the mechanical properties of PE. As an example, the silane cross-linking of PE was found to be a good way for this, in addition to the merit of its easiness for

manufacturing.

As mentioned above, various new informations given in this thesis should greatly contribute not only to the understanding of the fundamental breakdown characteristics but also to the improvement of the electric strength at high temperatures for polymeric insulating materials.